ELECTROCATALYTIC OXIDATION OF ALCOHOLS USING PLATINUM AND PALLADIUM NANOPOROUS SOLIDS

By

Margaretta Mary Dimos

A DISSERTATION

Submitted to
Michigan State University
in partial fulfillment of the requirements
for the degree of

DOCTOR OF PHILOSOPHY

Chemistry

2011

ABSTRACT

ELECTROCATALYTIC OXIDATION OF ALCOHOLS USING PLATINUM AND PALLADIUM NANOPOROUS SOLIDS

By

Margaretta Mary Dimos

As the world's supply of fossil fuels continues to diminish, there is an increasing need for the development of alternative energy sources. Fuel cell technology, coupled with renewable, biomass-derived fuel stocks such as methanol and ethanol, is one such energy source that will find increasing use in both the near- and long-term future. The present generation of catalysts for fuel cells is characterized by limited efficiency and durability, and as such there is a great need to improve upon and develop new catalytic materials. Nanoporous solids, also known as inverse opals, are potentially useful materials, due in part to their relatively regular structure and physical integrity. It is the purpose of this work to initiate and investigation of nanoporous catalytic materials.

We have developed nanoporous solids made from the electrodeposition of platinum and palladium metal around a silica nanosphere template. We used these materials to probe and interpret the catalysis of selected alcohols using cyclic voltammetry and chronoamperometry measurements. Initially we examined the electrocatalytic oxidation of methanol and ethanol, under acidic and basic conditions, using Pt and Pd nanoporous solid electrodes. Our results were then compared to planar Pt and Pd substrates, prepared using the same electrodeposition process as the nanoporous materials. The current density enhancement seen for the Pt nanoporous solids was more pronounced under basic conditions than acidic conditions. It was also

determined that the nanoporous Pd was more catalytically active for ethanol than for methanol, with the nanoporous Pt producing higher catalytic efficiency for methanol.

The enhancement that was observed with the nanoporous solids over their planar counterparts could be the result of either geometric factors or the catalyst surface morphology. The effect of morphology of the nanoporous Pt substrates was examined by studying the electrocatalytic oxidation of 1,2-propanediol under basic conditions. Our work was performed in alkaline media because, for this reactant, electrocatalytic oxidation is more efficient under these conditions. Our data for 1,2-propanediol point to metal morphology as the primary explanation for the enhanced current density relative to the planar solid electrode observed for the reaction with the nanoporous Pt.

Our work with 1,2-propanediol proved to be informative, and we continued to examine the geometric *vs*. morphological enhancement issue by examining the electro-catalytic oxidation of 1,3-propanediol and four butanediols at nanoporous Pt and planar solid Pt electrodes under basic conditions. These reactants were chosen based on the positions of the hydroxyl moieties, so that the role of functional group position could be studied. The electro-catalysis of the aforementioned diols was studied both in terms of their reaction mechanism(s) and their kinetics. Our data indicate that the dominant factor in mediating the electrocatalytic oxidation pathway is the proximity of the hydroxyl groups on the diol and that there is a difference in the morphology of the nanoporous Pt and the planar solid Pt. This work leads to the conclusion that it is the electrode morphology rather than the geometric considerations that appears to be the dominant factor in the enhancement observed for the nanoporous solids and that this enhancement also depends upon the reactants used.

ACKNOWLEDGEMENTS

First and foremost, I would like to thank Dr. Gary J. Blanchard for his help and support, not only in writing this document but in all aspects of the research and writing processes. Without his guidance I would not be the chemist that I am today and I am fortunate enough to have chosen him as my advisor.

As a student, there is no better place to be than in an environment where you can always find a helping hand. With that in mind, I would also like to thank my Guidance Committee: Doctors Merlin Bruening, Greg Swain, and David Weliky. Thank you all for your support and guidance throughout my graduate education.

I could not have made it through grad school without the help and support of my labmates, both past and present. Thank you for all of your help and support, and being friends as well as coworkers. In particular I would like to thank Dr. Janelle D. S. Newman and Dr. Alex Blevins for their help and encouragement the first few years of graduate school. A great big thank you also goes to those who joined the Blanchard group with me: Dr. Ben Oberts, Dr. Monika Dominska, & Dr. Heather Pillman. Although Gary may never take four graduate students in one year again, I'm glad he made an exception and that we all made it through together! Doug Gornowich, Christine Hay, Iwan Setiwan, Stephanie Wright, Kim Eggers & Katie Logan-Dinco: thank you for making the last few months of my graduate career so enjoyable.

I am extremely lucky to have a great extended family that includes a multitude of friends I have made along the way, without which I would not be the person I am today. Even though most of you are hundreds of miles away, I knew I could count on each and every one of you through the good and the bad. I would especially like to thank my grandparents, Marge & Phil Paladino, who from pre-school on, made sure that I made school a priority. Thank you also to my brother, Christos and my sisters, Aleka and Melissa. Graduate school was that much better knowing that I could turn to all of you when I needed a shoulder to lean on or a good laugh.

I would be completely remiss if I were to not thank my best friend and fiancé, Kristopher Koster. I do not know where I would be today if not for your love and support. Thank you for trying to keep me sane these past few months and I cannot wait to spend the rest of my life with you.

Finally, I would not have even thought about graduate school without the love and encouragement that I received from my parents, Debra Ann & Sotirios Dimos, to whom this dissertation is dedicated. Thank you both for your unconditional love and support, for pushing me when I needed to be pushed, and knowing exactly when all I needed was a hug. I love you both and hope to make you proud each and every day.

TABLE OF CONTENTS

LIST OF TABLES

LIST OF FIGURES

LIST OF SCHEMES

LIST OF SYMBOLS AND ABBREVIATIONS

Pt	Platinum
Pd	Palladium
USDOE	United States Department of Energy
CV	Cyclic Voltammetry (Voltammogram)
i_p	Peak Current (A)
n	Number of electrons
A	Area
D	Diffusion Coefficient
C	Concentration
v	Scan Rate
E_p	Peak Potential (V)
R	Gas Constant
T	Temperature (K)
F	Faraday's Constant
EtOH	Ethanol
MeOH	Methanol
TEM	Transmission Electron Microscope
SEM	Scanning Electron Microscope
TEOS	Tetraethylorthosilicate
ITO	Indium Tin Oxide
LB	Langmuir-Blodgett

E_0	Standard Reduction Potential (V)
Q_H	Coulombic Charge for Hydrogen Desorption
I_f/I_b	Ratio of forward and reverse anodic peak currents
$2(Dt)^{1/2}$	Diffusion Length (cm^2/s)
d	Nanosphere diameter (nm)
j	Current Density

CHAPTER 1

INTRODUCTION

Energy concerns are becoming greater all over the globe. With fossil fuels such as coal, petroleum and natural gas accounting for 83% of the total energy consumed, they are still the primary source of energy throughout the US and the world.[1] Although for the present these fossil fuel supplies are substantial, they are finite and are expected to be exhausted in the next 100 to 300 years. Therefore it is not surprising that there has been an increased effort to find alternate sources of energy, preferably sources that will not lead to the same environmental and supply concerns as fossil fuels, so that the standard of living can continue to be on par with what it is today.

One effort that is being explored to help address the world's energy requirements is development of technology that makes use of renewable, biomass-derived fuel stocks such as methanol and ethanol.[2-4] These renewable fuels can potentially be incorporated into fuel cell technology, which will likely see increased use in the near and long term future. The operation of fuel cells is based on the principle of elecrocatalytic oxidation of fuel and the reduction of gas phase O_2. It is important that the fuels used in this process do not degrade or poison the catalyst directly. Also, since a major concern of continuing to use fossil fuels is not only the limited supply, but also the rising costs, for fuel cell technology to be a competitive source of energy the fuel sources need to be readily available, renewable and inexpensive. Biomass-derived fuels meet these criteria, and provide an added bonus of producing less atmospheric pollutants than their fossil fuel counterparts.[3]

The critical component in fuel cells is the catalyst, which should be efficient and durable. Catalysts that are currently available for fuel cells include bi-metallic catalysts such as PtRu, PtSn and PtW,[5-6] and carbon-metal catalysts such as Pt-C and Pd-C.[7-8] Typically, the preferred anode catalyst for direct methanol fuel cells is Pt-Ru.[6] However, improvements still need to be made to develop these catalysts into fuel cells in a commercial setting. One problem with many of these direct alcohol fuel cells is the poisoning of the catalytic surfaces by carbon monoxide. This poisoning leads to the inhibition of catalysis and the consequent need to regenerate or replace the catalyst.[3,8-9] It would be helpful to develop catalytic materials that are more efficient and less susceptible to poisoning from the by-products of the alcohol catalysis.

As mentioned above, platinum and palladium catalysts have found some success when used as catalysts in direct alcohol fuel cells, but the issue of poisoning continues to be a problem. Moderate improvement of this issue has been seen with the use of bi-metallic catalysts, specifically with the incorporation of ruthenium.[5-6] The incorporation of the second metal provides the necessary oxygen for complete oxidation to CO_2.[10] The current consensus is that the optimal platinum to ruthenium ratio is 1:1, but even when using this ratio a high catalyst loading of approximately 2-8 mg/cm^2 is needed to reach acceptable fuel cell performance, especially considering the lifetime of the catalyst.[5]

Therefore, there needs to be a reduction in the cost and improvements in the catalyst to make their incorporation into commercial fuel cells feasible.

Since one of the main concerns in developing catalysts for fuel cell technology is the cost of the catalytic materials and the metals that are typically used as catalysts are expensive, more efficient catalysts in smaller quantities are desirable. For example, the USDOE has targeted a loading density of ≤ 0.15 mg Pt/cm^2 of surface area in order for fuel cells to be cost effective.[11] However, the current Pt catalyst loading density used in methanol fuel cell applications is on the order of 0.6 – 0.8 mg/cm^2. The lower loading densities needed for these applications can, in principle, be achieved by using high surface area catalysts. It is with this in mind that we looked to using nanoporous solids as catalytic materials.

We use the term "nanoporous solids" to describe inverse opal structures as it is an accurate descriptor of their structural properties. Inverse opals take their name from the colloidal crystal template used in their construction. Colloidal crystal silica nanoparticles are sometimes referred to as a synthetic opals due to their optical properties.[12] Using a colloidal crystal template allows for control over the average pore size within the material as changing the sphere size will naturally result in a corresponding change in the pore size of the nanoporous solid.[13] Advantages of using these materials include not only the comparatively low density of the resulting structure (*vide infra*), but also their comparitively robust physical structure. The synthesis of the nanoporous solids is depicted in Figure 1.1 and is discussed in detail in Chapter 2.

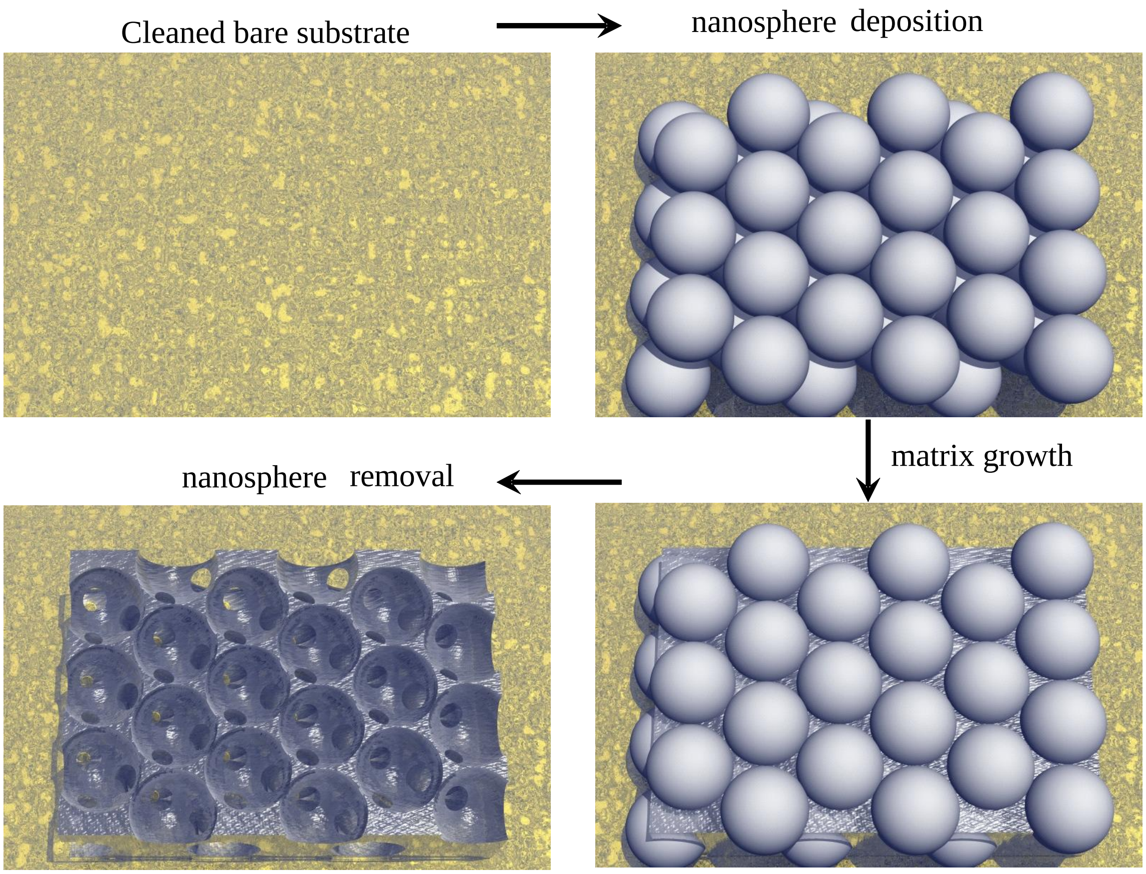

Figure 1.1: Depiction of the synthesis of the fabrication of a nanoporous solid, starting in the upper left with the bare substrate and continuing clockwise with the deposition of the colloidal crystal template, electrodeposition of the metal and the resulting nanoporous solid. <u>For interpretation of the reference to color in this and all other figures, the reader is referred to the electronic version of this dissertation.</u>

Nanoporous solids have been used in applications such as from photonic bandgap materials,[14-15] chemical separations,[16-18] and electrocatalysts.[19-20] We expect that nanoporous solids will be an efficient catalyst that can be incorporated relatively easily into fuel cell technology as a catalytic membrane (Figure 1.2). In this depiction the nanoporous solids would be at both the anode and the cathode, functioning as porous electrodes. Taking the direct methanol fuel cell as an example the reaction at the anode would be as follows:

$$CH_3 + H_2O \rightarrow CO_2 + 6H^+ + 6e^-$$

The H^+ will pass from the anode through a proton-permeable membrane to the cathode. At the cathode O_2 from the air will react with protons, producing water:

$$O_2 + 4H^+ + 4e^- \rightarrow 2H_2O$$

Combining the two half reactions leads to the overall net reaction:

$$2CH_3OH + 3O_2 \rightarrow 2CO_2 + 4H_2O$$

This simplified reaction sequence does not contain the detailed information that is known about the electrocatalytic oxidation of methanol on Pt.[4,21-22] There are multiple by-products that, specifically in the case of CO, will adsorb onto the catalytic surface and "poison" the metal. Furthermore, it has been demonstrated that methanol oxidation occurs differently depending on the crystal face of Pt on which it proceeds (*e.g.* Pt(111),

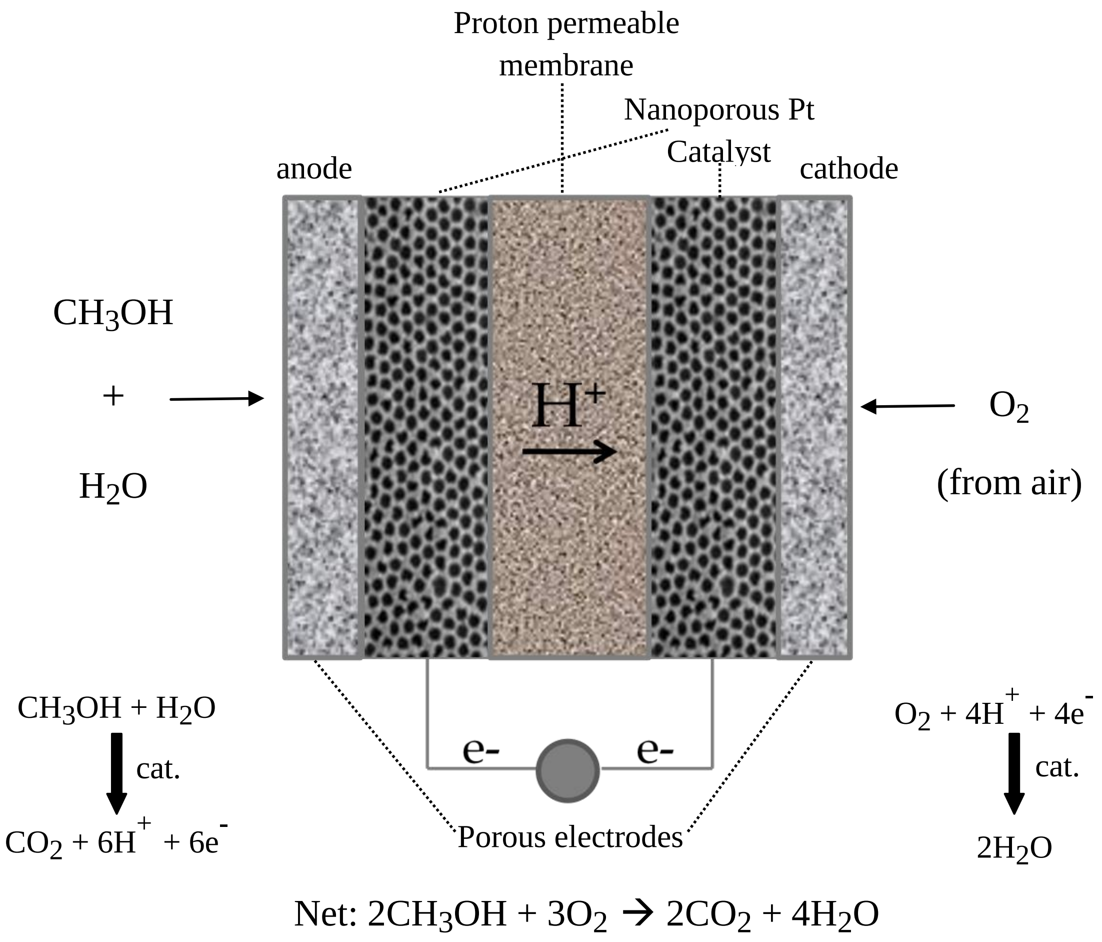

Figure 1.2: Schematic of a methanol fuel cell incorporating nanoporous solid catalysts.

Pt(100)).[23] The details of methanol electrocatalytic oxidation at nanporous solid Pt and Pd will be discussed further in Chapter 3.

Although the long-term goal of this project is to incorporate these nanoporous solids into fuel cells, before the these materials can be used to facilitate an alternative energy source, there needs to be careful studies of the efficiency of these materials as a catalyst as well as the development of a fundamental understanding of the enhanced electrocatalytic behavior reported in this dissertation. These goals are the focus of the work discussed in the forthcoming Chapters.

The methods used in the study of the electrocatalysis of the alcohols with the Pt and Pd nanoporous solids fabricated in the Blanchard lab were primarily cyclic voltammetry (CV) and chronoamperometry. Both of these electrochemical methods can provide useful information on catalytic activity and susceptibility to poisoning. Our experiments made use of a three-electrode cell that involved a working electrode (our nanoporous solid or planar solid electrode), a reference electrode (a Ag/AgCl (3M)) and a counter electrode (Pt wire). The potential was controlled using a CHI604A potentiostat, allowing for the potential to either remain constant or to be cycled, depending upon the application.

Cyclic voltammetry is a potential sweep method where the potential is changed as a function of time (Figure 1.3a) and what results is a current-potential curve (Figure 1.3b). The CV depicted in Figure 1.3 is that of a system that follows Nerstian behavior, meaning that it is a reversible system.[24] For these systems the peak current at 298K can be found using Equation 1.1.

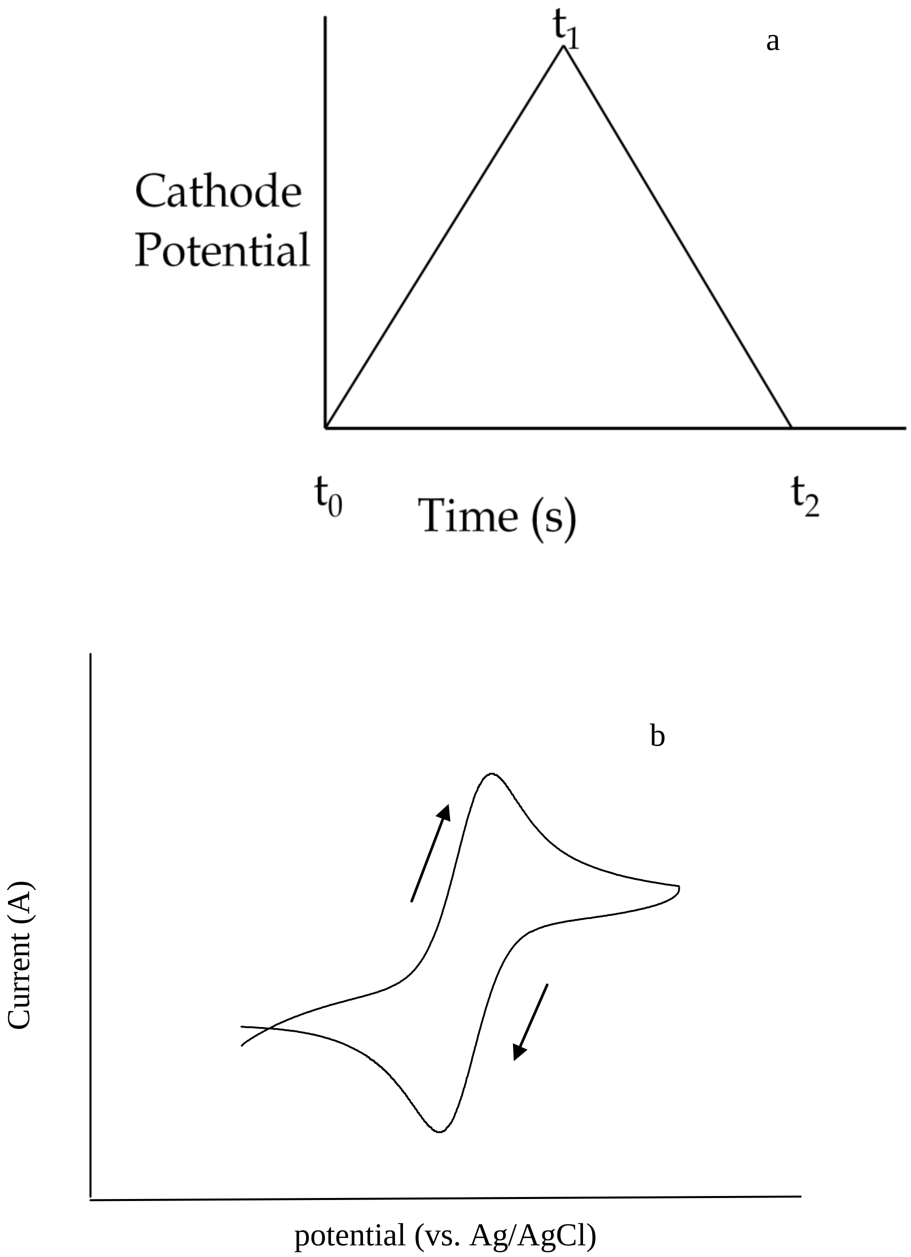

Figure 1.3: Depiction of the potential vs. time curve (a) and a typically CV resulting from a cyclic voltammetry scan (b).

$$i_p = (2.69\times 10^5) n^{3/2} A D^{1/2} C v^{1/2} \text{ (Eq. 1.1)}$$

It is the peak current that will determine the usefulness of the nanoporous solids as catalysts. The peak potential is another useful parameter in gauging the catalytic activity of the nanoporous solids. The peak potential for reversible systems is can be found using the relationship indicated in Equation 1.2.

$$E_p = E_{1/2} - 1.109\frac{RT}{nF} \text{ (Eq. 1.2)}$$

As mentioned earlier, the behavior of the electro-oxidation of even the simplest alcohol (methanol) is much more complicated than that of a simple reversible system. In fact, for electrocatalytic systems such as those we use here, instead of oxidation and reduction curves as seen in Figure 1.3, there are forward and reverse oxidations and an example CV is shown in Figure 1.4.

Chronoamperometry, another useful electrochemical technique, is a potential step method. In chronoamperometry, current is measured as a function of time after the potential is stepped from a potential in which faradaic processes do not occur to one which they do occur.[24] A typical waveform and response for chronoamperometry measurements is shown in Figure 1.5. These curves are useful for determining the extent of poisoning of the catalyst and in determining the relative number of active sites involved in the electrocatalysis.[8,22,25-26]

As most of the research on the use of alcohols focuses on the study of methanol and ethanol, it is with these two alcohols that our initial studies were completed.

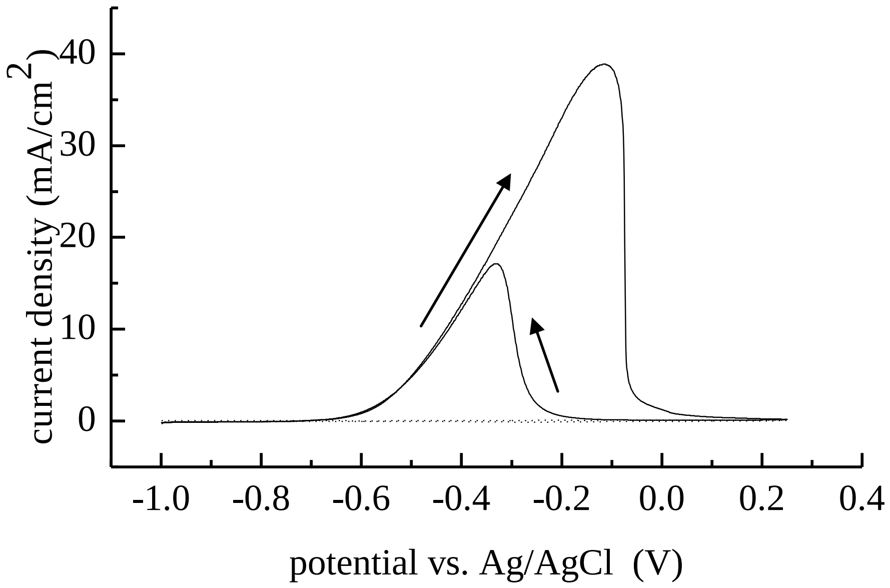

Figure 1.4: Typical oxidation curve observed for the electrocatalysis of methanol, with both a forward and reverse oxidation.

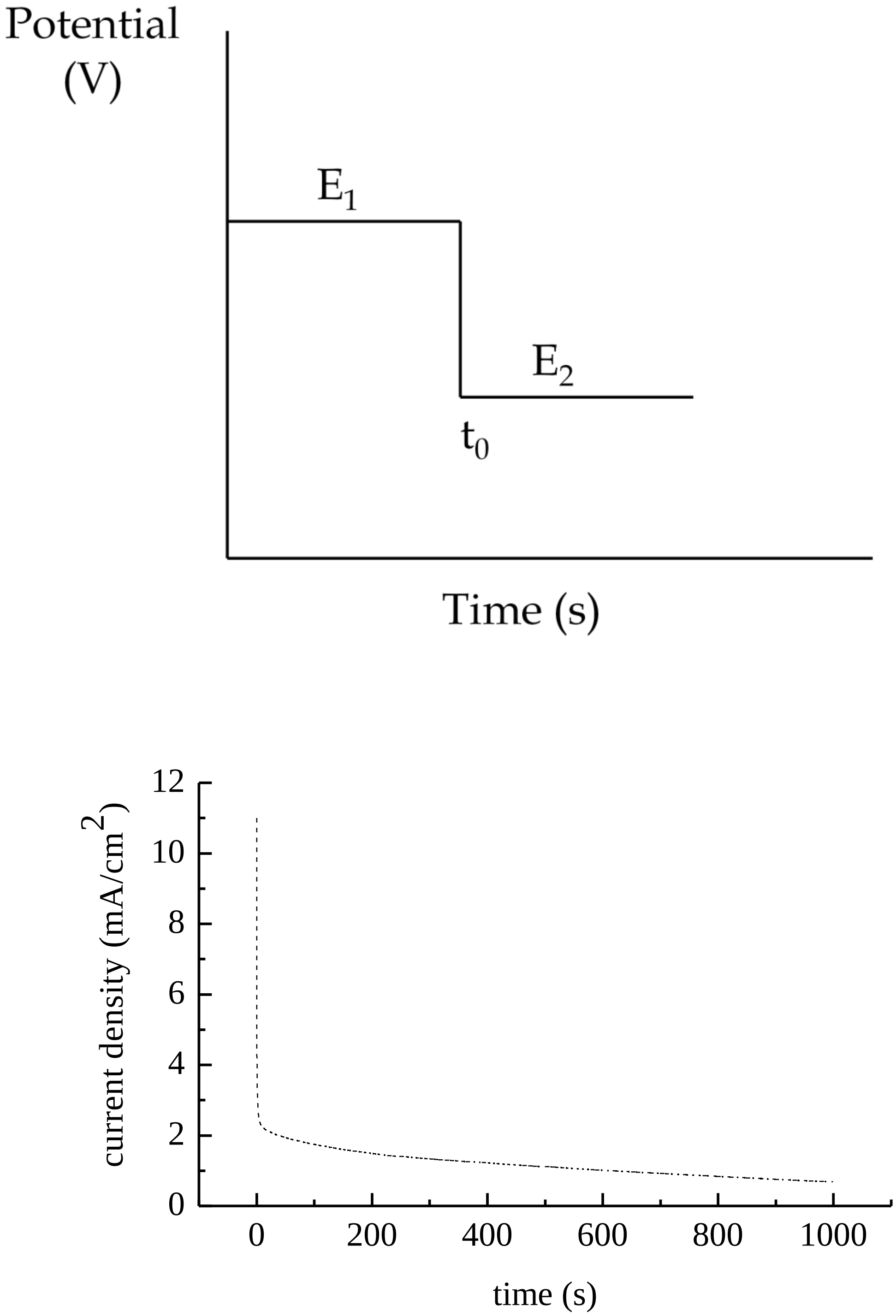

Figure 1.5: Chronoamperometry waveform and response curves.

However, electrocataltyic oxidation is not limited to the study of these simple alcohols. Longer chain alcohols and diols, although less studied than methanol and ethanol, can also potentially be used as fuels. The structure of diols can also potentially provide some insight into the factors relevant to the efficiency of electrocatalytic oxidation at different electrode surfaces.

The following Chapters will go into the details of our work, beginning in Chapter 2 with the development of the nanoporous solids in the Blanchard lab. Chapter 3 reports the role of Pt and Pd catalyst morphology on the electrocatalytic oxidation of methanol and ethanol, comparing the results under acidic and basic conditions. Chapter 4 builds upon the results explained in the previous chapter and explores the use of 1,2-propanediol as a probe to the geometric vs. morphology debate of the catalytic enhancement. The catalysis of diols are further explored in Chapters 5 and 6, which examine the electrocatalysis of 1,3-propanediol and the four isomers of butanediol from a mechanistic and a kinetic perspective, respectively. Chapter 7 concludes this dissertation and discusses the results the Chapters before it, as well as offers a perspective on the far-reaching goals of this project.

CHAPTER 2

DEVELOPMENT AND CHARACTERIZATION OF METALLIC NANOPOROUS SOLIDS

Introduction

The key first step in the work that follows is the construction of nanoporous solid materials. Because the creation of such structures was new to the Blanchard group, there is a substantial body of experimentation that went into gaining the expertise required to make nanoporous solids reproducibly and on a regular basis. It is the purpose of this Chapter to describe the details of constructing nanoporous solids, a family of materials sometimes known as inverse opals.[13-14,22] In this Chapter we focus on the experimental aspects of forming nanoporous solid materials, including the synthesis of silica nanospheres, the creation of layers and colloidal crystal assemblies of the nanospheres, the deposition of the metals around the nanosphere assemblies and the choice of substrates on which the nanoporous solids are grown. We start with the growth of silica nanospheres.

Silica Sphere Formation

Silica nanospheres enjoy wide use in a number of applications, and are available commercially in a range of sizes. As noted in Chapter 1, one of the virtues of the nanoporous solid structure is that the size of the pores between the void spaces in the structure is controlled by the size of the nanospheres used in creating the colloidal crystal scaffold.[13] Because of the importance of nanosphere size and uniformity to the formation of nanoporous solid structures, the Blanchard group undertook an effort to synthesize silica nanospheres in-house. Silica nanospheres were synthesized using a modified Stöber method.[12-13,27-28] In this method, alkoxysilanes are introduced to an ethanolic aqueous solution and the resulting hydrolysis produces silicic acid (1). Subsequent condensation of the silicic acid leads to the formation of spherical silica particles (2). This process requires the use of ammonium hydroxide, which acts as a catalyst.[28]

$$Si(OC_2H_5)_4 + 4H_2SO_4 \rightarrow Si(OH)_4 + 4C_2H_5OH \ (1)$$

$$Si(OH)_4 \rightarrow SiO_2 + 2H_2O \ (2)$$

Although a fairly facile synthesis, there is still some debate in the literature on the exact mechanism of the nanosphere formation by the Stöber synthesis.[28-36] There are two main models that are presented: one where, after the initial nucleation process, the particles proceed to grow through monomer addition,[30-31,35-36] and the other where there is continuous growth through aggregation.[29,35] Recently, van Blaaderen and Vrij proposed that the silica particles are initially formed by the controlled aggregation of nuclei, which is then followed by monomer addition growth.[36]

Hydrolysis is thought to be the rate limiting step for this synthesis, and it is through this step that the active monomer is produced.[30-31,35-36] Van Blaaderen and Vrij offer a convincing theory on the formation of these Stöber particles, in which their experimental findings support the notion that nucleation does not seem to continue throughout the entire growth process; if growth were to continue through aggregation of subparticles, the surface of the resulting spheres would not be as smooth as their TEM images indicate. Furthermore, although both the kinetic model presented by Matsoukas and Gulari and expressions from classical nucleation do explain parts of the synthesis, neither model can explain all of the features. The combined theory presented by van Blaaderen and Vrij offer a more complete possibility of understanding. For instance, if one considers the issue of particle morphology, the irregularity that is sometimes observed in particles would be due to the initial controlled aggregation where the monomer growth that would result in the smooth surface was unable to occur.

Despite the literature extant on the Stöber method, there were several experimental efforts required to refine the synthetic method to the point of producing monodisperse nanospheres. The first attempts at synthesizing the nanospheres were moderately successful. In these experiments, the solution into which tetraethylorthosilicate (TEOS) was added was comprised of either 35 mL or 70 mL of methanol, 11.5 mL Milli-Q water, and 4.8 mL of 25% v/v ammonium hydroxide. The TEOS (7.5 mL) was added to the solution and the solution was stirred at room temperature for 24 hours. The reaction product solution was centrifuged at 3000 rpm for 30 minutes at 25°C, producing a turbid solution, with the turbidity being more pronounced for the solution containing 70 mL of methanol. The resulting silica nanospheres were examined using a JEOL 100CX Transmission Electron Microscope (TEM), revealing a *ca*. 9 nm average diameter for the synthesis using 70 mL of methanol and *ca*. 21 nm average diameter for the synthesis using 35 mL of methanol. In addition to the relatively small size of the nanospheres, their shape was irregular and non-uniform (Figure 2.1). Neither of these experimental conditions is conducive to the formation of nanoporous solid structures.

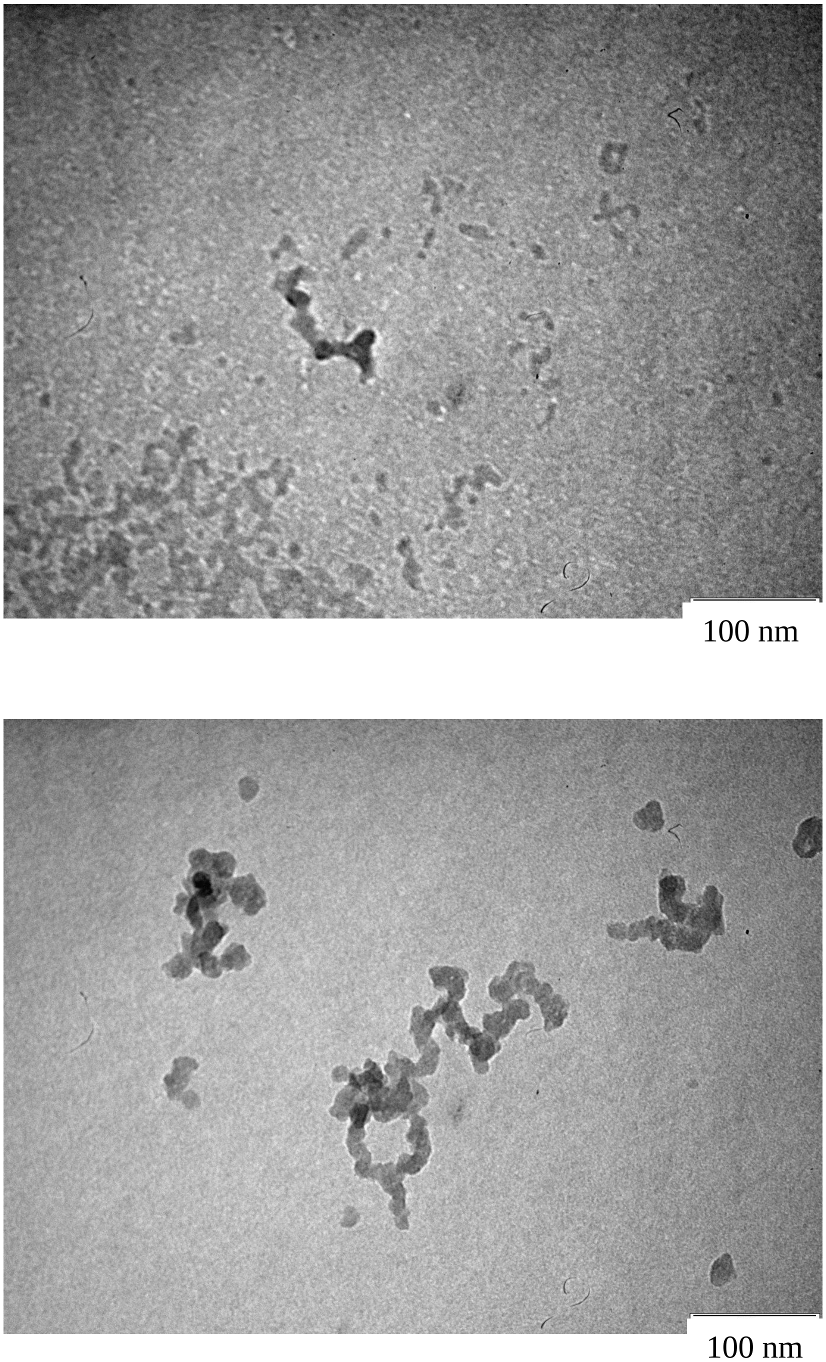

Figure 2.1: TEM images of silica spheres using methanol as the solvent. The silica spheres in the top image are approximately 9 nm in diameter, while those in the bottom are approximately 21 nm in diameter. The silica spheres in the bottom image were synthesized using half the volume of methanol as was used to synthesize those in the top image.

Since the synthesis using methanol did not result in sufficiently large, spherical or monodisperse silica spheres, modification of the synthesis was required. The two most widely utilized variables in this synthesis are the identity and concentration of the alcohol used, and it is known that these two factors influence the size of the resulting spheres.[28] We repeated the experiments described above, using ethanol (35 and 70 mL) instead of methanol. The solution was stirred overnight and a milky-white suspension was observed for both ethanol concentrations. Portions of these solutions were centrifuged at 3000 rpm for 30 minutes at 25°C and the supernatant was decanted. The silica spheres were put through three cycles of washing with Milli-Q water followed by centrifugation, and three cycles of washing with ethanol followed by centrifugation. TEM examination of the reaction product showed spherical, relatively monodisperse nanospheres, with average diameters of 175 nm for the synthesis using 70 mL ethanol and 400 nm for the synthesis using 35 mL of ethanol (Figure 2.2).

The spheres from this synthesis contained a modest distribution of sizes, so modifications to the Stöber method were examined.[12,27] It was found that the size distribution of the silica spheres could be narrowed if the reactants were not added at the start of the reaction. We modified the synthetic procedure by adding the ethanolic TEOS solution drop-wise to a reaction vessel containing an aqueous solution of ethanol and ammonium hydroxide. This reaction was stirred while the TEOS solution was added and following completion of this step, the reaction was stirred for *ca.* 12 hours. As before, the solution was centrifuged and the separated nanospheres washed. The initial experiments resulted in a distribution of silica sphere sizes, ranging from 320 nm to 533 nm (Figure 2.3). It was found that the rate of addition of the TEOS solution was not

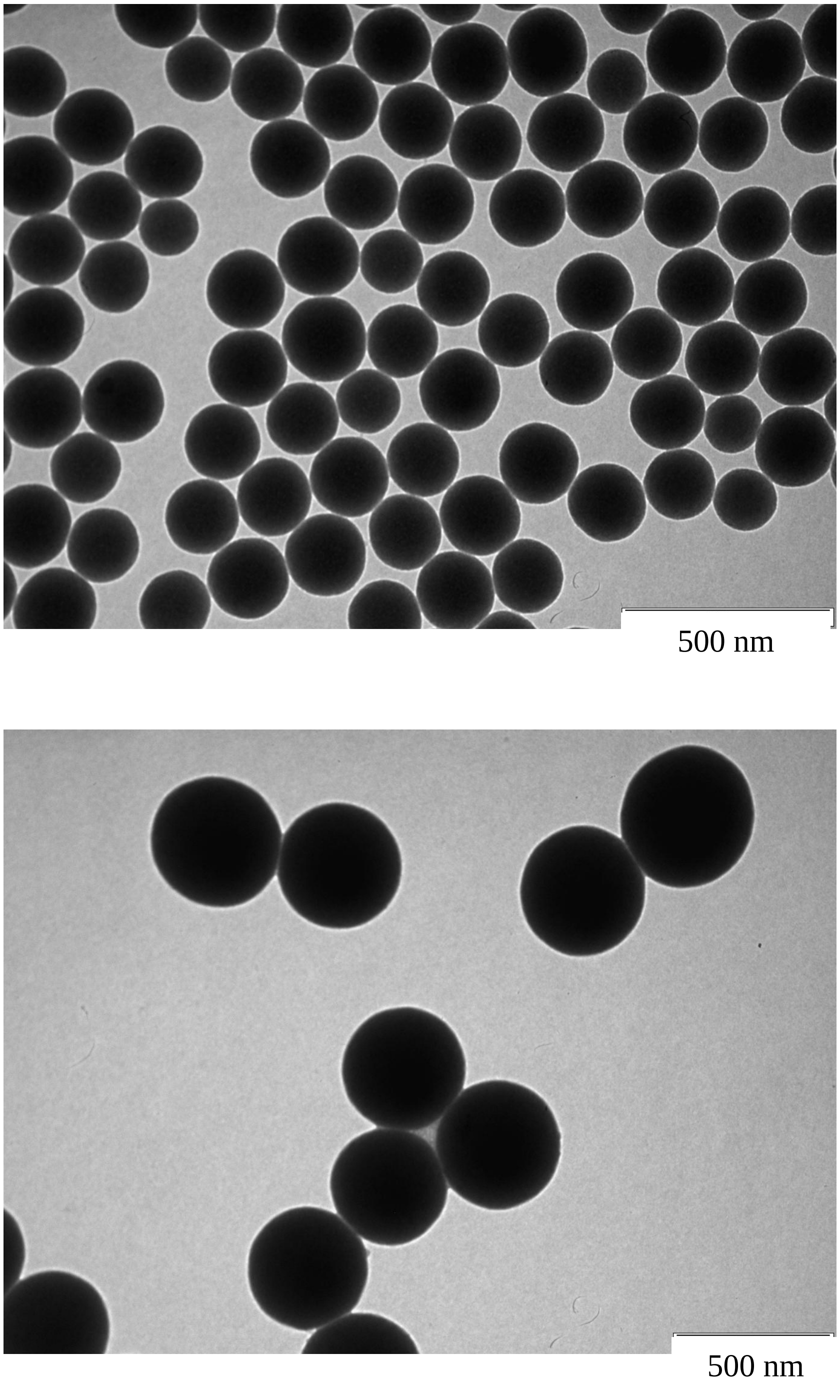

Figure 2.2: TEM images of silica spheres using ethanol as the solvent. The silica spheres in the top image are approximately 175 nm in diameter, while those in the bottom image are approximately 400 nm in diameter. The silica spheres in the bottom image were synthesized with half the volume of ethanol as was used in the synthesis of the silica spheres in the top image.

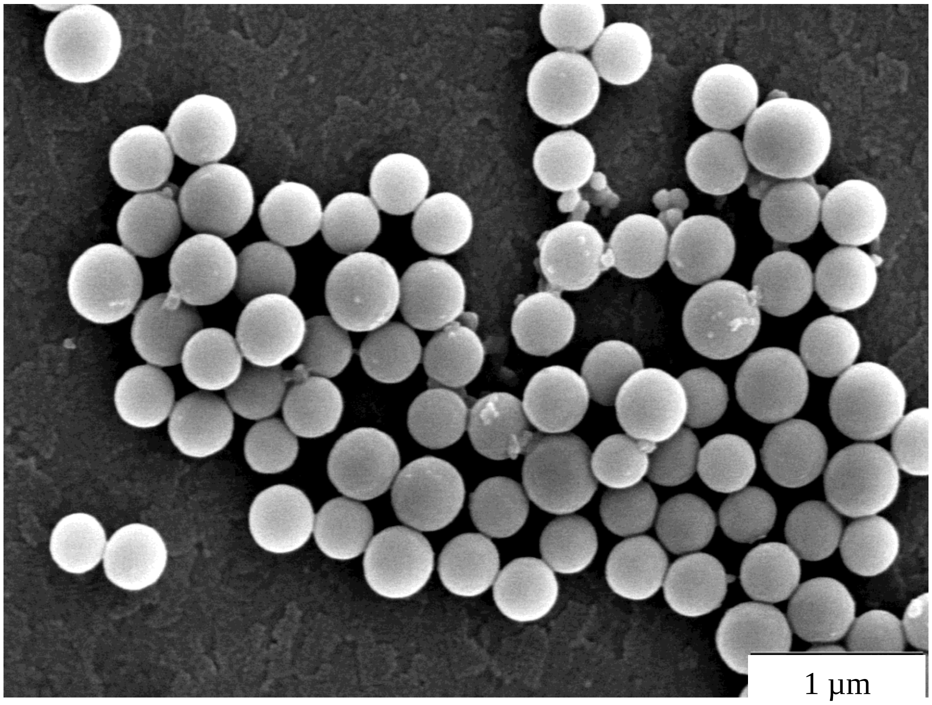

Figure 2.3: SEM images of silica spheres ranging in size from 320 nm to 533 nm. The silica spheres were synthesized using a drop-wise addition of ethanol

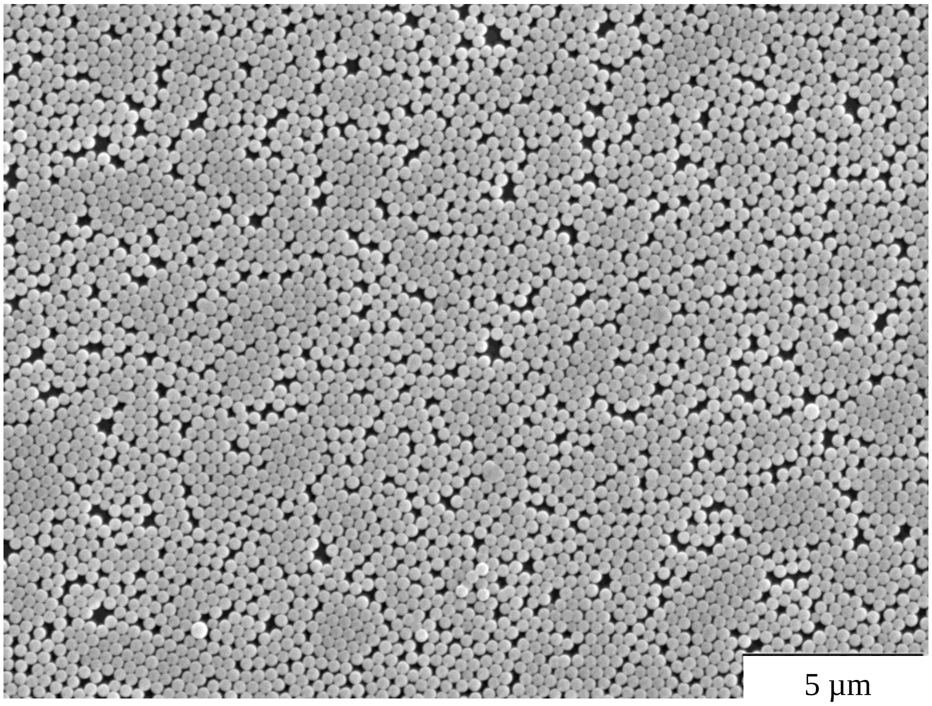

Figure 2.4: SEM image of silica spheres of approximately 300 nm in size, resulting from the slow addition of a TEOS ethanol solution to and ethanol/ammonium hydroxide solution.

uniform, and subsequent experiments were performed where the rate of TEOS addition was made more consistent by making sure the addition tube did not clog, resulting in a more uniform distribution of sphere size, *ca*. 300 nm for the conditions used here (Figure 2.4). Subsequent experiments demonstrated that the size of the nanospheres can be controlled through the amount of ethanol and ammonium hydroxide in the reaction vessel (Table 1.1). This synthetic strategy has proven to be useful in producing silica nanospheres of controllable size and with a relatively narrow size distribution. The next task in the creation of nanoporous solid structures is to assemble the spheres into well-organized, multi-layered structures. We discuss first the substrates for these assemblies.

Solid Support

Assemblies of silica nanospheres cannot be free-standing, but must reside on a (planar) support for the work we report here. The properties of the support, such as conductivity and porosity, will play an important role in determining the organization and utility of the resulting nanosphere assembly. In this work, the nanoporous solids that are of ultimate interest will be made of metals such as Pt and Pd, it is important for the substrate to be conductive and capable of undergoing electro-deposition. Initially, silica nanospheres were deposited onto indium tin oxide (ITO) coated glass slides. This substrate material was chosen because it is electrochemically active and transparent across much of the spectrum, thus allowing for optical spectroscopic measurements to be made. In addition, because ITO exists as a thin layer on the glass substrate, it may be possible to chemically remove it subsequent to the formation of the nanoporous solid, leaving a free-standing nanoporous structure. Ultimately, however, it was not possible to create a free-standing nanoporous solid film, primarily for reasons of spatially irregular

Table 2.1: Relationship between solution composition and silica sphere size.

Ethanol (mL)	25% Ammonium Hydroxide (mL)	Average Size of Silica Spheres (nm)
35	4.8	400.0
70	4.8	175.0
100	22	333.52
50	22	599.71
150	22	421.64
100	11	< 100

adhesion of the nanoporous solid to the ITO. Once it was determined that ITO was not a suitable substrate for the formation of Pt and Pd nanoporous solid structures, another solid support had to be identified. Previous work has used gold as a substrate successfully,[13] and it is for this reason that we chose to use gold also. On gold substrates, nanoporous solids were formed and exhibited sufficiently regular and robust adhesion that it was possible to use these materials for experiments described in the later chapters. We consider the details of Pt and Pd deposition on gold substrates below.

Flow-Through Supports

The ITO and gold substrates are solids and thus do not allow for flow through them normal to the surface plane. For a nanoporous solid to function as a flow-through catalyst, it must be constructed on a porous substrate. For a porous substrate to support a nanoporous solid, it must first be possible to create an organized nanosphere assembly on the surface, requiring one of two conditions to obtain; either there needs to be regular openings in the substrate that would allow for the packing of the nanospheres within them, or the characteristic pore size of the porous substrate must be smaller than the diameter of the nanospheres used in creating the template assembly. Our initial attempt used TEM grids as support structures where the nanospheres could, in principle, organize within the open grid spaces. This structural motif had a number of attractive features, including structural robustness and facile connectivity for electrochemical processes. Unfortunately, however, it was not possible to reliably fill the void spaces in the grids with nanospheres. The silica nanospheres would partially fill the grid holes and electrodeposition of the metal was incomplete (Figure 2.5).

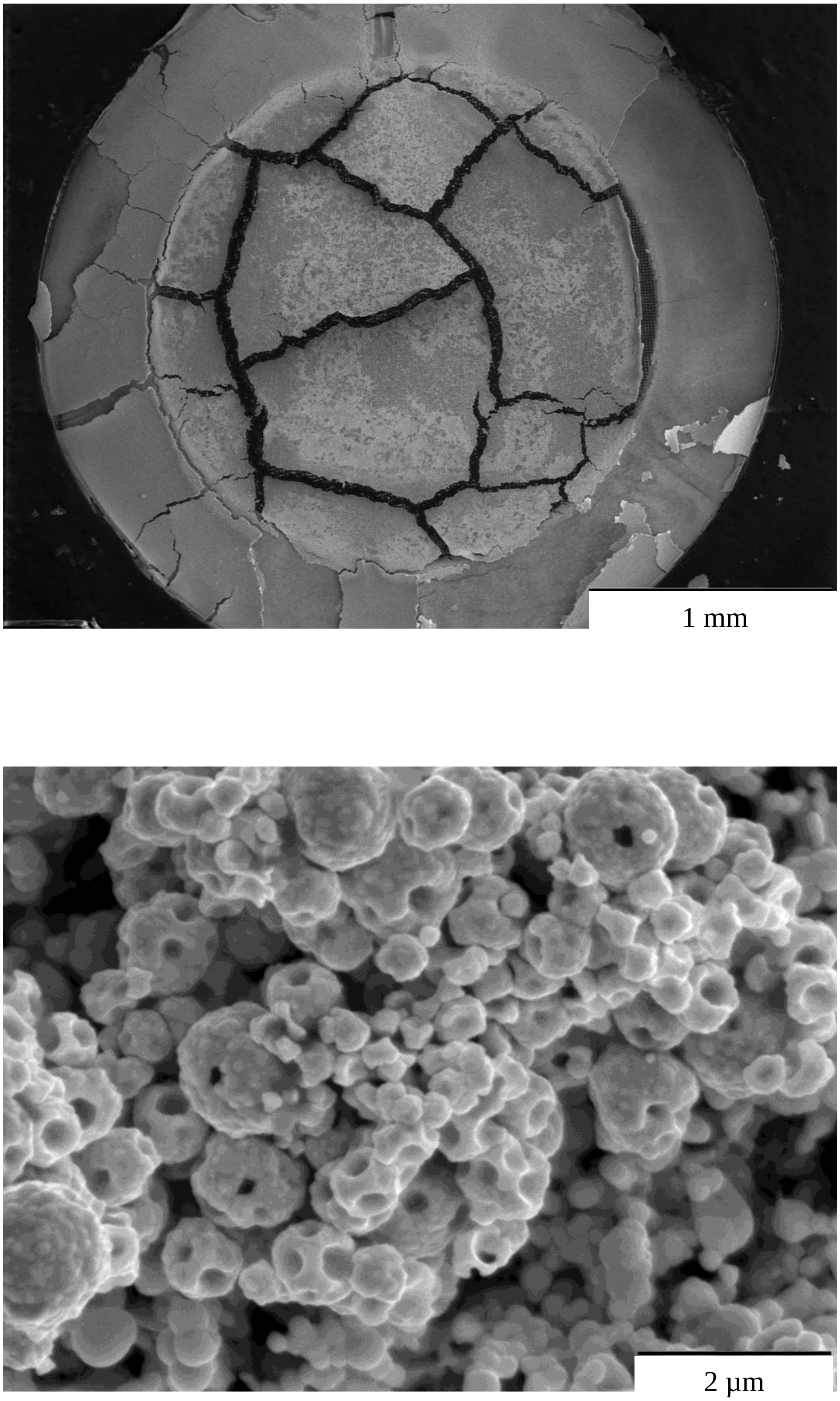

Figure 2.5: TEM grid with silica spheres deposited within the grid spaces and platinum metal deposited around the spheres. The silica was then removed using HF.

Subsequent efforts to utilize track-etched alumina as porous supports has met with success for the deposition of silica nanoporous solids,[37] but such filters are not of use for the work discussed in this dissertation because of the inability of the alumina membranes to provide electrical continuity with a deposited metal nanoporous solid. The work we present here thus focuses on gold as the support.

Deposition of Silica Template

Silica nanosphere assemblies function as the template for the construction of nanoporous solids. It is thus imperative that the silica nanosphere assembly is well organized and regular across macroscopic distances on the supporting substrate. Accomplishing this assembly task can, of course, be a challenge, and we have utilized several methods of nanosphere deposition. Ideally, the nanospheres should exhibit a hexagonally closed-packed structure, allowing the nanoporous solid to have a regular array of interconnected pores. Regardless of the method used to deposit these nanosphere assemblies, defects will be present, giving rise to corresponding defects in the nanoporous solid structure. The primary issue in selecting a method for nanosphere deposition is the minimization of the defects in the resulting structure, and the discussion below details the experiments that lead to selection of nano-dipping as the deposition method of choice.

The first technique used to deposit silica nanospheres was Langmuir-Blodgett (LB) deposition.[12-13,27] The rationale for the use of this method was that the use of a fluid underlayer and control over surface pressure that a LB trough afforded would allow for the facile organization of the nanospheres into a hexagonal close-packed array. In order to facilitate the deposition of nanospheres using a LB trough, it is necessary to have nanospheres that will float on the surface of the water sub-phase. Silica nanospheres will not, by themselves, float on the surface of an aqueous phase, and it was necessary to modify the surfaces of the nanospheres to make them hydrophobic. The silica nanosphere surfaces were reacted with allyltrimethoxysilane (Scheme 2.1). Allylsilane derivatization afforded the correct amount of surface polarity reduction. Previous work had shown that if the surface of the silica nanospheres is too hydrophilic, aggregation occurs in solution, and if the nanosphere surface is too hydrophobic, the silica nanoparticles aggregate at the air-water interface.[27] Neither possibility leads to a well organized interfacial assembly. Modification of the silica surface was performed by adding *ca*. 0.6 mL of allytrimethoxysilane to *ca*. 30 mL of a solution containing silica nanospheres at a concentration of *ca.* 20 mg/mL in a round-bottom flask containing a stir bar. The solution was stirred for 4 hours, and the flask heated to 90°C with stirring using a hot oil bath for two hours.[27] The reaction system was cooled to room temperature and was then centrifuged for 30 min. at 3000 rpm. The supernatant was decanted and the surface-modified silica nanospheres were washed several times with water and ethanol to remove any remaining reactants, with centrifugation between washings.

A LB trough (NIMA 312D) was used for deposition. It is constructed of a trough and two movable arms, which sweep over the surface of a liquid sub-phase, compressing a layer of molecules or nanospheres floating on top of the sub-phase into a well-packed monolayer. As this layer is compressed, a Wilhelmy plate balance is used to measure changes in the surface tension. This change in pressure, resulting from compression of the surface layer, can be displayed as a pressure-area isotherm and is characteristic of the molecules or nanospheres comprising the film. Dipping a solid substrate into the

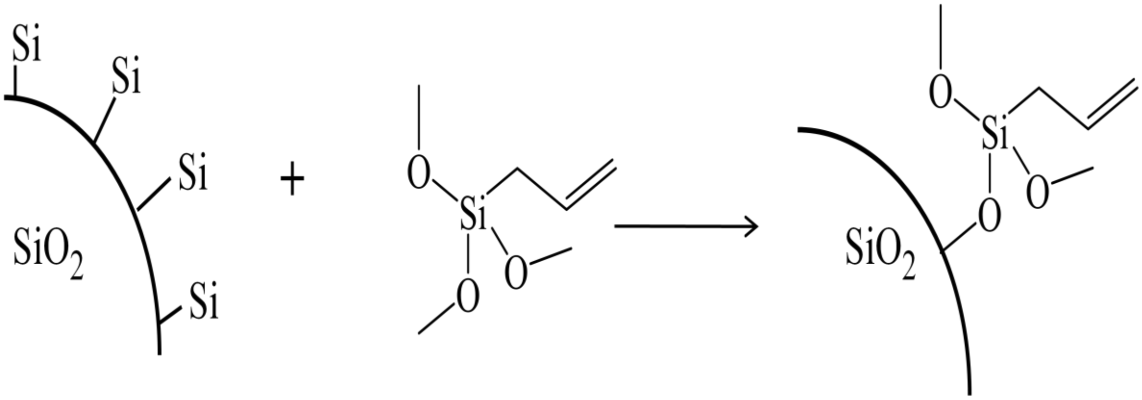

Scheme 2.1: Modification of silica sphere surface with allyltrimethoxysilane. The silica spheres were modified in order to reach the surface polarity needed to float on the water sub-phase of the Langmuir-Blodgett trough.

compressed monolayer (Langmuir film), allows monolayer deposition onto the substrate. For this phenomenon to function correctly, the nanospheres have to possess the appropriate balance between hydrophobic and hydrophilic forces, to allow for the formation of a uniform surface layer. Sequential deposition strokes of the substrate through the surface-layer leads, in principle, to the formation of a multilayer silica template.

To create the surface nanosphere layer, modified silica nanospheres were suspended in ethanol and transferred to a 20-mL scintillation vial, where the ethanol was allowed to evaporate. The nanospheres were then re-suspended in an 80:20 (v/v) ethanol : chloroform solution to make a 20.0 mg/mL solution and sonicated for *ca.* 20 minutes. A 0.5 mL aliquot of this suspension was spread on the LB trough water sub-phase. The surface-layer of nanospheres was compressed, producing an isotherm (Figure 2.6). These data show that the collapse pressure for the film is *ca*. 37 mN/m. However, because the collapse pressure is seen at a point when the film irretrievably loses its mono-molecular form[38], layer transfer is not performed at this pressure. Layer transfer was performed at a pressure of 30 mN/m, and at this pressure the resulting deposited layer can be seen as an iridescent film on the substrate surface.

It is useful to consider the details of nanosphere deposition onto the substrate. Prior to spreading the silica nanosphere monolayer onto the water subphase, the solid support onto which the nanospheres are to be deposited was immersed (vertically) into the subphase. Deposition onto the substrate thus occurs on the upward stroke rather than the more typically used downward path. This deposition method is used typically for monolayer deposition onto a hydrophilic surface, where initial down-stroke deposition is

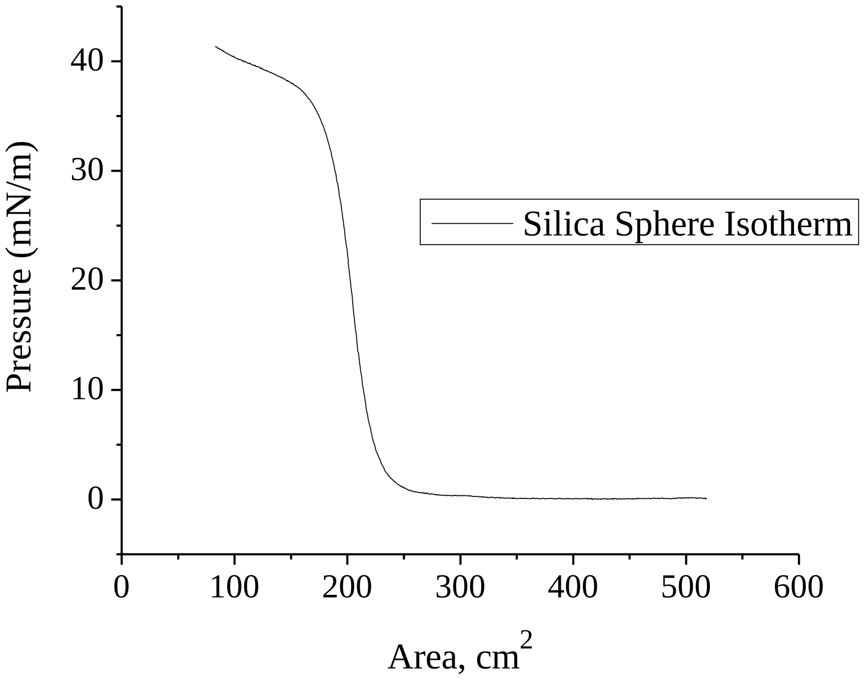

Figure 2.6: Typical pressure isotherm produced using the Langmuir-Blodgett method to deposit silica spheres onto a solid support. This indicated collapse pressure for the film produced by the silica spheres on the water sub-phase is approximately 37 mN/m.

used when the substrate is hydrophobic. For the deposition of our nanospheres, where we have controlled the hydrophilic character of their surfaces by modification, either upstroke or downstroke deposition could be used, in principle. We have found experimentally that deposition of the initial adlayer on the upstroke produces higher quality nanosphere assemblies. For these experiments, surface compression was completed with the substrate immersed, and the upstroke deposition proceeding at a withdrawal rate of 1.0 mm/min. Once completely removed from the subphase, excess water was allowed to evaporate before the substrate was re-immersed into the water subphase at a rate of 44 mm/min, as the faster rate will prevent the spheres from depositing on the downstroke.[27] This process was repeated to deposit consecutive layers. The resulting multilayer silica nanosphere templates consisted of areas of hexagonally close packed spheres, but large cracks and gaps could also be seen (Figure 2.7). This result is characteristic of this deposition method, exhibiting little or no dependence on the variables amenable to experimental control such as substrate withdrawal rate, surface pressure, and spreading solution concentration. While this deposition method may be acceptable for certain nanoporous solid requirements because the cracks and void spaces in the nanosphere arrays would be filled in by metal upon deposition, the existence of such features will limit the porosity of the resulting assembly. For this reason, we have sought other means of creating nanosphere assemblies.

One method that has been used in the past for the deposition of colloidal crystal assemblies is evaporative deposition. In this method, a substrate is suspended in an ethanolic solution of silica nanospheres and the solvent is allowed to evaporate slowly.[39-42] As the alcohol evaporates, the silica nanospheres self-assemble and adhere to the solid

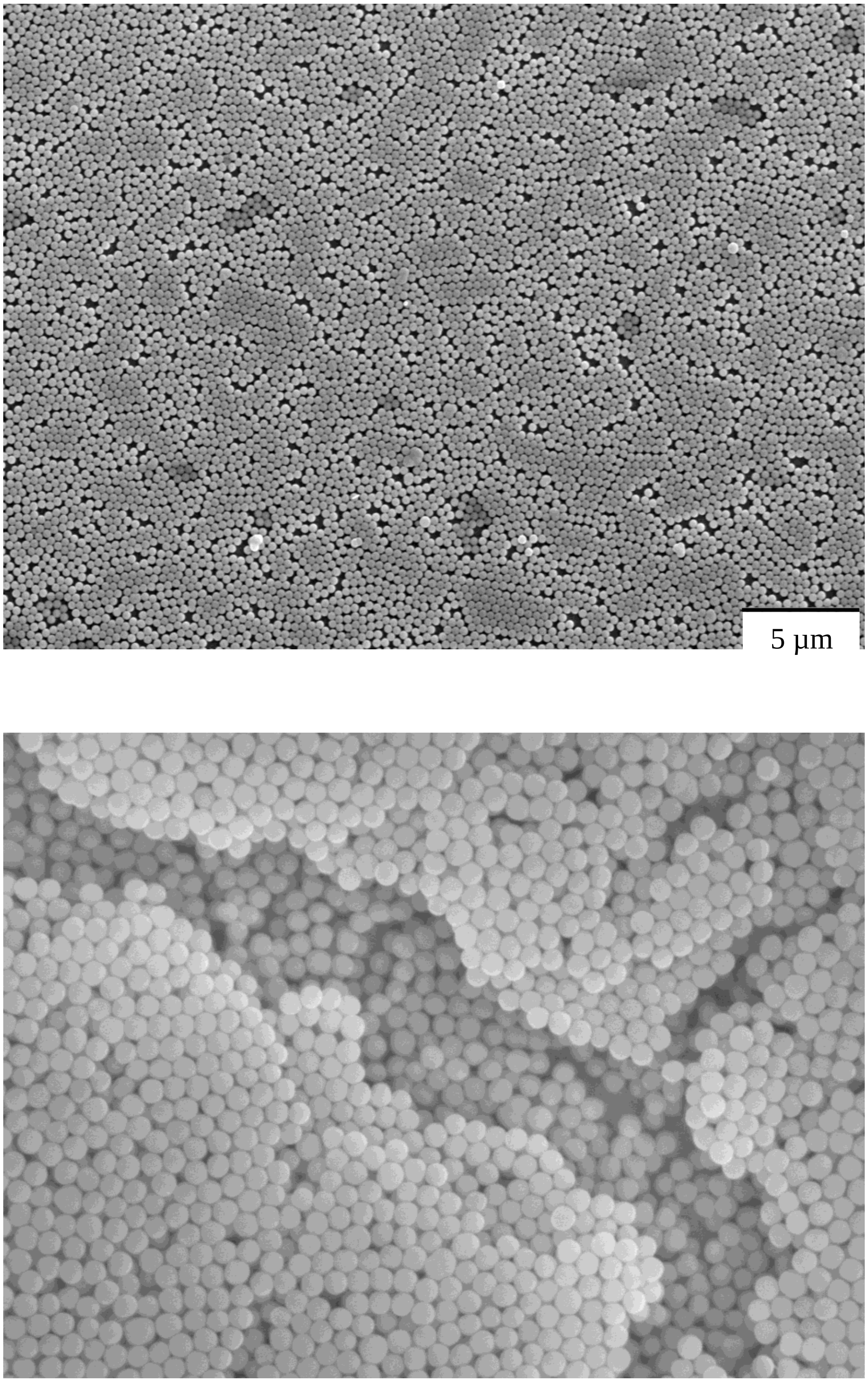

Figure 2.7: SEM images of the silica nanosphere template made using the Langmuir-Blodgett method. Although there are areas of hexagonally closed-packed spheres, there are also areas of large cracks and gaps.

support. This method lead to results that were marginally better than those obtained by LB deposition, but the time required to achieve a colloidal crystal assembly by this method was substantially longer, and there was little or no control over the number of layers that were deposited onto the substrate (Figure 2.8). The nanosphere assemblies were irreproducible in terms of macroscopic organization, with the product structure and organization depending sensitively on experimental conditions. It was clear from the LB and evaporative deposition experiments that neither method was ideal. Rather, what was needed was some method that combined the advantages of both methods while minimizing the disadvantages.

The combination of substrate dipping/withdrawal and solvent evaporation can be realized experimentally by removing the substrate slowly from a suspension of silica nanospheres.[40] This procedure requires the use of a SDI Nanodip Coater, which allows for control of the deposition area, the deposition rate, and also features a time control option. The user is able to program the nanodipper for multiple consecutive dips and each dip can be completed at the same deposition rate or at different deposition rates, depending upon the application. The number of layers that are deposited on the surface of the solid substrate is controlled by the deposition rate and the total concentration of the ethanolic silica nanosphere suspension. To optimize the silica nanosphere deposition for our applications, deposition rates were compared (Table 1.2). Useful nanosphere assemblies could be formed with 300 nm diameter silica nanospheres, where the deposition was performed at a substrate withdrawal rate of 0.15 μm/s from a 9.2 mg/mL nanosphere suspension. For these experimental conditions, two adlayers of nanospheres were deposited per withdrawal stroke, and three strokes were used. The resulting six-

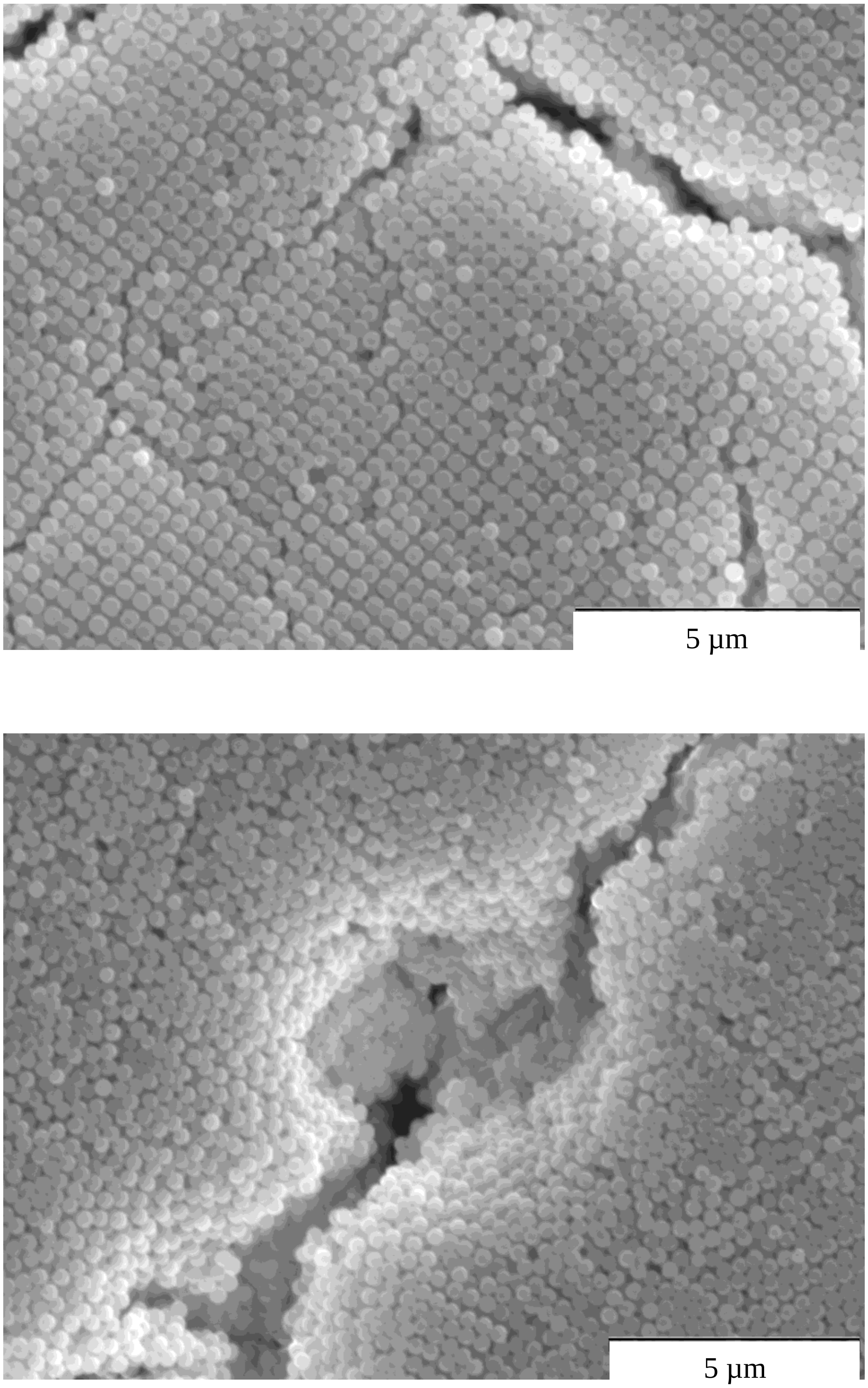

Figure 2.8: SEM image of the silica sphere template formed on a substrate using a slow evaporation method deposition.

Table 2.2: Effect of Deposition Rate on Silica Nanosphere Deposition

Silica Sphere Size (nm)	Concentration of Silica Spheres (mg/mL)	Rate of Deposition (µm/s)	Number of Adlayers
300	9.2	1.25	1
300	9.2	1.30	1
300	9.2	0.15	2
300	15.0	0.48	3
450	15.0	0.34	4

layer nanosphere assemblies were useful as templates for the formation of nanoporous solids. For the 450 nm diameter nanospheres, the optimum deposition rate was found to be 0.34 µm/s from a 15.0 mg/mL nanosphere suspension, resulting in 4 adlayers. Under these experimental conditions, a single deposition was required. The characteristic nanosphere packing achieved by this dip-coating method is shown in Figure 2.9. Once formed, the silica nanosphere templates were characterized using a JEOL 6400 scanning electron microscope. The substrates were first mounted onto a stub with epoxy and then coated with a thin layer of Os. The coating of the substrates was necessary to make the sample conductive, and Os coating was found to produce higher quality images than Au coating. For all measurements, the accelerating voltage was 12 kV, and both the condenser lens (which controls the spot size) and the working distance (objective focal length) were 14 mm. These parameters led to high quality pictures using this microscope, although changes in working distance (*e.g.* to 8 mm) was found to be helpful for some measurements, depending on the size of the nanospheres used.

It was found that simple deposition of the nanosphere assemblies was not sufficient to ensure high quality nanoporous solids. Electrodeposition of Pt or Pd on nanosphere assemblies (*vide infra*) gave rise to highly disrupted materials (Figure 2.10). Images such as these suggested that the silica nanosphere template may not possess the requisite structural integrity. To address this issue, the silica nanosphere template was heated to 200°C for two hours prior to metal deposition. This heating procedure appeared to "sinter" the silica nanospheres, producing a more robust template that was capable of withstanding the electrodeposition process.

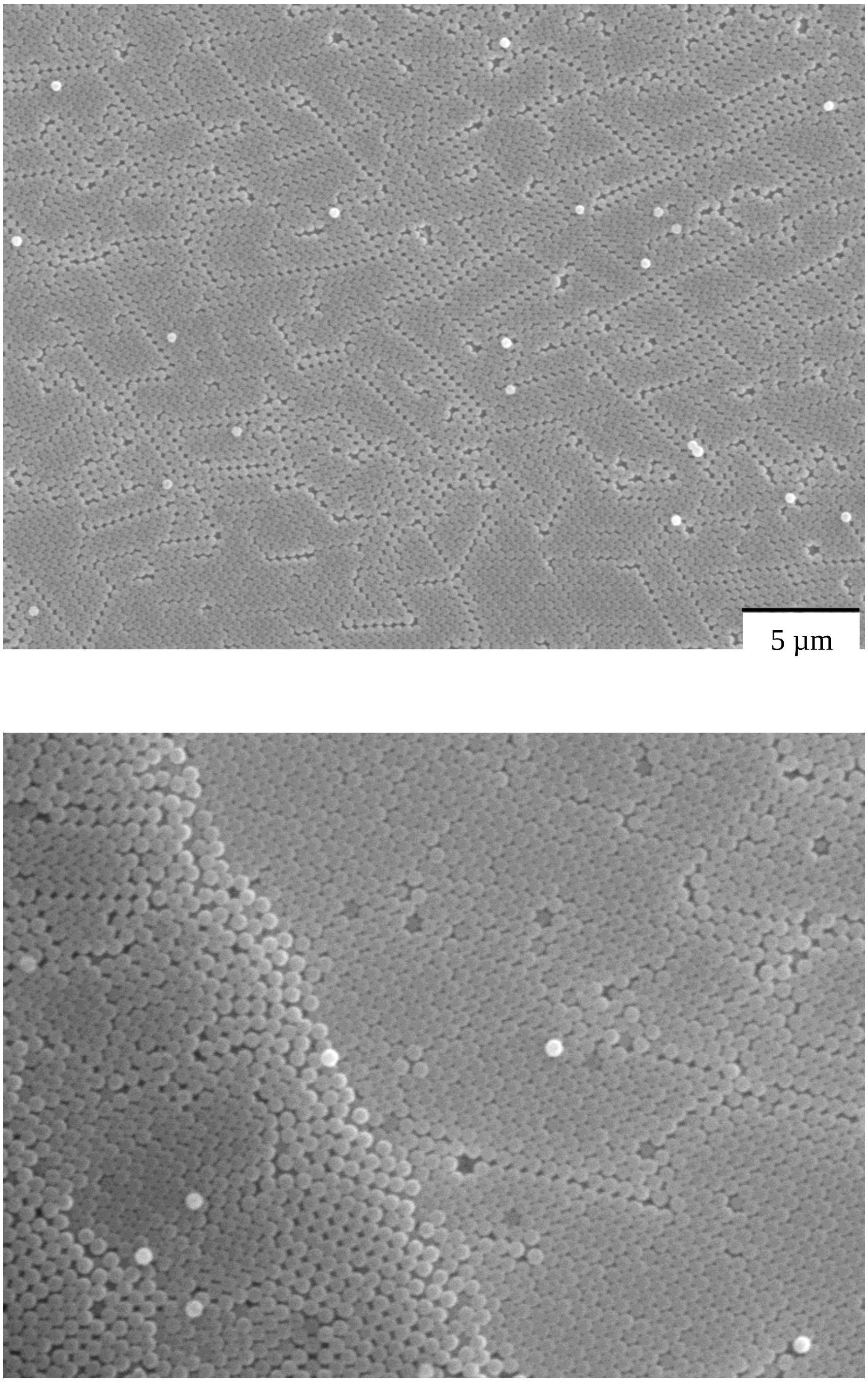

Figure 2.9: SEM images of silica sphere template formed using the SDI Nanodip Coater, which allows for greater control of parameters including the area and rate of deposition.

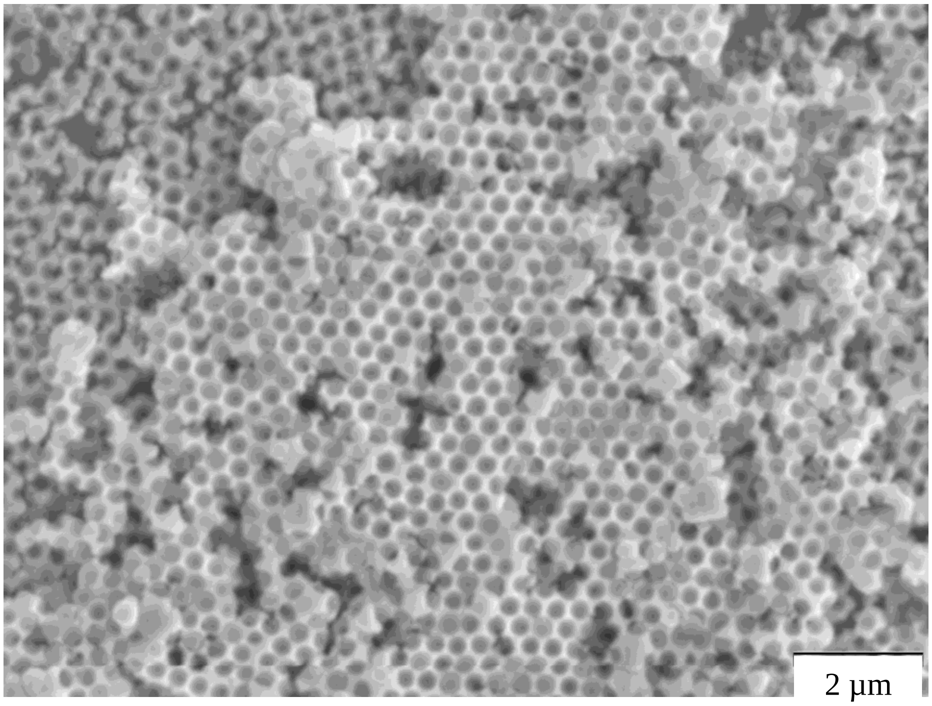

Figure 2.10: SEM images of platinum deposition that indicate that there may have been non-planar deposition of the metal due to the silica spheres not adhering to the surface once the electrodeposition potential was applied.

Electrodeposition of Metal Nanoporous Solid Structure

The initial electrodeposition experiments were an attempt to deposit Au into/onto the silica template. There is literature precedent for the formation of Au inverse opal structures, with the Kuhn laboratory reporting the formation of high quality Au structures around silica nanosphere templates.[13] Initial attempts to produce the analogous Au nanoporous solid structure in the Blanchard lab were unsuccessful (Figure 2.11). In these experiments, the deposition of the gold was performed using chronoamperometry at a potential of 0.5 V vs. Ag/AgCl 3M KCl for 480 seconds with a 0.01 M solution of $HAuCl_4 \cdot 3H_2O$. In the first experiments, the working electrode was ITO, the reference electrode was Ag/AgCl (3 M KCl), and the counter electrode was a platinum wire. The deposition area was controlled with a mask. SEM images of these attempts at deposition indicated that Au was depositing around the spheres, but not in a uniform manner. While there may be a variety of possible explanations for this finding, surface contamination and/or the structural integrity of the nanosphere template may have played a role.

In subsequent experiments, Au was deposited on nanosphere templates formed on a gold substrate. The resulting Au growth produced uneven coverage of the nanosphere structure and structures that appeared to be crystalline gold (Figure 2.12). This result obtained despite variation of the applied potential and deposition time. Greater success with the electrodeposition of gold was achieved when the surface of the gold substrate was modified with cysteamine, producing a hydrophilic surface.[13] To accomplish this surface modification, 5.0 mL of a 35 mM cysteamine solution was placed in a 20 mL scintillation vial that contained the gold-coated substrate. The gold substrate was reacted

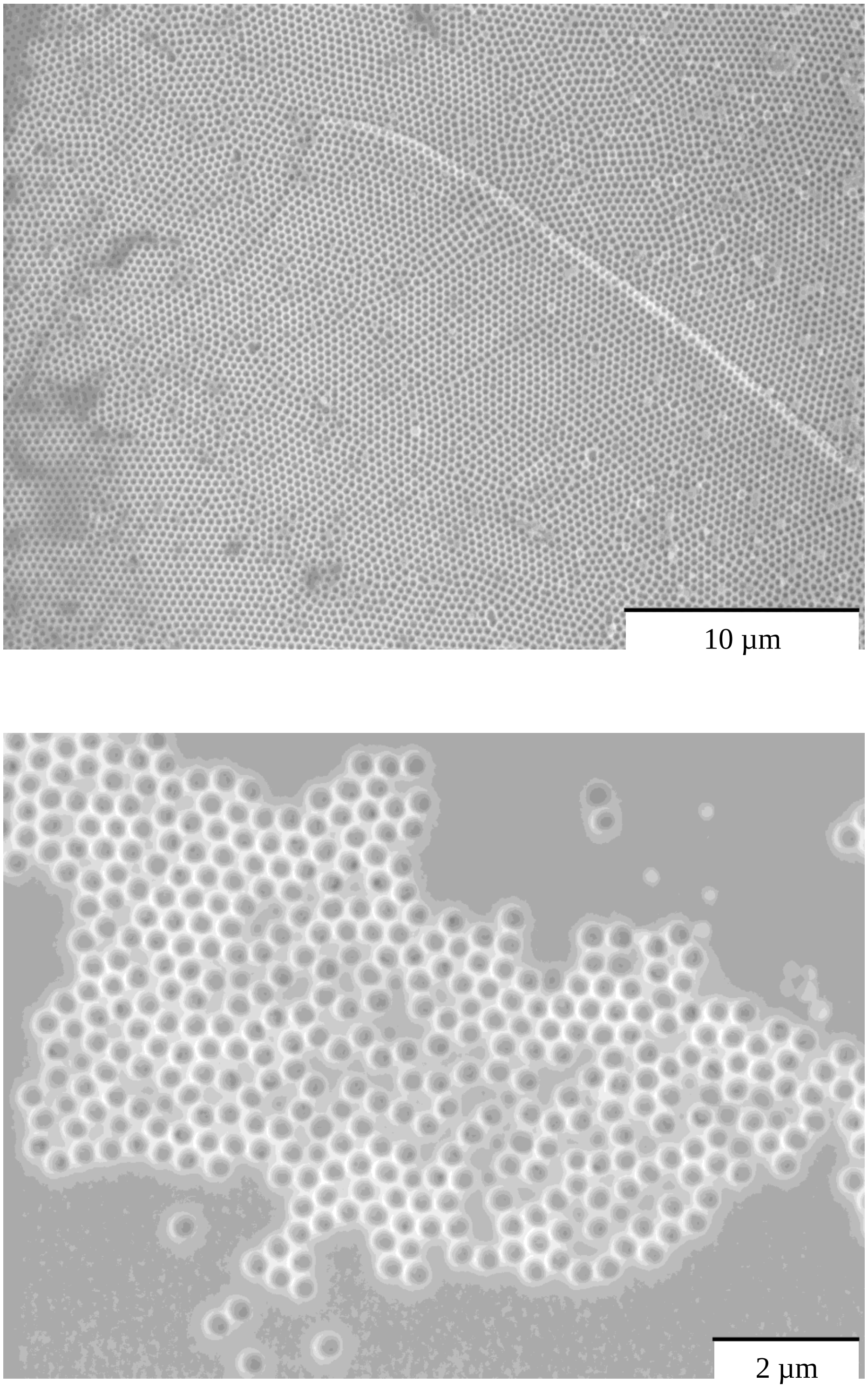

Figure 2.11: Initial gold deposition experiments did not produce the desired honeycomb that is typical of the nanoporous solids as evidenced by the SEM images above.

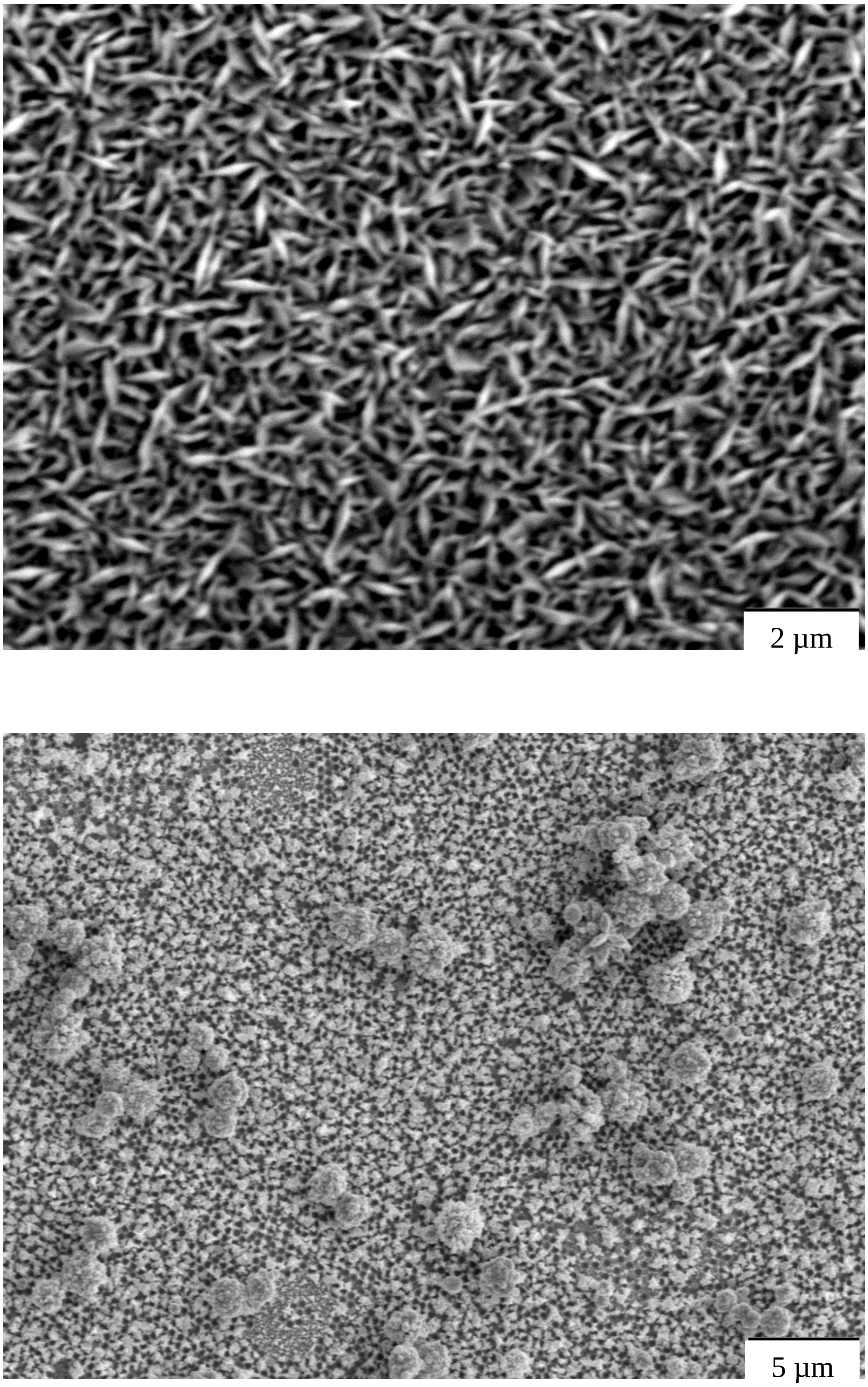

Figure 2.12: SEM images of the deposited gold indicating the presence of crystalline metal instead of the desired honeycomb that is expected when gold is deposited around the silica sphere template. The silica spheres were removed prior to imaging.

for 12 hours, then removed from the solution, washed with ethanol and water, and dried with a stream of N_2 gas. The modified gold substrate was then used as the substrate for dip-coat formation of a nanosphere assembly. After heating the nanosphere assembly to 200°C, the resulting template was coated with Au using chronoamperometry at 0.5 V (*vs.* Ag/AgCl 3M KCl) for two 600 s cycles with a 49.9 mM solution of 99.999% $HAuCl_4 \cdot H_2O$. The result is shown in Figure 2.13. In this figure, the nanoporous solid is shown. Subsequent to the electrodeposition of Au, the silica nanosphere template was removed using a 10% (v/v) solution of hydrofluoric acid (HF). The electro-deposited substrates were immersed in the HF solution typically for *ca*. 15 minutes to effect dissolution of the nanospheres. This same procedure was used throughout, for removal of the template from the Au, Pt and Pd nanoporous solids (*vide infra*).

Although chronoamperometry proved to be useful for the electrodeposition of gold onto the solid substrate, a different approach was used for the deposition of Pt and Pd. The use of a different approach to the deposition of these metals is due, in part, to the large amount of hydrogen that can be released during the deposition of these metals. To ameliorate this issue, deposition was performed using cyclic voltammetry. Liu *et al.* demonstrated previously that Pt can be deposited around polystyrene nanospheres on an ITO substrate by cycling the potential between -0.4 V and 1.6 V at 50 mV/s in a 10% w/w solution of H_4PtCl_6.[22] This procedure proved useful for the deposition of Pt into our nanosphere templates as well. As for the case of Au deposition, heating of the nanosphere template to 200°C resulted in sufficient structural integrity to allow the deposition of Pt (Figure 2.14). For comparison, the same cyclic voltammetric deposition

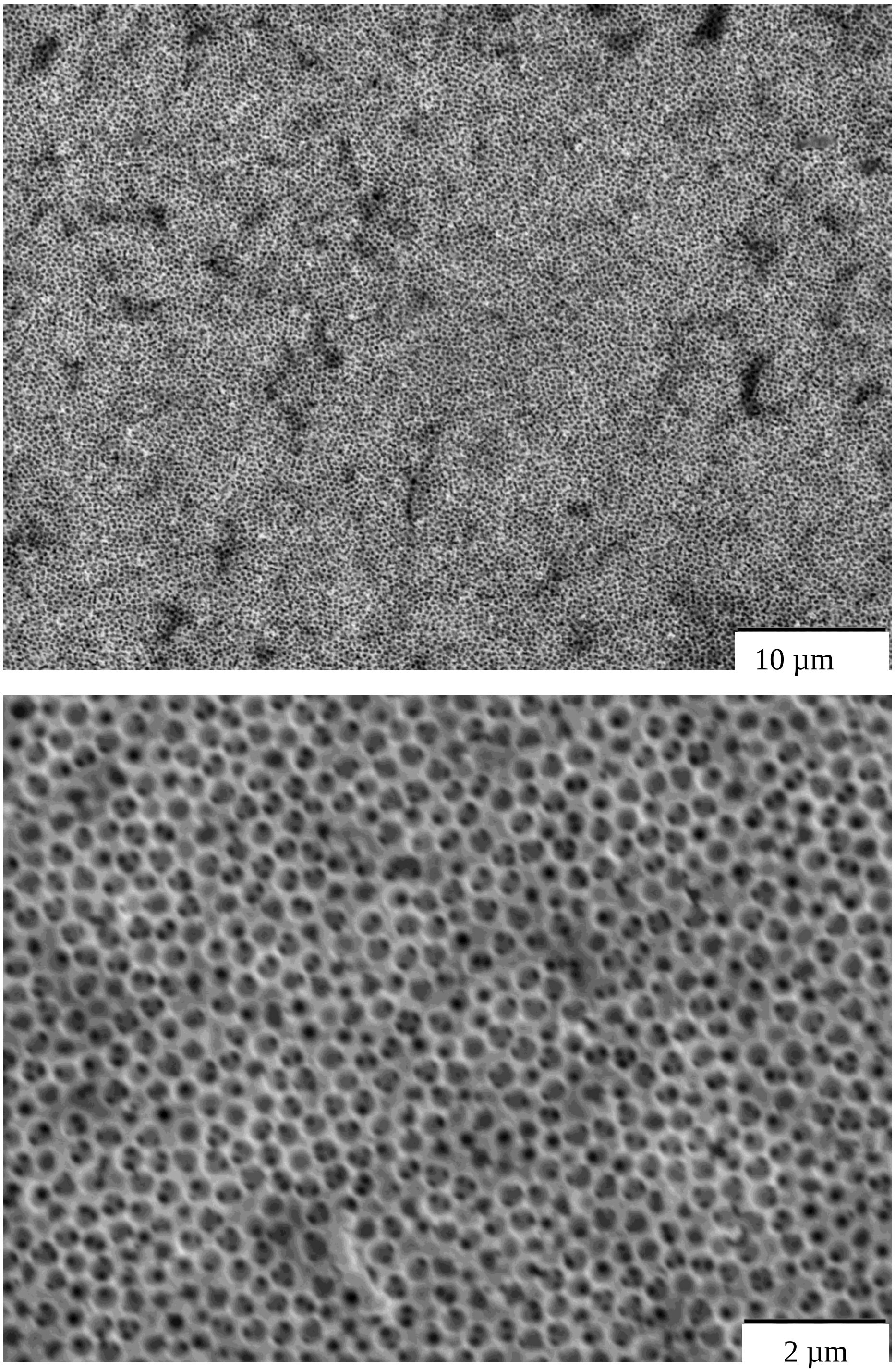

Figure 2.13: SEM images of the gold nanoporous solid made using chronoamperometry. The surface of the gold substrate was modified with cysteamine before the deposition of the silica template.

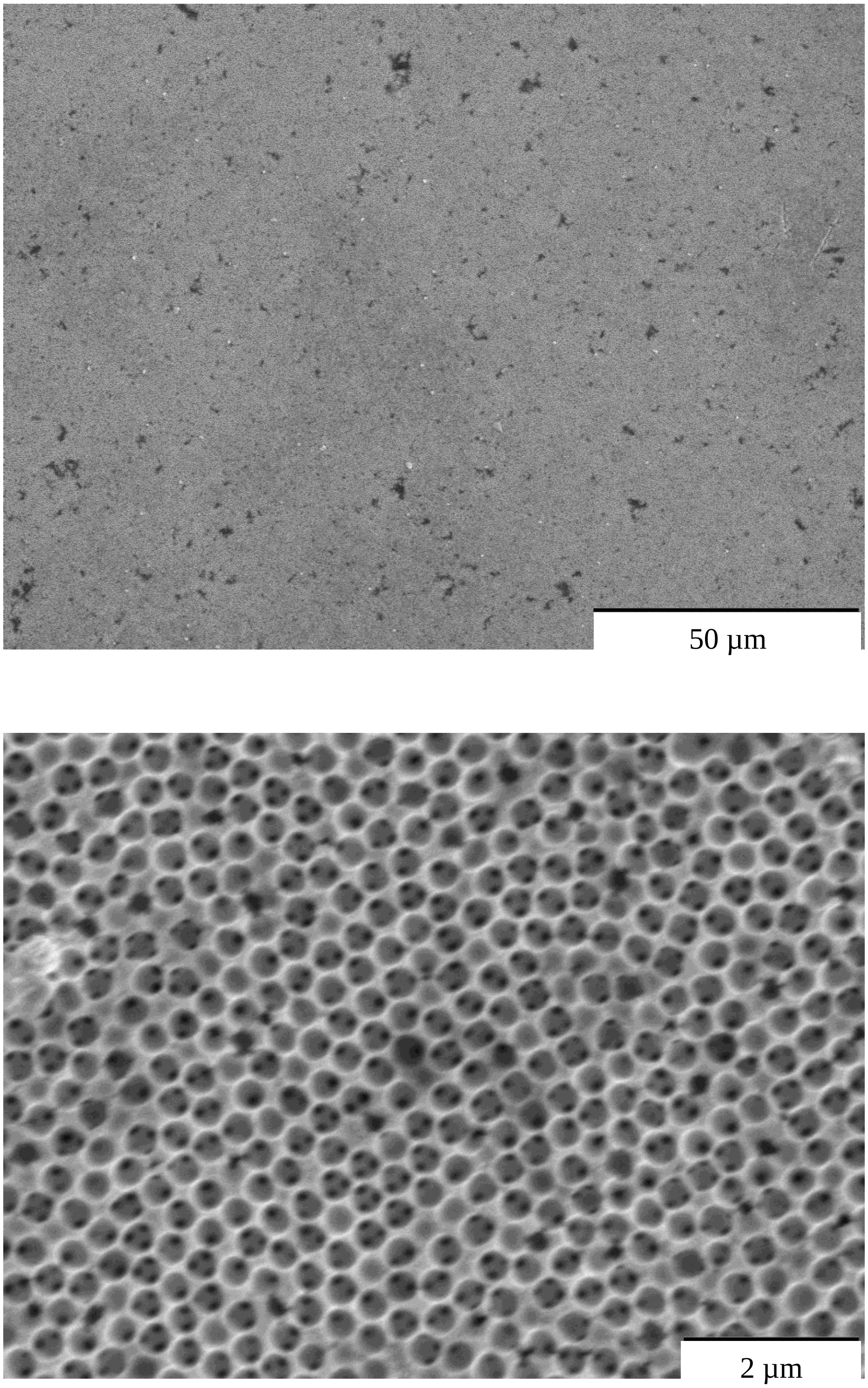

Figure 2.14: SEM images of platinum nanoporous solids formed from the electrodeposition of platinum around a silica sphere template on a gold substrate. The electrodeposition was performed using cyclic voltammetry. The silica spheres were removed with HF prior to imaging.

procedure was used on a gold substrate without the silica template, resulting in a planar Pt-coated substrate. There is a difference in the appearance of the two types of Pt-coated substrates, and this difference can be explained on the basis of refraction of light from the nanoporous Pt and the reflection of light from the planar Pt.

Developing the deposition process for Pd was not as straightforward as for Pt. From literature reports as well as our own experimentation, it was determined that a viable Pd nanoporous solid could be produced. Initial deposition experiments focused on changing the CV deposition scan rate, the number of cycles, and the concentration of the Pd^{2+} solution. The optimum deposition solution was found to be 16.0 mM Na_2PdCl_4 (Aldrich) in 50 mM H_2SO_4 and the potential was cycled from 0.0 V to 1.2 V vs. Ag/AgCl 3M KCl at a scan rate of 20 mV/s for 10 cycles. The resulting nanoporous solid is shown in Figure 2.15. The same deposition procedure was also used to deposit Pd onto a planar gold substrate for comparison in the catalysis experiments reported in later Chapters.

At various times throughout the production of the nanoporous solids, the electrodeposition did not proceed as expected. In these circumstances, contamination of either the substrate or the nanospheres is the typical cause, and replacement of these materials with freshly coated substrate or synthesized nanospheres is required.

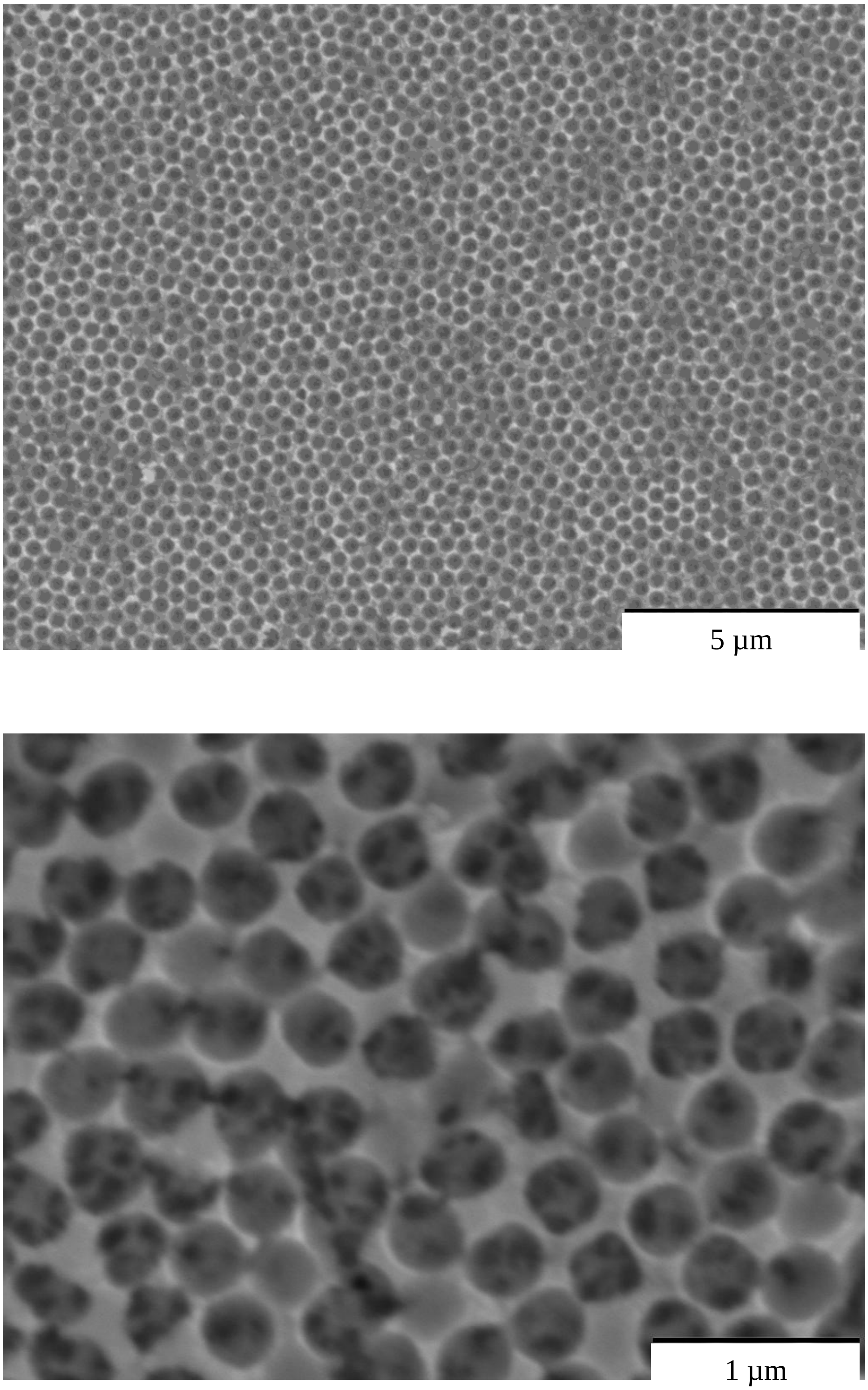

Figure 2.15: SEM images of palladium nanoporous solids formed from the electrodeposition of palladium around a silica sphere template on a gold substrate. The electrodeposition was performed using cyclic voltammetry. The silica spheres were removed with HF prior to imaging.

Conclusion

Achieving the routine fabrication of nanoporous solids has required a substantial amount of trial-and-error, with the result being that it is possible to create these structures reproducibly. One of the primary purposes of this Chapter has been to document the experimental body of work that went into gaining this ability, in the hope that future students on this project will be able to avoid repeating these attempts. In the following Chapters, the application of these metallic nanoporous solids to the electro-catalytic oxidation of alcohols and diols will be described.

CHAPTER 3

EVALUATING THE ROLE OF PT AND PD CATALYST MORPHOLOGY ON ELECTRO-CATALYTIC METHANOL AND ETHANOL OXIDATION

Introduction

In recent years the importance of materials with high surface area and an ordered internal structure has increased for applications such as photonic bandgap materials,[14-15] chemical separations,[16-18] and electrochemical catalysis.[19-20] While these applications appear to be largely unrelated, there exists some commonality based on the materials and structural requirements of each. Specifically, a highly periodic assembly will be characterized by moderately enhanced surface area compared to the corresponding planar solid, rendering it useful for a range of applications, depending on the material used in its construction. One way to obtain a structurally regular material is through the use of a colloidal crystal template formed from nanospheres as a support structure for the deposition of either metals or dielectric materials.[13-14,22,43] Once the nanospheres are removed, the resulting inverse opal structure of interconnected voids can be used in a variety of applications.

One potential use for metallic nanoporous solids is in the catalytic oxidation of alcohols, an area of particular importance to the operation of fuel cells. The oxidation of methanol and ethanol are particularly important for fuel cell applications because they can be derived from biomass.[2-4] Using the energy produced from these sources provides advantages over petroleum-derived fuels in terms of decreased production of atmospheric pollutants.[3] However, one problem with many means of direct alcohol oxidation is the poisoning of catalyst surfaces by carbon monoxide, leading to inhibition and the consequent need to regenerate or replace the catalyst.[3,8-9] Both Pt and Pd have been used as catalysts for alcohol oxidation, and have been examined in the form of pure metals as well as in bimetallic systems.[7,9,26,44] Both metals have been shown to function as catalysts, with similar issues relating to surface poisoning. We are interested in exploring the use of Pt and Pd as alcohol oxidation catalysts in the structural form of nanoporous solids. We recognize that a variety of materials have been used as catalysts for the oxidation of alcohols, and have chosen to use Pt and Pd in this work because of the ability to electrochemically deposit these metals and to avoid potential issues relating to the identity of the catalytic site(s) for more complex systems.[45-48] Our motivation for this work is two-fold. The first is that there is a straightforward surface area enhancement for nanoporous solids relative to planar metal substrates for use as catalysts, and we intend to evaluate the extent to which this enhancement can be accessed experimentally. Second, we are interested in exploring the possibility that the formation of the nanoporous solids gives rise to microcrystalline surface morphologies that may be useful for catalytic processes.[48] Specifically, the deposition of Pt and Pd in the form of nanoporous solids may give rise to a different distribution of microcrystalline surface structures (*e.g.* Pt(111), Pt(755), Pt(332)) than is seen for a typical planar surface, and the presence of edges at the connection points between voids in the nanoporous solid structures could serve, in principle, to produce catalytic behavior with different efficiency than that seen for planar metal surfaces.

To explore the utility of nanoporous Pt and Pd for catalytic alcohol oxidation, we have constructed these materials and compared their electro-catalytic behavior to planar metal substrates in both acidic and basic media. The catalytic stability of the nanoporous solids is investigated as well as the tolerance to the accumulation of potential catalyst poisons resulting from the oxidation of the alcohols. Our data reveal system-specific, reproducible behavior that suggest in some instances an enhancement associated with the use of nanoporous solids compared to planar metal substrates.

Experimental

Nanoporous Solid Fabrication: Silica nanospheres of *ca*. 300 nm diameter were synthesized in house using a modified Stöber method, as discussed in detail in Chapter 2.[12-13,27-28] As a quick reminder, a mixture of tetraethylorthosilicate (TEOS, Fluka) and ethanol was added slowly to a solution of ethanol and 25% ammonium hydroxide. The solution was allowed to stir overnight and the resulting suspension was centrifuged and washed several times with ethanol. To deposit nanosphere adlayers, a gold substrate was immersed in an ethanolic suspension of silica nanospheres and withdrawn from the solution at a rate of 0.15 µm/s using a SDI Nanodip Coater. Using a nanosphere concentration of 9.2 mg/mL, this withdrawal rate produces 2 adlayers of nanospheres. The immersion and withdrawal sequence was repeated three times to create a nanosphere assembly containing 6 nanosphere layers for use as a template for growth of the metallic nanoporous solid (Figure 3.1). The silica nanosphere assembly was sintered at 200°C for 2 hours to enhance the structural integrity of the template during the electrodeposition process.

Electrodeposition of the metals was performed using a CHI650A electrochemical analyzer. The three-electrode set-up utilized a Ag/AgCl, 3M KCl reference electrode (E_0 = 0.210 V *vs*. SHE), a Pt wire counter electrode and the silica/gold substrate as the working electrode. For the Pt deposition, a solution of 10 % w/w H_4PtCl_6 (Fluka) was used and the potential was cycled between -0.4 V and 1.6 V[22] for 10 cycles at a scan rate of 50 mV/s. For Pd deposition a solution of 16 mM Na_2PdCl_4 (Aldrich) in 50 mM

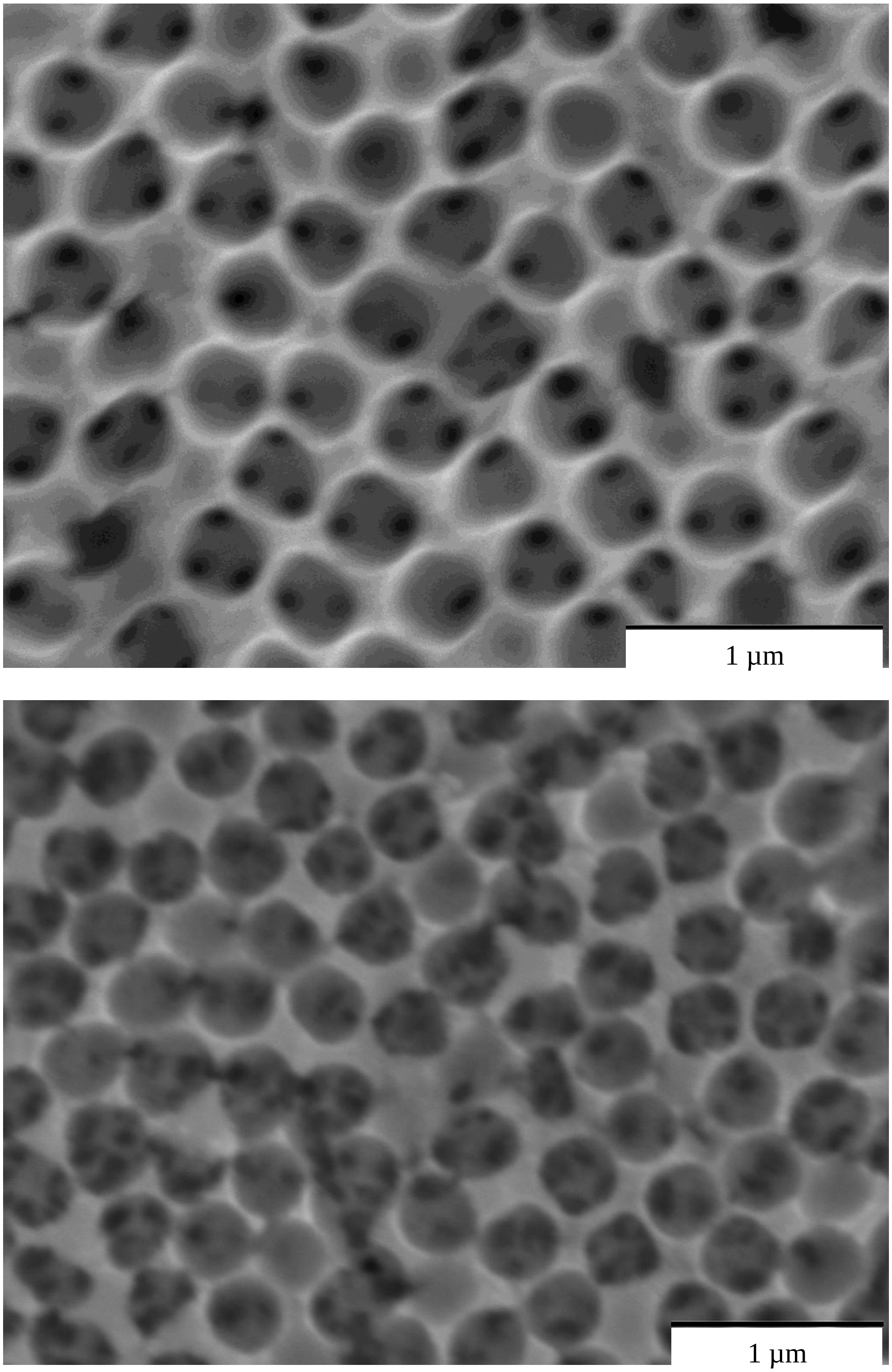

Figure 3.1: SEM micrographs of nanoporous solids of (a) Pt and (b) Pd. Both metals were electrodeposited onto silica nanosphere layered assemblies.

H_2SO_4 was used and the potential cycled from 0.0 V to 1.2V for 10 cycles at a scan rate of 20 mV/s. The area of deposition on the Au surface was controlled using an insulating mask. The same parameters were also used to deposit Pt and Pd on planar gold substrates for comparison measurements. We used a potential cycling method rather than constant potential deposition because, in our hands, this method yielded more reproducible nanoporous solid materials. Following metal deposition onto the nanosphere assembly, the silica template was removed by immersing the substrate in a solution of 10% hydrofluoric acid for *ca*. 15 minutes.

Characterization: Characterization of the nanoporous solid structure was performed first by scanning electron microscopy (Figure 3.1) (JSM-6400). The active surface area for both the nanoporous and planar substrates was determined electrochemically using cyclic voltammetry (CV) in a solution of either 1.0 M H_2SO_4 or 1.0 M KOH. The potential was scanned from -0.25 V to 1.25 V (*vs*. Ag/AgCl) under acidic conditions and -1.0 V to 0.25 V (*vs*. Ag/AgCl) under basic conditions using Pt wire as the counter electrode and either the nanoporous solids or planar substrates as the working electrode (Figure 3.2). The electrochemically active surface area (A) can then be found using the area of hydrogen adsorption/desorption peaks, which is the coulombic charge for hydrogen desorption (Q_H), and the charge associated with monolayer adsorption of hydrogen, so that $A = Q_H/210\ \mu C\ cm^{-2}$.[49-51]

Alcohol Oxidation: Electrochemical experiments were conducted at 20°C. Aqueous solutions of 1.0 M methanol (MeOH) or 1.0 M ethanol (EtOH) were made with either 1.0 M sulfuric acid (H_2SO_4) or 1.0 M potassium hydroxide (KOH). For the cyclic

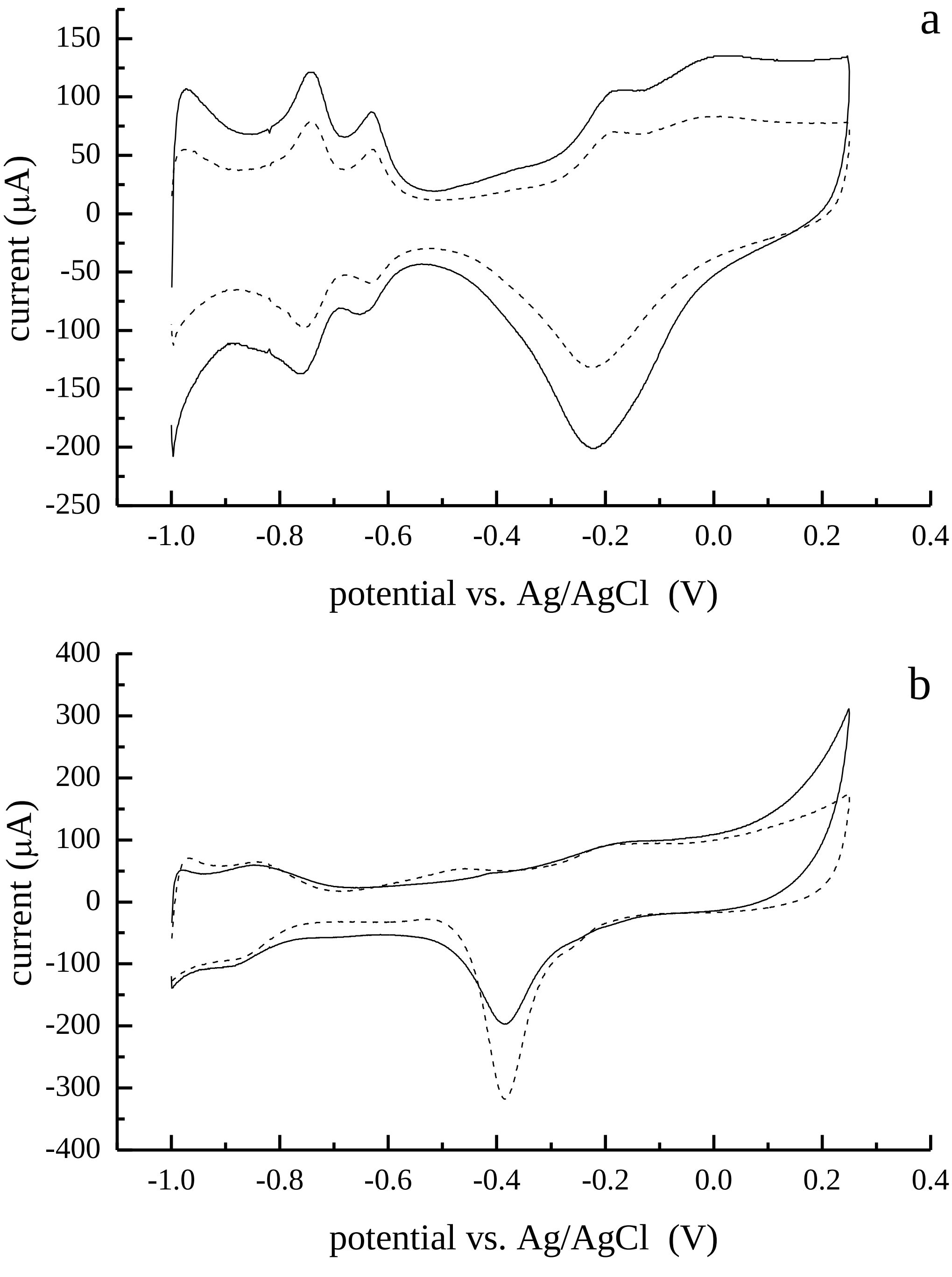

Figure 3.2: Cyclic voltammograms showing current as a function of potential for nanoporous solid (solid line) and planar substrate (dashed line) electrodes. Panel (a) shows CV data for Pt, and panel (b) shows data for Pd.

voltammetry experiments, the potential was cycled between 0.0 V and 1.0 V (*vs.* Ag/AgCl) under acidic conditions and between -1.0 V and 0.25 V (*vs.* Ag/AgCl) under basic conditions. Chronoamperometry experiments were performed at 0.7 V in acidic solution and -0.355 V in basic solution.

Results and Discussion

In the comparison of nanoporous solids to planar metallic surfaces, there are several issues to consider. The first is the geometric advantage that the nanoporous solid enjoys over the planar metallic electrode. The second issue is the susceptibility of both materials to contamination, which is essentially an issue of accessibility of both reactants and potential catalyst poison(s) to the surface of each metallic structure. These first two issues are largely geometric and diffusional processes, and are expected to play a significant role. The third issue that remains to be determined is whether or not the morphology of the nanoporous solid creates regions of comparatively high catalytic activity. We consider the first two issues individually and, based on these results, we examine whether or not nanoporous solids exhibit a catalytic enhancement relative to a planar metal substrate that cannot be accounted for by geometric considerations.

The first and perhaps most obvious advantage of using nanoporous solids instead of planar substrates is the increased surface area relative to the planar substrate that results from the inverse opal structure of the metal. To determine the expected geometric enhancement, we calculate the surface area of the nanoporous solid. The surface area of the nanoporous solid is given by the sum of the surface areas of the nanoporous spheres used in the construction of the nanoporous solid, minus the area of the points of contact between the silica spheres, which accounts for the surface area lost due to pore formation. We calculate this nanoporous solid surface area per geometric cm^2 of planar substrate. Assuming that the diameter of the resulting pores is 20% of the diameter of the nanospheres[13] and that the nanospheres exist in a hexagonally close-packed array, the surface area of each void in the nanoporous solid is given by: $A_{void} = A_{nanosphere}$ –

$10A_{pore}$ for the layer in contact with the planar substrate and $A_{void} = A_{nanosphere} - 12A_{pore}$ for each subsequent layer (Figure 3.1). This formula is based on the number of contact points each nanosphere makes with its neighbors and, for the first layer, with the supporting surface. We take the surface area of each nanosphere to be $4\pi r^2$ and the (circular) area of each pore to be $0.2\pi r^2$. Thus the surface area for per nanosphere is $2\pi r^2$ for the first layer and $1.6\pi r^2$ for subsequent layers. The surface area per layer is independent of the size of the nanospheres because the surface area of interest is (A_{void} per nanosphere)×(number of nanospheres per geometric cm^2). Thus for a nanoporous solid n layers thick the resulting surface area is expected to be $(1.57 + (n-1)*1.26)$ cm^2 per cm^2 of geometric area. The area of our nanoporous substrates was determined electrochemically to be substantially lower than predicted by calculation (Table 3.1), a reason for which may be that the nanoporous solid is grown on a solid surface, precluding access to its interior regions by any means other than diffusional permeation. Given the observed level of surface area enhancement, our results are consistent with *ca*. three layers of the nanoporous solid participating in the catalytic process, and we recognize that this is possibly a conservative estimate. With this information in hand, we turn to the consideration of catalytic activity for these nanoporous solids.

Pt/KOH: To determine if the nanoporous solid does indeed provide an advantage over a planar substrate, the oxidation of methanol under basic conditions was examined for both substrates using a 1.0 M MeOH/1.0 M KOH aqueous solution. The cyclic

Table 3.1: Experimental Surface Area Enhancement of Nanoporous Solids

Nanoporous Metal	Electrochemically Determined Surface Area (cm^2)	Geometric Area (cm^2)	Enhancement
Pt	1.453	0.282	5.15
Pd	0.7766	0.282	2.75

voltammetry of this system shows two oxidation peaks for both the nanoporous and the planar substrates (Figure 3.3). The oxidation wave seen at -0.14 V in the positive-going scan is due to the oxidation of methanol,[7] and the wave seen in the negative-going scan is attributed to the oxidation of the methanol oxidation reaction products (*e.g.* CO, CO_2 and HCOOH) adsorbed on the Pt surface (Scheme 3.1).[4,21-22] The slight difference in potentials seen for methanol oxidation for the two Pt surface structures is likely due to different catalytic activity of the two surfaces. The slightly more negative onset potential (Table 3.2) of the nanoporous solid demonstrates that the alcohol oxidizes more readily on this surface.[25,51] We report our results in terms of current density to make comparison of the data for each surface more facile. We use the electrochemically determined surface area of the interfaces to calculate current densities (*vide infra*). The resulting current density for methanol oxidation with the Pt nanoporous solid is almost three times that of methanol oxidation at the planar substrate. This increased electro-catalytic response indicates that there is indeed a morphologically-mediated dependence of catalytic activity in our nanoporous solid. This morphological difference may result from the physical structure of the nanoporous solid, or the crystalline nature of the electro-deposited Pt. In previous studies it has been established that Pt(111) typically produces greater anodic current density than other Pt surface structures, such as Pt(100) and Pt(110).[52-54] If this is the case, our data are consistent with the nanoporous Pt solid containing a higher fractional amount of Pt(111) than the planar Pt substrate. Furthermore, exposure to alkaline solutions has been demonstrated to affect surface

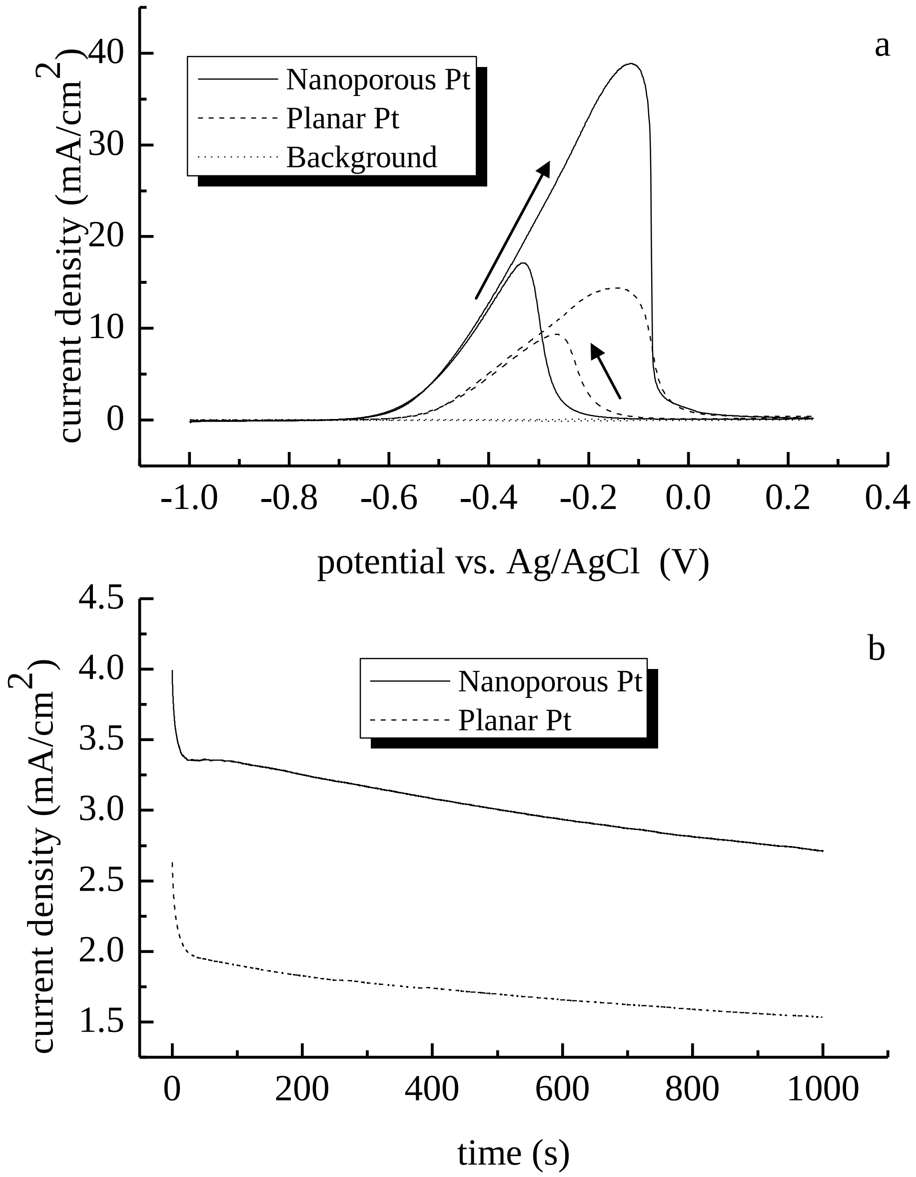

Figure 3.3: Comparison of electrocatalytic response of Pt substrates. (a) Cyclic voltammogram of 1.0 M MeOH/1.0 M KOH aqueous solution at a scan rate of 10 mV/s. (b) Chronamperometric scan of nanoporous and planar Pt for 1.0 M MeOH/1.0 M KOH acquired at a potential of -0.355 V vs. Ag/AgCl.

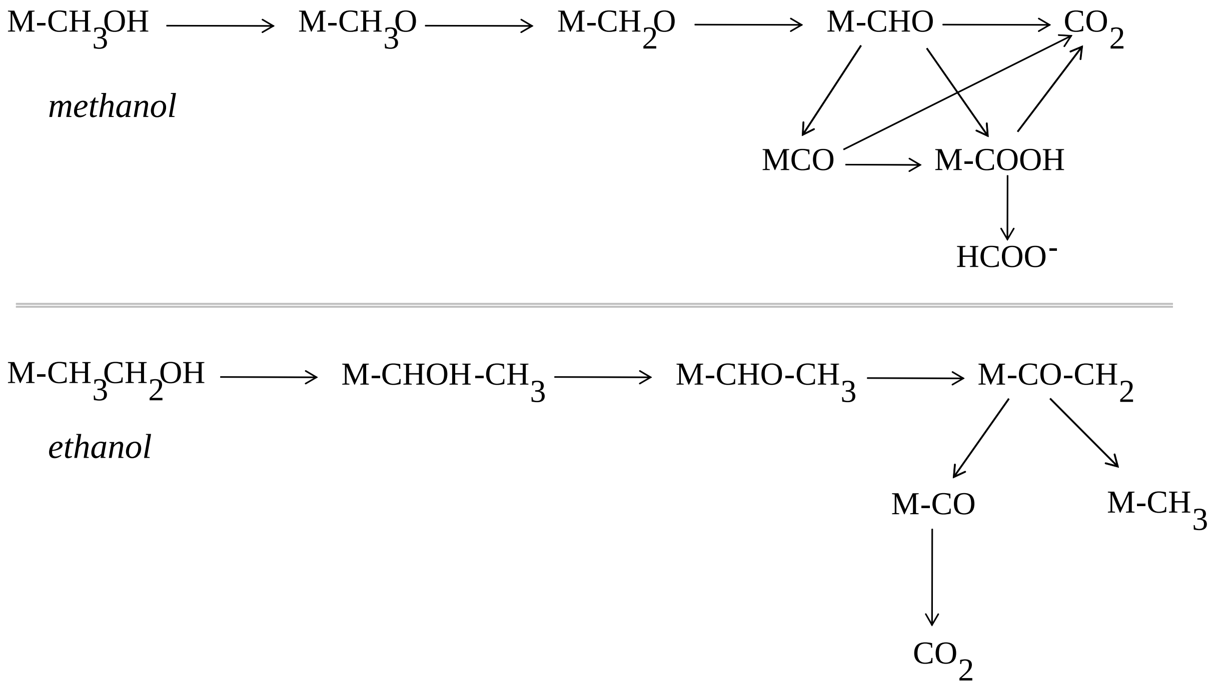

Scheme 3.1: Reaction pathways for methanol and ethanol. M designates an active site on the metal surface.

Table 3.2: Comparison of Electrochemical Performance of Methanol and Ethanol: Pt/KOH

Platinum Substrate	MeOH Onset Potential (V)	MeOH Peak Potential (V)	MeOH Current Density (mA/cm^2)	I_f/I_b Ratio MeOH
Nanoporous	-0.571	-0.115	37.6	2.26
Planar	-0.542	-0.145	14.4	1.54

Platinum Substrate	EtOH Onset Potential (V)	EtOH Peak Potential (V)	EtOH Current Density (mA/cm^2)	I_f/I_b Ratio EtOH
Nanoporous	-0.715	-0.175	24.3	1.79
Planar	-0.728	-0.283	9.45	0.94

reconstruction, depending on the morphology of the Pt. The more open the surface arrangement (*i.e.* Pt(110)), the greater the surface expansion that occurs when the electrode is exposed to the solution.[55] This surface reconstruction may then contribute to the difference observed between the nanoporous and planar Pt solids. A reason for the resulting difference with a change in morphology is the surface's ability to support the formation and adsorption of CO.[52]

The effect of poisoning the Pt nanoporous and planar surfaces was examined using chronoamperometry at a potential of -0.355 V (Figure 3.3). Upon application of the potential to the electrode, a steady decrease in current is seen within the first few minutes for both the nanoporous solid and planar Pt electrodes, followed by the establishment of a nearly constant current at longer times. Since the current density plateau was higher for the nanoporous solid than for the planar substrate, the Pt nanoporous structure appears to be more catalytically stable than the Pt planar electrode.[7,22,26] Furthermore, the higher initial current that is observed for the nanoporous solid is indicative of a greater number of active sites available for oxidation.[25] In this case, the loss of activity for the nanoporous solid is 32%, compared to a 42% loss for the planar Pt solid. This finding, combined with a slower overall decay, also suggests enhanced stability for the nanoporous solid relative to the planar surface. The tolerance of the catalyst to CO can be gauged by the ratio of the forward and reverse anodic peak currents, I_f/I_b.[4,21] A small ratio indicates a relatively large amount of carbonaceous material resides on the surface of the catalyst, the result of incomplete oxidation of methanol to carbon dioxide (Scheme 3.1).[9] For the Pt nanoporous solid, the ratio of the two peaks is 2.26, and for the Pt planar solid the ratio is 1.54. The higher peak ratio for the nanoporous solid indicates this structural motif is more efficient at reducing the adsorbed carbon monoxide than a planar metal surface.[4,21]

To further evaluate the utility of the nanoporous solid under basic conditions, the electro-oxidation of a 1.0 M EtOH/1.0 M KOH aqueous solution was also performed. For this system two anodic peaks are observed for both the nanoporous solid and the planar Pt electrode (Figure 3.4). The oxidation potential of ethanol at the nanoporous solid is slightly more positive than that observed at planar Pt substrates, reported here, and potentials reported for other Pt catalysts under analogous conditions.[7,26,56] For ethanol under basic conditions, the onset potential for oxidation at the nanoporous Pt electrode is less negative than that seen for the planar substrate. This finding indicates a smaller enhancement in the catalytic activity for nanoporous Pt relative to planar solid Pt for ethanol in basic conditions, the reasons for which may be morphological.

As was seen for methanol, the Pt nanoporous solid produced a *ca.* three-fold greater current density than the planar Pt electrode, as well as enhanced current density compared to other reported values.[26] When the results from ethanol oxidation are compared to those for methanol oxidation, it is clear that the Pt nanoporous solid produces a greater current density for methanol than for ethanol under basic conditions (Table 3.2). Chronoamperometry data for ethanol (Figure 3.4) indicate the Pt nanoporous solid is catalytically only slightly more stable than the planar substrate for ethanol oxidation. The overall loss of activity was essentially the same for the Pt nanoporous

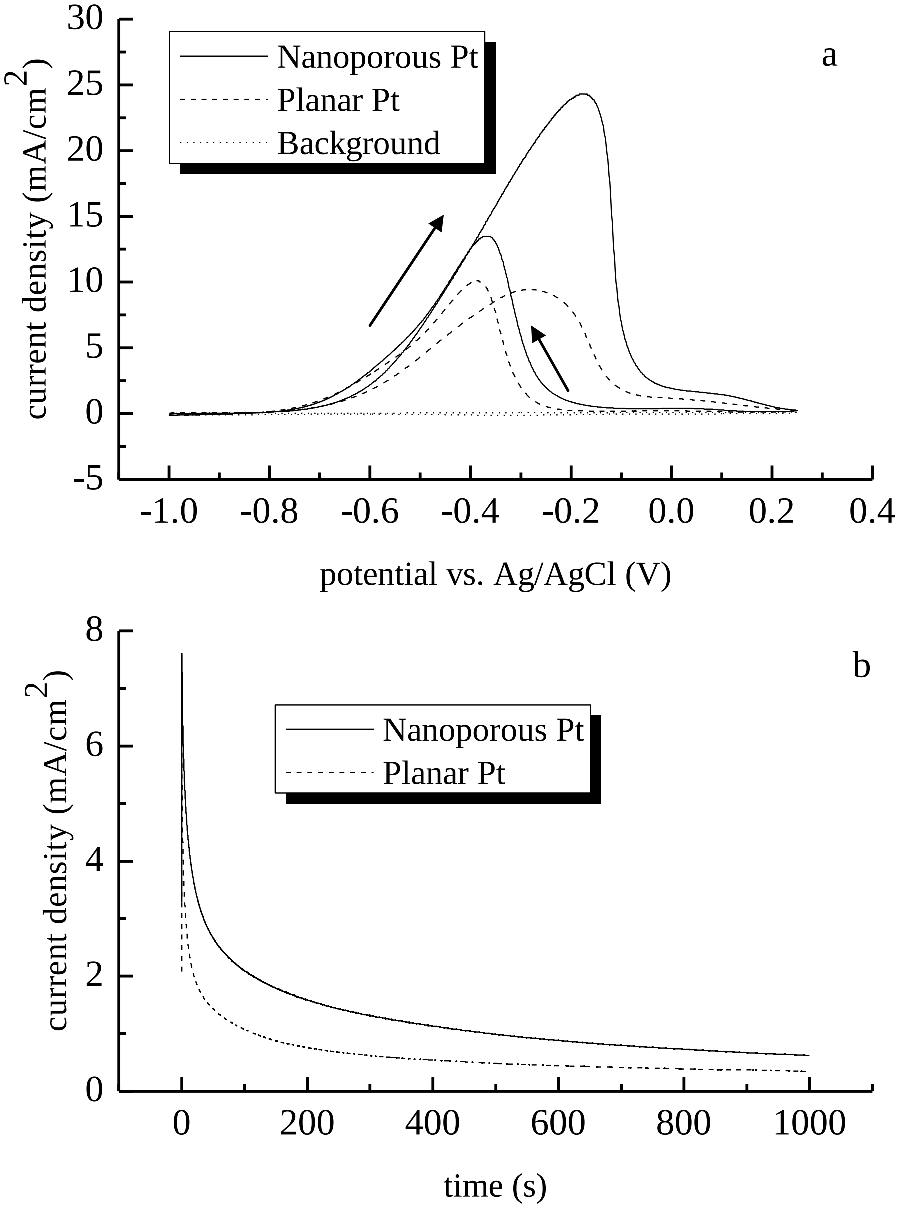

Figure 3.4: Comparison of electrocatalytic response of Pt substrates. (a) Cyclic voltammogram of 1.0 M EtOH/1.0 M KOH aqueous solution, acquired at a scan rate of 10 mV/s. (b) Chronamperometric scan of nanoporous and planar Pt for 1.0 M EtOH/1.0 M KOH at a potential of -0.355 V vs. Ag/AgCl.

solid (92%) and the Pt planar solid (94%). The increased loss relative to what was observed for methanol may be the result of differing catalytic activity at the surface of the solids and the relative stability of different crystalline faces of the Pt. The anodic peak ratio for the Pt nanoporous solid is 1.79 and for the planar substrate the ratio is 0.94, indicating that the nanoporous solid electrode is more efficient at reducing adsorbed CO than the planar substrate. Our comparative results for methanol and ethanol oxidation are in agreement with previous literature reports.[26]

Pd/KOH: Pd catalysts are also of interest in terms of catalytic efficiency and their ability to withstand surface contamination. We first compare the catalytic activity of nanoporous Pd to a planar Pd surface under basic conditions. The cyclic voltammetry data for methanol and ethanol oxidation at Pd are characterized by two anodic waves, as expected (Figures 3.5, 3.6). The Pd nanoporous structure exhibits a higher current density than the planar Pd electrode for ethanol, yet a lower current density than the planar Pd for methanol (Table 3.3). We also note that the Pd electrocatalyst produces higher current densities for ethanol than for methanol, which is the reverse of the behavior seen for the Pt catalysts. The current densities for methanol using the Pd nanoporous solid are similar to, while those for ethanol are higher than, other reports.[7,26]

Both the peak and onset potentials for methanol oxidation at the Pd nanoporous solid are shifted negative relative to the analogous data for the planar Pd electrode (Table 3.3), indicating greater catalytic activity for the nanoporous solid structure. The onset and peak potentials for ethanol oxidation at the Pd nanoporous solid are the same as, or positively shifted from those for the planar Pd electrode. This finding suggests that the nanoporous Pd solid is as active catalytically as the planar Pd electrode for ethanol.

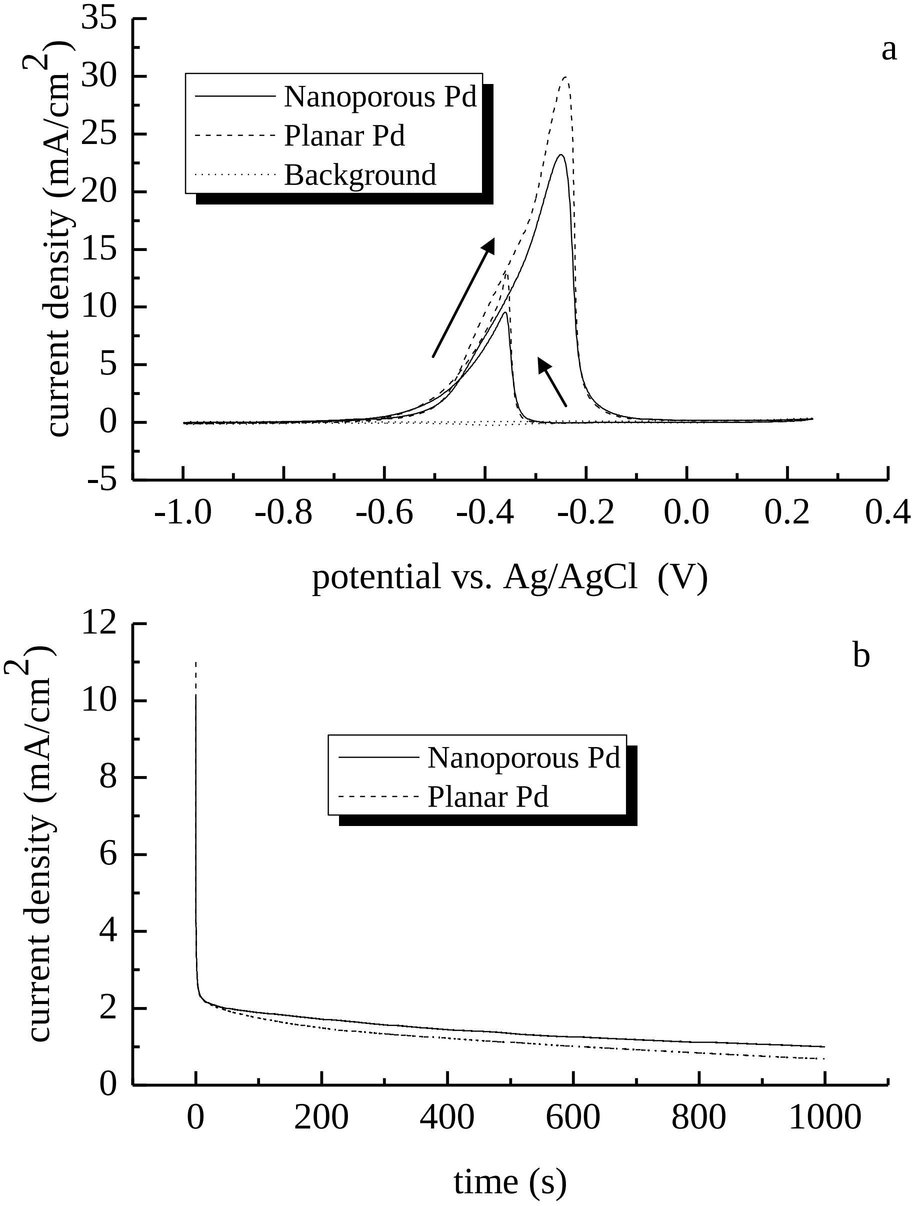

Figure 3.5: Comparison of electrocatalytic response of Pd substrates. (a) Cyclic voltammograms of 1.0 M MeOH/1.0 M KOH, acquired at a scan rate of 10 mV/s. (b) Chronoamperometric scans of nanoporous and planar Pd for 1.0 M MeOH/1.0 M KOH at a potential of -0.355 V vs. Ag/AgCl.

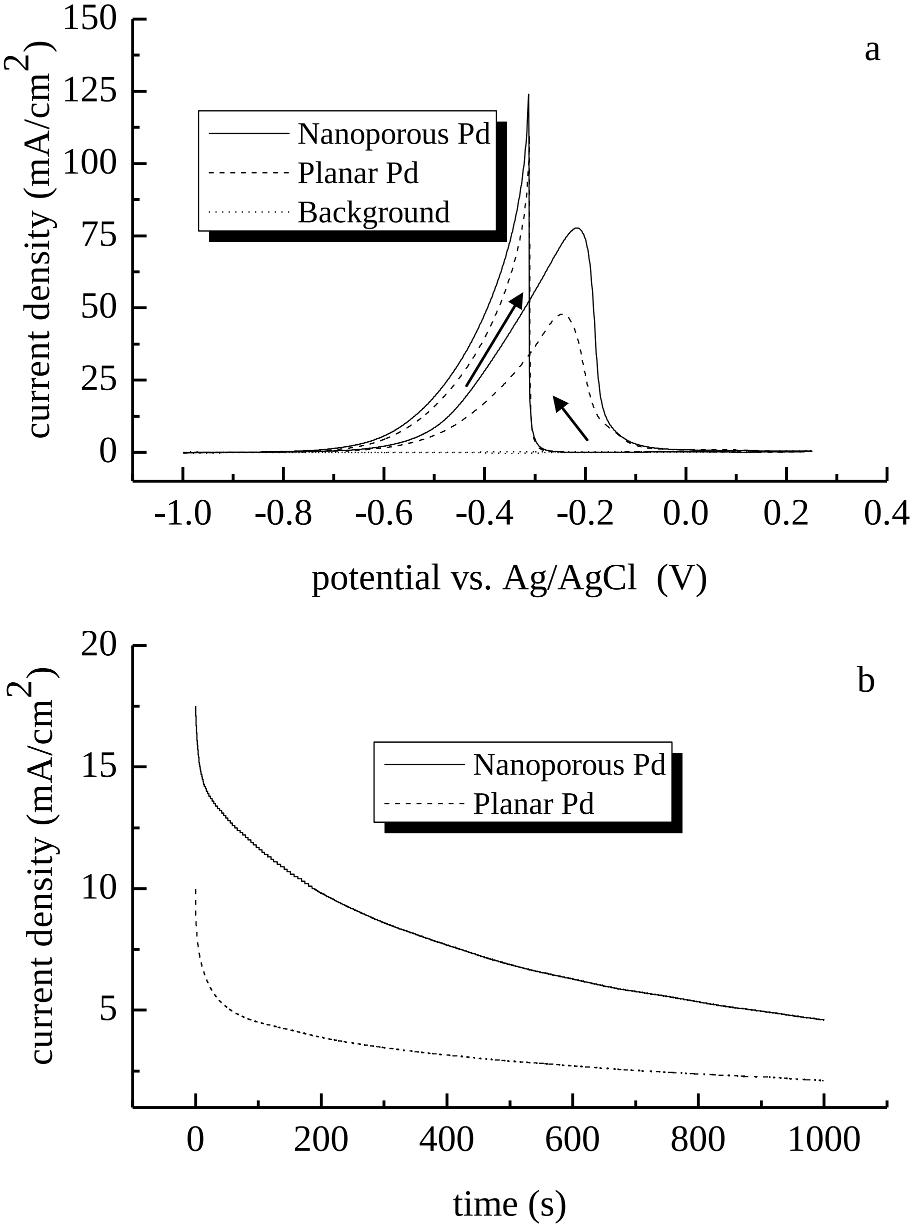

Figure 3.6: Comparison of electrocatalytic response of Pd substrates. (a) Cyclic voltammograms of 1.0 M EtOH/1.0 M KOH, acquired at a scan rate of 10 mV/s. (b) Chronoamperometric scans of nanoporous and planar Pd for 1.0 M EtOH/1.0 M KOH at a potential of -0.355 V vs. Ag/AgCl.

Table 3.3: Comparison of Electrochemical Performance of Methanol and Ethanol: Pd/KOH

Palladium Substrate	MeOH Onset Potential (V)	MeOH Peak Potential (V)	MeOH Current Density (mA/cm^2)	I_f/I_b Ratio MeOH
Nanoporous	-0.530	-0.249	23.3	2.43
Planar	-0.522	-0.241	29.9	2.28

Palladium Substrate	EtOH Onset Potential (V)	EtOH Peak Potential (V)	EtOH Current Density (mA/cm^2)	I_f/I_b Ratio EtOH
Nanoporous	-0.538	-0.216	77.7	0.63
Planar	-0.553	-0.245	47.8	0.43

There appears to be less morphologically-mediated dependence of catalytic activity with Pd than with Pt, as it has been found that the reaction pathway of ethanol is the same on Pd(110) and Pd(111) surfaces, in contrast to what has been determined for Pt.[57] When our peak and onset potential data are compared to potentials reported for other Pd catalysts, our data for both methanol and ethanol oxidation are shifted negative.[7,56]

Chronoamperometric measurement of alcohol oxidation at the Pd nanoporous solid results in higher current densities than the corresponding planar Pd electrode (Figures 3.5, 3.6). This finding is consistent with our results for Pt, indicating that the nanoporous solid morphology provides a more catalytically active surface than the corresponding planar solid. The time-resolved current densities for the alcohols showed that the initial decay for methanol oxidation was more rapid than for ethanol oxidation and, at long times, methanol oxidation produced a lower current density than ethanol oxidation. The loss of activity for the Pd nanoporous solids was less than that observed for the Pd planar solids for both alcohols, specifically 90% *vs*. 94% for methanol and 74% *vs*. 79% for ethanol. However, in contrast to the Pt nanoporous solids, greater overall loss of performance was seen for methanol. The observed I_f/I_b ratio is greater for the Pd nanoporous solid than for the planar Pd electrode, for oxidation of both alcohols (Table 3.3). This ratio is smaller for ethanol (0.63) than for methanol (2.43), due to the very large and narrow anodic wave for the reverse scan of ethanol, which is not observed for methanol under either acidic or basic conditions. One possible explanation for the smaller ethanol I_f/I_b ratio is the generation of byproducts that result from the oxidation, where the higher current density of ethanol oxidation on Pd gives rise to a higher adsorbate density on the Pd surface.

Pt/H_2SO_4: There are literature reports that indicate electro-oxidation of alcohols under basic conditions results in higher activity and faster reaction kinetics than under acidic conditions.[7] To determine if the same is true for the nanoporous solid, we have examined the electro-catalytic oxidation of 1.0 M MeOH/1.0 M H_2SO_4 and 1.0 M EtOH/1.0 M H_2SO_4 aqueous solutions at nanoporous solid and planar Pt electrodes. The cyclic voltammetry data for these solutions showed two oxidation peaks for each alcohol (Figures. 3.7, 3.8). The measured current density for the nanoporous solid was about half that of the planar Pt electrode for methanol and essentially equal to that of the planar Pd electrode for ethanol (Table 3.4). Although the resulting current densities do not reveal an enhancement, the more negative onset potential observed with the nanoporous solid, as well as the negative shift of the methanol oxidation potential, which is typically reported as 0.78 V *vs*. Ag/AgCl,[4] indicates a higher catalytic activity than that of the planar solid. In ethanol, the nanoporous solid electrode produced an anodic wave at 0.695 V, essentially the same as the observed potential of 0.701 V for the planar substrate, and shifted *ca*. 0.5 V negative from the value of 0.75 V reported for Pt catalysts.[8] This result indicates that there is a slightly greater catalytic activity for the nanoporous solid than for the planar solid, in agreement with our findings for methanol oxidation. Since the negative shift in oxidation potentials, which was not observed for basic conditions, is seen for acidic conditions (Table 3.4), the Pt nanoporous solid

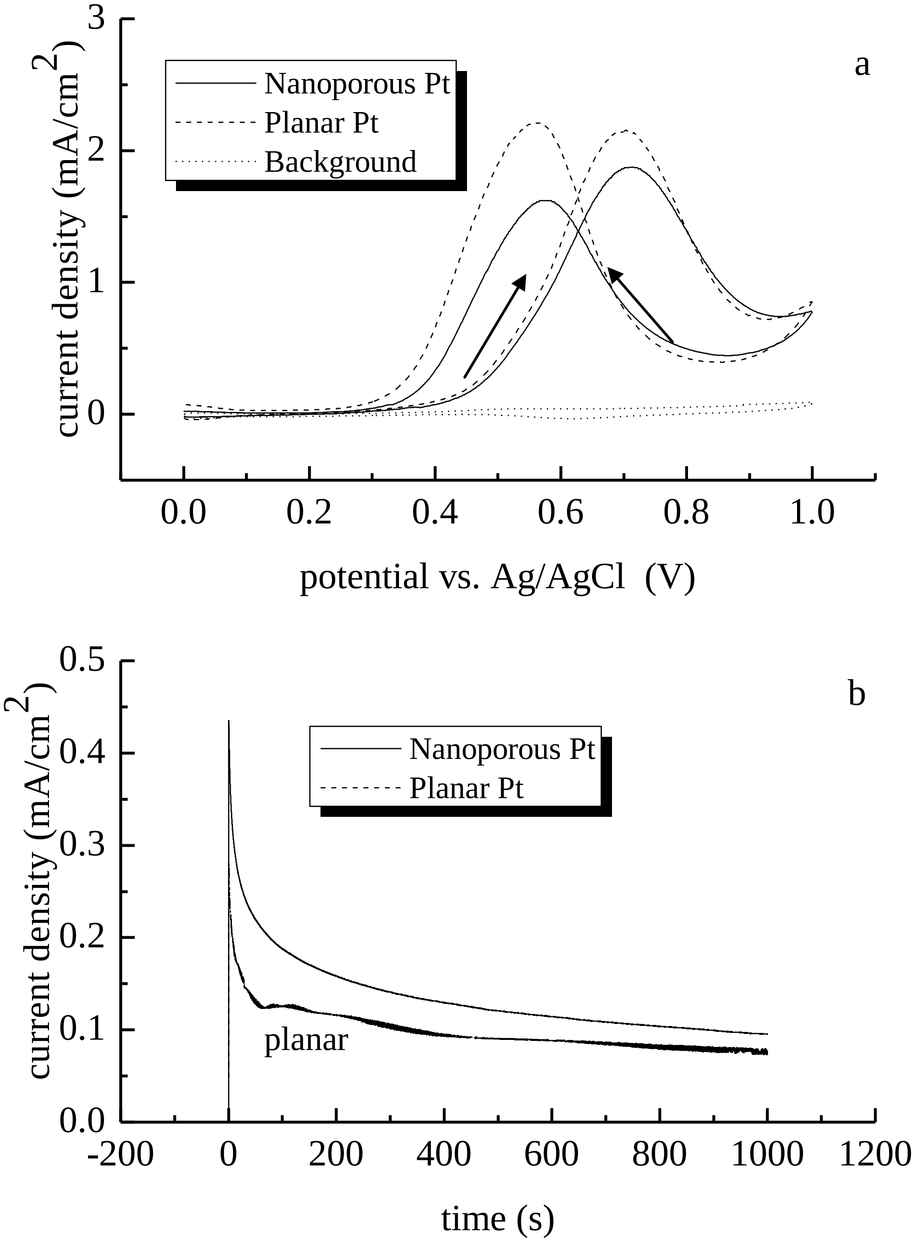

Figure 3.7: Comparison of electrocatalytic response of Pt substrates. (a) Cyclic voltammograms of 1.0 M MeOH/1.0 M H_2SO_4 aqueous solution acquired at a scan rate of 10 mV/s. (b) Chronoamperometric scans of nanoporous and planar Pt of 1.0 M MeOH/1.0 M H_2SO_4 at a potential of 0.70 V vs. Ag/AgCl.

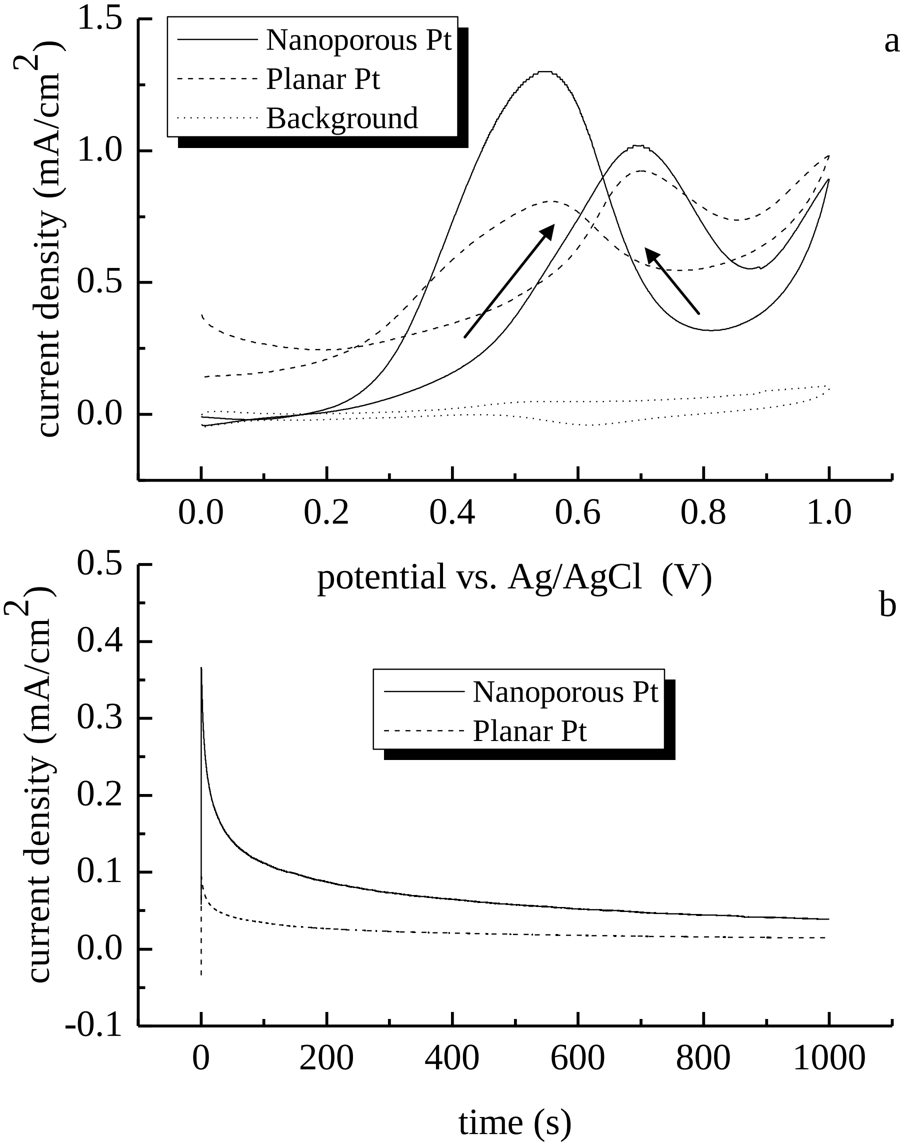

Figure 3.8: Comparison of electrocatalytic response of Pt substrates. (a) Cyclic voltammograms of 1.0 M EtOH/1.0 M H_2SO_4 aqueous solution acquired at a scan rate of 10 mV/s. (b) Chronoamperometric scans of nanoporous and planar Pt of 1.0 M EtOH/1.0 M H_2SO_4 at a potential of 0.70 V vs. Ag/AgCl.

Table 3.4: Comparison of Electrochemical Performance of Methanol and Ethanol: Pt/H_2SO_4

Platinum Substrate	MeOH Onset Potential (V)	MeOH Peak Potential (V)	MeOH Current Density (mA/cm^2)	I_f/I_b Ratio MeOH
Nanoporous	0.416	0.713	1.87	1.15
Planar	0.451	0.703	2.15	0.97

Platinum Substrate	EtOH Onset Potential (V)	EtOH Peak Potential (V)	EtOH Current Density (mA/cm^2)	I_f/I_b Ratio EtOH
Nanoporous	0.353	0.695	1.02	0.783
Planar	0.426	0.701	0.92	1.141

appears to be more catalytically active under acidic conditions than under basic conditions. However, the observed enhancement in current density seen for nanoporous solid Pt is greater under basic conditions than under acidic conditions.

The effect of poisoning of the Pt nanoporous solid was also examined for both methanol and ethanol under acidic conditions using chronoamperometry at a constant potential of 0.7 V (*vs.* Ag/AgCl) (Figures 3.7, 3.8). For both alcohols, the platinum nanoporous solid produced a higher final current density than the planar substrate, thus the nanoporous solid appears to provide greater catalytic stability. Furthermore, the initial current density for the Pt nanoporous solids is much greater than that for the corresponding Pt planar solids, indicating a greater number of active sites available per unit of surface area. We note that the overall decrease in catalytic activity is greater for the Pt nanoporous solid than for the Pt planar solid, yet when comparing the final current densities for both structures, the nanoporous solid appears to retain a higher level of activity. Comparing the Pt nanoporous solid response for the two alcohols, we find that methanol yields a higher current density than ethanol. This finding is also seen in the anodic peak ratio of methanol (Table 3.4). For ethanol, the peak ratios indicate that the Pt planar solid (1.14) is more efficient at reducing absorbed CO than the nanoporous solid (0.78) under acidic conditions. This finding could be the result of defects in the Pt nanoporous solid (unlikely) or it could be the result of ethanol exhibiting a unique affinity for each of the exposed facets of the Pt electrodes. In other words, the relative electro-catalytic efficiency of the Pt crystalline faces may be different for ethanol and methanol.[23,52,58-59] Another contributing factor may be the surface reconstruction that the different facets undergo when exposed to the electrolyte solution. Hydrogen adsorption from the solution can result in surface reconstruction, the degree of which is dependent on the crystalline face of the Pt.[55,60-61]

Pd/H_2SO_4: To complete the comparison between Pt and Pd under both basic and acidic conditions, we attempted the same experiments as described above at both nanoporous and planar Pd solids. The electro-catalytic oxidation of 1.0 M MeOH/1.0 M H_2SO_4 and 1.0 M EtOH/1.0 M H_2SO_4 aqueous solutions were examined. In contrast to our results for the Pt surfaces, there were no detected oxidation peaks for either the forward or the reverse scans at Pd surfaces under acidic conditions. Chronoamperometric measurements of alcohol oxidation at both nanoporous and planar Pd solids resulted in near background current densities. Furthermore, the decay that was observed with the Pt surfaces was not detected with the Pd surfaces for either alcohol.

These results are not altogether that surprising, because it has been demonstrated that the oxidation of both methanol and ethanol is less favorable under acidic conditions than under basic conditions.[7,26,62] One reason given for this finding is that the kinetics of the oxidation reaction(s) are limited by reaction intermediates generated under acidic conditions that bind efficiently to Pt and Pd, serving to poison the catalytic metal surfaces.[63] Under basic conditions, this situation is less likely because of competition for metal active sites between methanol and hydroxide, resulting in fewer reactive sites being occupied for long periods without undergoing competitive displacement by a solution phase species.[64] The reason that there were no observable results for either the nanoporous or planar Pd solids could be due to the combination of slow oxidation kinetics and the absence of competitive binding at the active catalytic sites.

Pt vs. Pd: Comparing our results for the Pt and Pd catalysts, we find that the Pt nanoporous solid produced higher current densities for methanol oxidation while the Pd nanoporous solid produced higher current density for ethanol oxidation (Figures 3.9, 3.10). For both metals, the nanoporous solid structural motif provided a higher current density than the corresponding planar metal electrode, demonstrating in both cases that there is a structural and morphological component to the catalytic behavior of these metals, with the morphology-dependence of Pt being more pronounced than for Pd. Studies on the effect of contamination on the electrodes were performed using chronoamperometry, and they showed that nanoporous Pt is catalytically more stable for the oxidation of methanol than it is for the oxidation of ethanol, while the reverse is true for the Pd nanoporous solid under basic conditions. This finding is in agreement with literature reports on the behavior of Pt and Pd catalytic systems.[7,56] The overall tolerance for CO, shown by the anodic peak ratio of the forward and reverse scans, was greatest for nanoporous Pd, although the greatest increase in the ratio between the nanoporous solid and the planar substrate was with Pt for methanol in sulfuric acid. Thus, both Pt and Pd demonstrate enhanced catalytic behavior for the oxidation of alcohols in a nanoporous solid structural format.

In comparing Pt under acidic and basic conditions, our data suggest that the surface of the nanoporous Pt solid may rearrange to produce a more catalytically active surface under acidic conditions. We found that, in correspondence with our data under acidic conditions, that Pt under basic conditions exhibits higher current densities than for

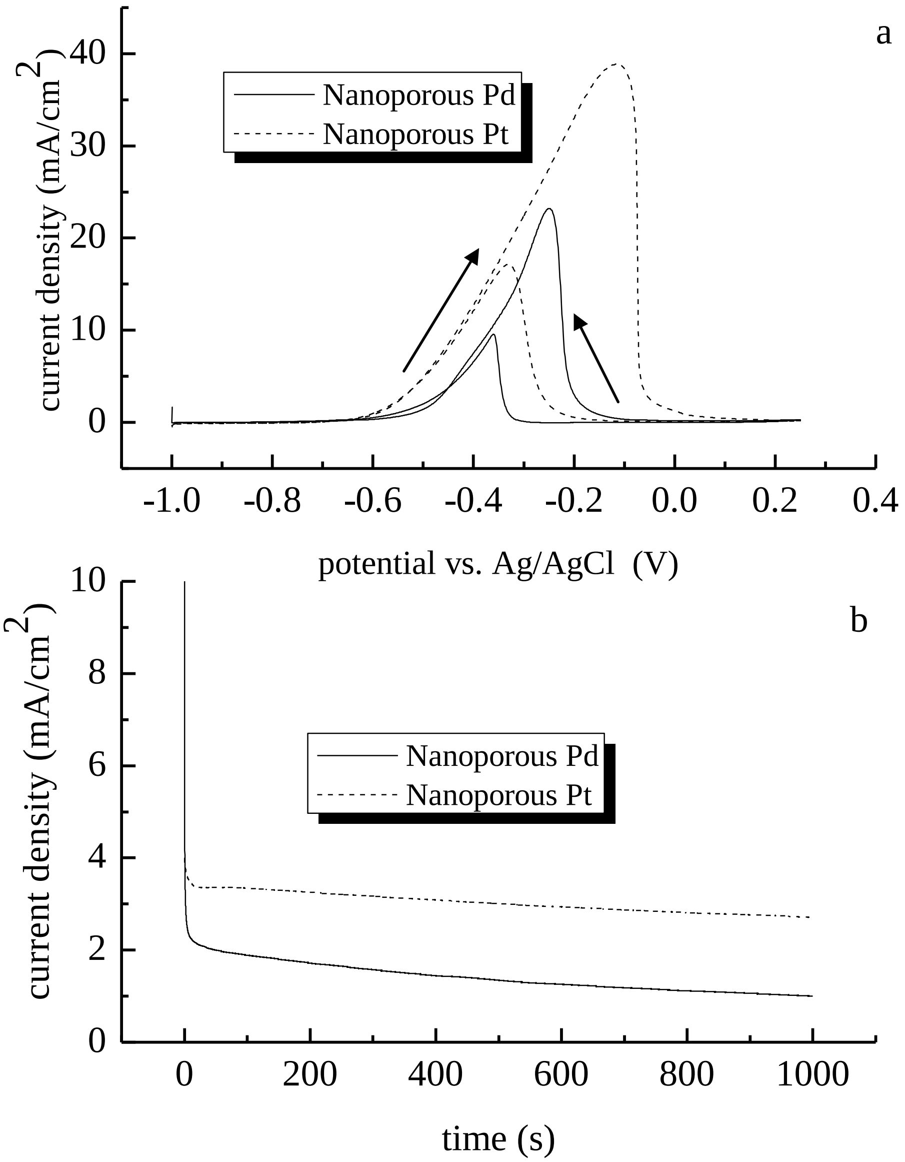

Figure 3.9: Comparison of electrocatalytic response of Pt and Pd nanoporous solids. (a) Cyclic voltammograms of 1.0 M MeOH/1.0 M KOH aqueous solution at a scan rate of 10 mV/s. (b) Chronoamperometric scans of 1.0 M MeOH/1.0 M KOH at a potential of -0.355 V.

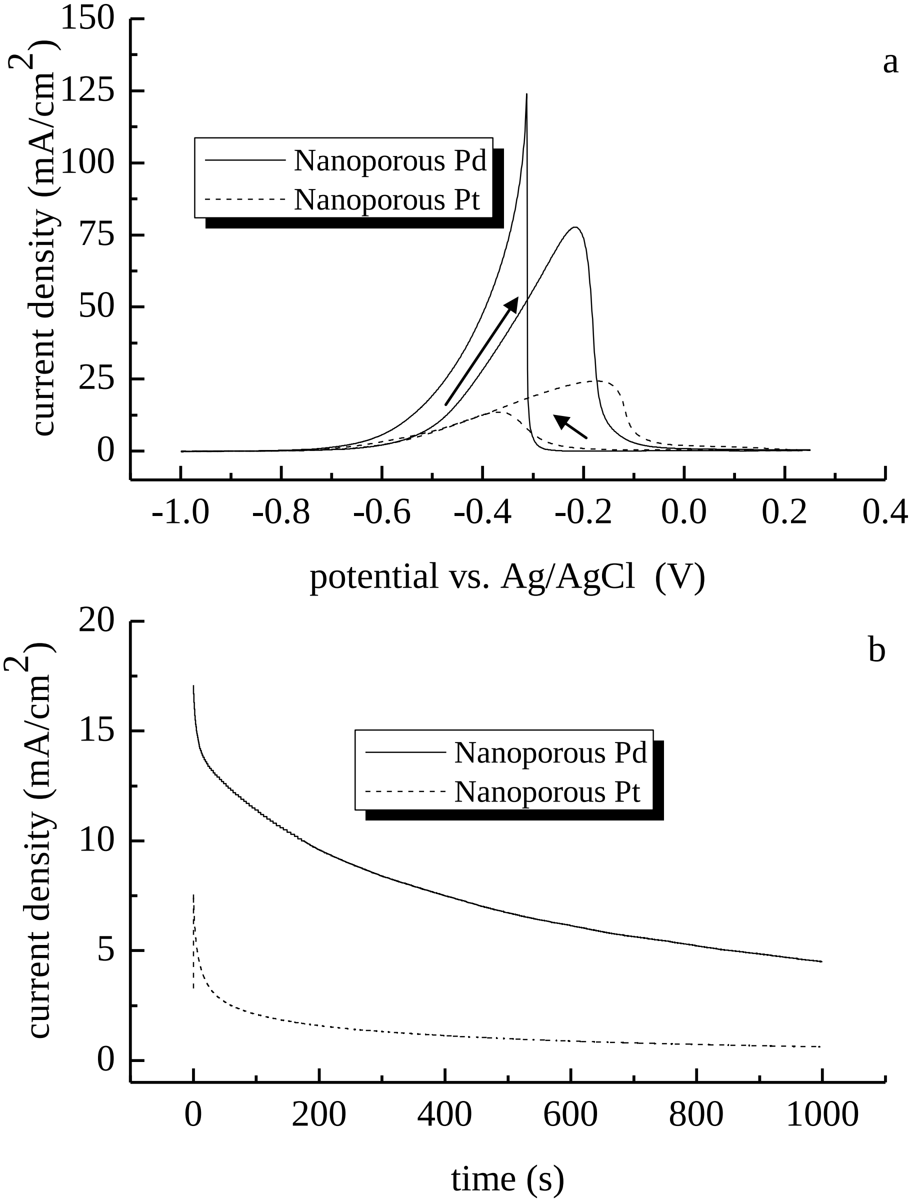

Figure 3.10: Comparison of electrocatalytic response of Pt and Pd nanoporous solids. (a) Cyclic voltammograms of 1.0 M EtOH/1.0 M KOH aqueous solution at a scan rate of 10 mV/s. (b) Chronoamperometric scans of 1.0 M EtOH/1.0 M KOH at a potential of -0.355 V.

the corresponding planar solid electrode. This finding may be due to different facets of Pt that were exposed during deposition onto the nanoporous solid scaffold. This effect is more pronounced with the Pt nanoporous solid due to the different reactions that can take place on the different surfaces. With the Pd structures, the reactions of both methanol and ethanol have been found to be the same on both Pd(110) and Pd(111).[57]

Conclusions

Nanoporous solids made from a silica nanosphere template and the electrodeposition of either Pt or Pd metal offer higher electro-oxidation current densities for both methanol and ethanol under basic conditions relative to the corresponding planar metallic substrates. The nanoporous solids also exhibit enhanced catalytic stability relative to the planar solid, as seen by chronoamperometry measurements. The current density enhancement seen for Pt nanoporous solids was more pronounced under basic conditions than acidic conditions, which is an expected result. The catalytic activity of Pd was found to be higher for ethanol than for methanol, with Pt producing higher catalytic efficiency for methanol. With the enhanced catalytic activity of nanoporous solids having been demonstrated, work is underway to determine the fundamental basis for this enhancement. Our initial work for this determination is discussed in part in Chapters 4, 5 and 6. We also anticipate that the use of a flow-through structural format for nanoporous solids will allow the intrinsic surface area enhancement for this class of materials to be realized, the possibility of which will be discussed in Chapter 7.

CHAPTER 4

ELECTROCATALYTIC OXIDATION OF 1,2-PROPANEDIOL AT NANOPOROUS AND PLANAR SOLID PT ELECTRODES

Introduction

As mentioned in Chapter 1, there are a number of potential applications for nanoporous materials, ranging from chemical separations[16-18] to electro-catalytic processes.[19-20] The work discussed in Chapter 3 demonstrated that nanoporous metal (Pt and Pd) structures exhibit higher electro-catalytic oxidation current densities for methanol and ethanol under basic conditions than the corresponding planar solid metal.[65] In that work, the nanoporous structures were formed using colloidal crystal templates made of silica nanospheres, and the reason for the alcohol oxidation current density enhancement we observed was not resolved fully.[65] Because the earlier work reported enhanced current density, the effect is not simply an enhancement in electrode surface area. There is the possibility of a geometrically based enhancement in catalytic reaction efficiency, which we describe below, but the distinction between electrode geometry and metal morphology[52-54] as the primary cause of the observed enhancement remained unresolved in our initial work.[65] The primary purpose of the work described in this chapter is to address this issue.

Electro-catalysis of simple organic molecules is becoming increasingly important in areas such as the development of alternative fuel sources.[66] The importance of alcohol electro-catalytic oxidation lies in the central role this process plays in the operation of fuel cells. Before nanoporous solids can be utilized to full advantage for electro-catalytic oxidation, the mechanism of the enhancement we have observed[65] needs to be understood. Although the electro-catalytic oxidation of methanol and ethanol have been examined extensively,[7,22,26,62] there has been much less effort on the study of longer chain alcohols and diols. The structure of diols, with two oxidatively accessible groups, can potentially provide some insight into the factors relevant to the electrocatalytic oxidation of hydroxyl-containing species. We have studied the electro-catalytic oxidation of 1,2-propanediol at nanoporous and planar solid Pt electrodes and we find that the cyclic voltammetric response of this diol depends on electrode morphology. With the oxidation of any alcohol there will be reaction products, and the identity and relative amount of these products will reflect the reaction pathway followed by the electro-catalytic oxidation. Certain of these reaction products will bind to the electrode, producing a voltammetric response and potentially poisoning the catalytic surface sites. Both of these effects will be mediated by the catalyst used and its morphology. Planar Pt electrodes have been used to study the electro-catalytic oxidation of 1,2-propanediol in both acidic and basic conditions,[67-69] and it is known that alcohols exhibit more efficient electro-catalytic oxidation under basic conditions.[7] We are interested in comparing the electro-catalytic oxidation of 1,2-propanediol at nanoporous and planar solid Pt electrodes. Our data are consistent with the reaction efficiency and pathway being influenced by the presence of higher order crystal faces at the electrode.

Experimental

Nanoporous Solid Fabrication: The construction of nanoporous Pt has been detailed previously,[65] and we recap the essential aspects of the synthesis here. Full details on the procedure can be found in the previous chapters. Silica spheres of *ca*. 450 nm diameter were synthesized in-house using a modified Stöber method[12-13,27-28] and deposited on a gold substrate by vertical withdrawal from an ethanolic solution of nanospheres at a rate of 0.34 µm/s (SDI Nanodip Coater). The resulting silica template was sintered at 200°C for two hours to enhance the integrity of the colloidal crystal structure prior to Pt deposition.

Electrodeposition of Pt was performed using a CHI650A electrochemical bench, in a three electrode configuration with a 3M Ag/AgCl reference electrode (E_0 = 0.210 V *vs.* SHE), a Pt counter electrode, and the silica nanosphere/gold substrate as the working electrode, the details of which can be found in Chapter 2. An insulating mask was used to control the area of deposition on the substrate. The same procedure was also used to deposit Pt on planar gold substrates. Following electrodeposition, the silica nanosphere template was removed by immersion of the substrate in a 10% (v/v) HF solution for *ca*. 15 minutes. It is important to note that while the diameter of the Si nanospheres is *ca*. 450 nm, the openings between the voids are much smaller, being on the order of 20% of the diameter of the templating nanospheres,[13] or roughly 90 nm. The size of the openings is a consequence of contact points between the nanospheres preventing deposition of Pt.

Characterization: The nanoporous solid was characterized using a JEOL 6400 scanning electron microscope (Figure 2.14). The electro-active surface areas of both the nanoporous and planar substrates were determined electrochemically using cyclic voltammetry and a solution of 1.0 M H_2SO_4 (Sigma-Aldrich). The potential was cycled between 0.25 V and 1.25 V (vs. Ag/AgCl), using Pt wire as the counter electrode and either planar solid or nanoporous Pt as the working electrode. The area of the adsorption/desorption hydrogen peaks (the Coulombic charge of hydrogen desorption, Q_H) can then be used to determine the electrochemically active surface area (A), along with the charge associated with the adsorption of a monolayer of hydrogen, so that $A = Q_H/210\ \mu C\ cm^{-2}$.[49-51] For our samples, we recovered $A = 2.74\ cm^2$ for the planar electrode and $A = 3.11\ cm^2$ for the nanoporous electrode.

1,2-Propanediol Oxidation: All electrochemical experiments were conducted at 20°C. Aqueous solutions of 1.0 M 1,2-propanediol (Jade Scientific), 1.0 M hydroxyacetone (Sigma-Aldrich), 1.0 M methylglyoxal (Sigma), and 1.0 M pyruvic acid (Sigma) were made with 1.0 M KOH(*aq*). All solutions were deoxygenated with nitrogen gas before use. For the cyclic voltammetry experiments the potential was cycled between -1.0 and 0.65 V (*vs.* Ag/AgCl) at a scan rate of 10 mV/s unless specified otherwise. Scans were initiated at -1.0 V. Chronoamperometry experiments were performed at -0.355 V (*vs*. Ag/AgCl), stepped from 0.0 V at the start of the experiment.

Results and Discussion

The previous report of enhanced electro-catalytic current density for alcohol oxidation with nanoporous Pt structures is significant, but the reason(s) for this enhancement remain to be understood fully. Two possible reasons for the observed current density enhancement with nanoporous solids are electrode geometry and morphology. We have examined the electro-catalytic oxidation of 1,2-propanediol in an effort to resolve which of these issues dominates. We consider the basis for each of these enhancements individually.

Geometric enhancement: Nanoporous solids offer the potential for enhanced catalytic activity based on the length scales characteristic of such structures. To illustrate this point, we use the example of a fluid flowing through a nanoporous solid structure. The reason we have chosen a flow-based example is because it is a facile means of controlling the exposure time of the reactant to the catalyst. We are interested in determining the dependence of contact time between reactant molecules and the catalytic surface on the interior of the nanoporous solid. For a 1 cm^2 geometric area nanoporous solid, with fluid flow through the nanoporous solid at a rate of 1 cm^3/min, the fluid velocity is 0.0167 cm/s. The diameter of the nanoporous solid voids determines the residence time of a molecule within the void, and during this residence time the molecule will exhibit diffusional motion. The diffusion length is given by $2(Dt)^{½}$ where D is the diffusion coefficient. We take D to be 1.5×10^{-5} cm^2/s for methanol in water, as an example.[70] The diffusion length of the reactant molecule is an average distance that the molecule travels while in the void space. The catalytic reaction requires contact between the metal surface and the reactant molecule, so the diffusion length divided by the diameter of the nanopore void will provide a relative measure of the number of molecule-surface interactions that occur during the passage of the molecule through the nanopore. A plot of $2(Dt)^{½}/d$ vs. nanopore diameter, d, provides an estimate of the probability of a catalytic reaction occurring as a function of the void size within the nanopores (Figure 4.1). This plot indicates that the probability of catalytic reaction increases markedly with decreasing nanopore void size, and thus provides one means to account for current density enhancements associated with the nanoporous solid electrodes (*vide infra*).

Morphological issues: Another key issue with the use of nanoporous solids vs. planar metal is the distribution of metal crystal faces at the surface of each structure. It is typically the case that planar Pt deposits primarily with the (100) crystal face exposed.[71] The presence of curvature and edges at the holes between individual voids in nanoporous Pt allows for different crystal faces to be present. It is not known, *a priori*, whether a given crystalline face of Pt will exhibit a higher or lower catalytic reactivity than Pt(100), but it is known that the catalytic reaction efficiency of a given metal surface depends on the crystalline face[66,68] and, in general, higher index surfaces are more reactive.[72-74] Owing to the structure of the nanoporous solid, the characterization of the crystalline face distribution of this type of material is difficult at best. For monofunctional species, discerning crystal face-dependent reaction efficiencies is likely not possible under our experimental conditions, because of the need to make absolute current density comparisons and the sample-to-sample variations in the nanoporous Pt. A bifunctional

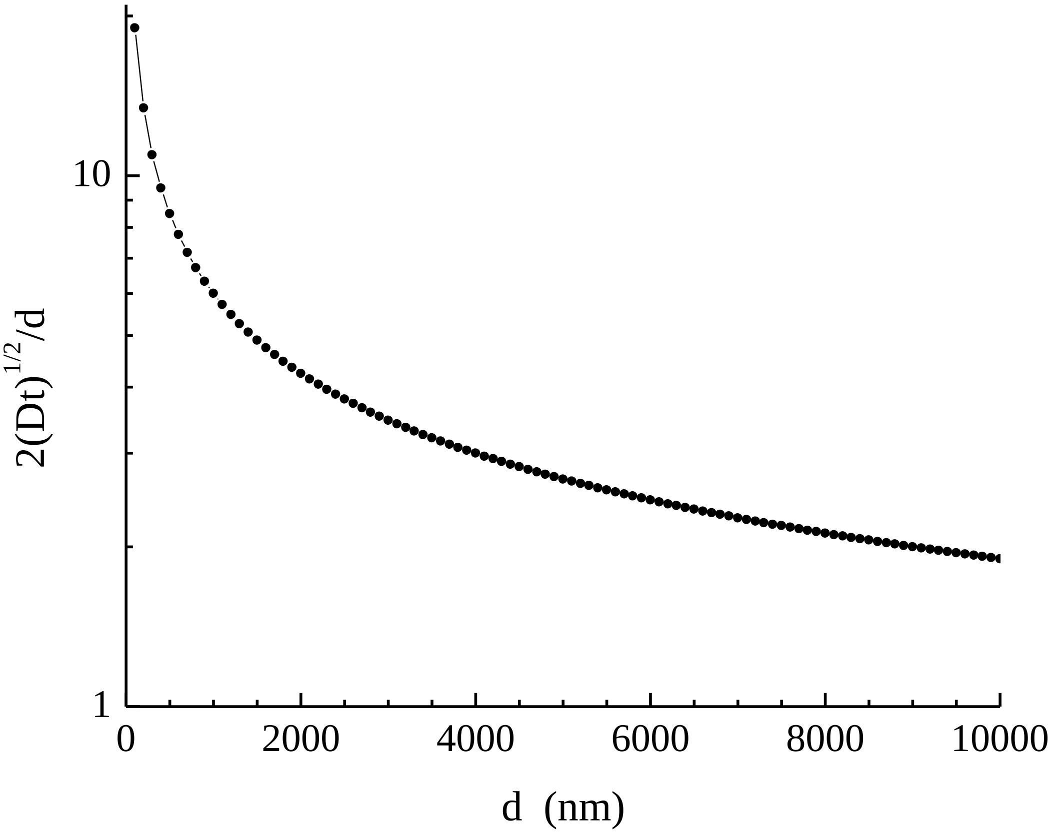

Figure 4.1: Plot of $(2Dt)^{1/2}/d$ *vs.* d, where D is the reactant diffusion coefficient and d is the diameter of the void spaces in the nanoporous solid structure.

molecule, however, with two reactive sites may prove to be a useful means of identifying the presence of specific crystalline face(s) that possess the geometric properties that allow for preferential surface-molecule interactions. This assertion is based on the *ansatz* that a two-point surface binding of the reactant will lead to a different catalytic reaction efficiency than for reactants that interact with the Pt surface at a single site (*i.e.* with only one –OH group).

Nanoporous vs. Planar Pt: The first step in evaluating nanoporous and planar solid Pt is to compare the cyclic voltammograms of 1,2-propanediol in KOH(*aq*) using the two Pt structures as electrodes (Figure 4.2). These data reveal a noticeable difference in CV form for the nanoporous and planar solid Pt substrates. This difference is more pronounced than any of the data reported previously for methanol and ethanol,[22,65] suggesting the importance of reactant and substrate steric issues (*e.g.* existence of surface defect sites and step edges, distance between and orientation of diol hydroxyl groups) in determining catalytic efficiency. In contrast to methanol and ethanol, 1,2-propanediol produces two oxidation waves for nanoporous Pt and one wave with a poorly-defined shoulder for the planar solid electrode. The two peaks seen for the nanoporous Pt electrode could be either the result of two oxidation steps, one for each hydroxyl group, or the second wave could result from an oxidation product of the first oxidation reaction (Scheme 4.1).[66,68-69,75-77] On the reverse scan, oxidation of the initial reaction products is seen, similarly producing two waves for the nanoporous Pt and a single wave at -0.292 V for the planar Pt substrate. For the nanoporous Pt electrode, the second forward

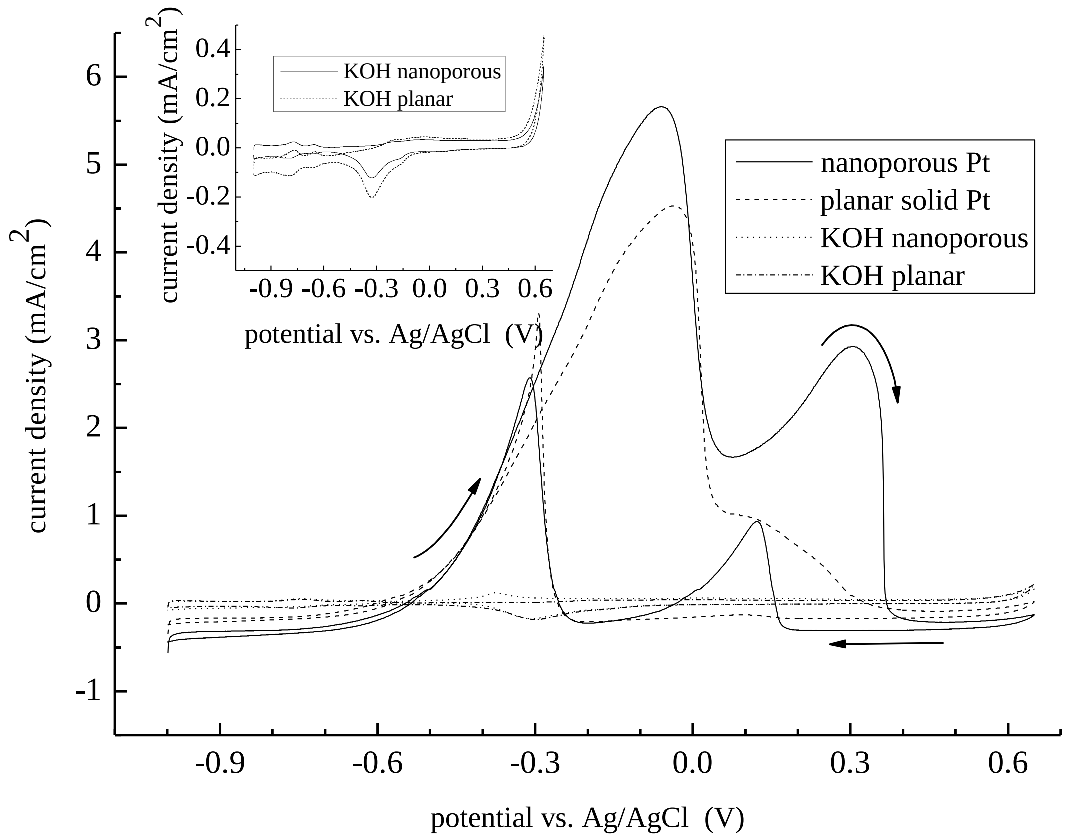

Figure 4.2: Cyclic voltammograms of 1.0 M 1,2-propanediol/1.0 M KOH aqueous solution, acquired at a scan rate of 10 mV/s, for nanoporous Pt (solid line) and planar solid Pt (dashed line). Arrows indicate potential scan direction. Inset: Background scans in KOH for both nanoporous Pt and planar solid Pt on an expanded current scale for comparison purposes.

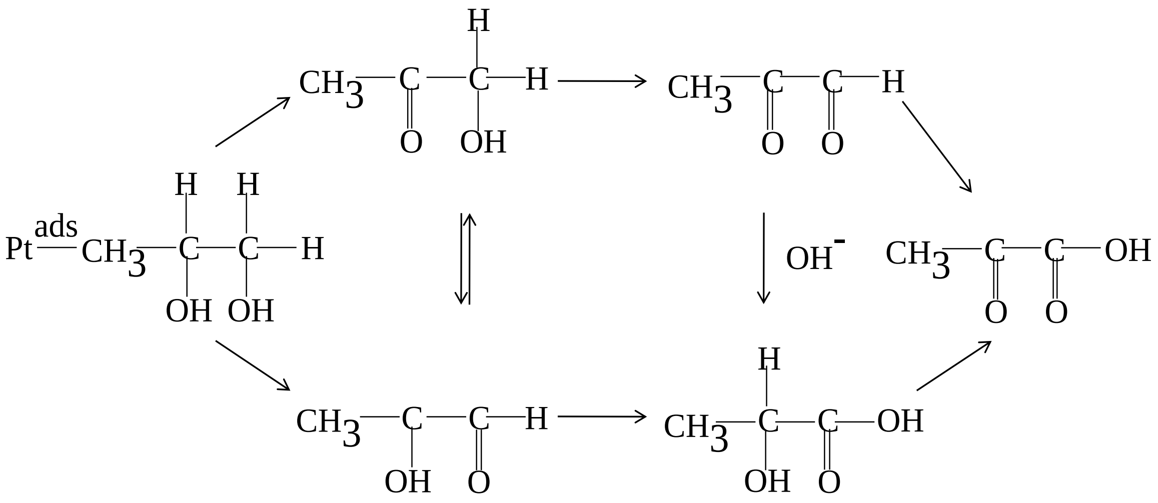

Scheme 4.1: Reaction pathways for the electrocatalytic oxidation of 1,2-propanediol.

oxidation wave also exhibits a product oxidation wave on the reverse scan, a feature that is missing for 1,2-propanediol at the planar solid Pt electrode.

In addition to the difference in the electro-catalytic oxidation behavior of the two substrates, there are indications that nanoporous Pt is more catalytically active than planar solid Pt based on the more negative peak potentials observed for the oxidation waves with the nanoporous substrate (Table 4.1).[25,51] Onset potentials were determined by overlapping the CVs of the substrates with and without 1,2-propanediol present,[78-79] and indicate only a slight difference between the nanoporous Pt and planar solid Pt. The values for onset potential and peak potential observed for both the nanoporous and planar Pt are shifted negative relative to the corresponding literature data,[69] indicating that the Pt electrodes we have constructed are comparatively efficient catalysts for the oxidation of 1,2-propanediol. The nanoporous Pt also produces slightly higher current densities than those measured for planar solid Pt and reported in the literature.[69] The differences in CVs for the two Pt morphologies reported in Figure 4.2 and the enhanced current density for nanoporous Pt point collectively to energetically and/or sterically favorable interactions between 1,2-propanediol and the nanoporous Pt surface.

Our results are reported in terms of current density, calculated using the electrochemically determined surface areas of the electrodes, so that the comparison between the nanoporous and planar Pt substrates can be made directly. The nanoporous Pt substrate produces a current density for 1,2-propanediol oxidation that is 1.3 times that observed for the first oxidation peak seen for the planar Pt substrate, and the corresponding current density enhancement for the second oxidation peak is almost a

Table 4.1: Comparison of Electrochemical Performance of 1,2-Propanediol. Current densities are reported as the average of at least 3 scans with uncertainty of ± 1σ. Uncertainties in the reported potentials are *ca*. 5 mV.

Platinum Substrate	Onset Potential (V)	Peak Potential I (V)	Peak Potential II (V)	Current Density PI (mA/cm^2)	Current Density PII (mA/cm^2)
Nanoporous	-0.540	-0.060	0.305	5.52 ± 0.13	3.46 ± 0.49
Planar	-0.595	-0.036	0.110	4.39 ± 0.25	0.95 ± 0.15

factor of four. We note that this enhancement is somewhat less than was observed for the oxidation of methanol under basic conditions,[65] suggesting a reactant-dependence to the enhancement. Chronoamperometry measurements for both electrodes were conducted at -0.355 V (Figure 4.3) to examine the poisoning of the Pt substrates during electro-oxidation of 1,2-propanediol. Following the initial application of -0.355 V, there is a steady decrease in current density for both the nanoporous and planar solid electrodes, and for both a plateau is reached at long times. Although the loss of current density for both substrates is the same (97%), the higher initial and final currents of the nanoporous substrates suggest that the nanoporous Pt is more catalytically active than the planar solid. Furthermore, a higher initial current density is displayed by the nanoporous Pt indicating either a greater number of active sites available per unit area of Pt or a more rapid turnover rate per site in the nanoporous electrode.[25]

The Effect of Scan Rate. The electro-oxidation kinetics of 1,2-propanediol can be examined through the scan rate dependence of CV data. For both nanoporous and planar solid Pt, the current density of the first oxidation peak increases with increasing scan rate. However, the oxidation of the initial reaction products seen in the reverse scan produces current densities that are substantially independent of scan rate. For both the nanoporous and planar solid Pt, there is a scan rate-dependent shift of the potentials for all four peaks observed (Figure 4.4). This finding is consistent with reactions that are not diffusion-limited. For both nanoporous and planar solid Pt, the dependence of current on the square root of the scan rate shows that the oxidations are diffusion-limited at lower scan rates, but at higher scan rates there appears to be the onset of saturation of the current

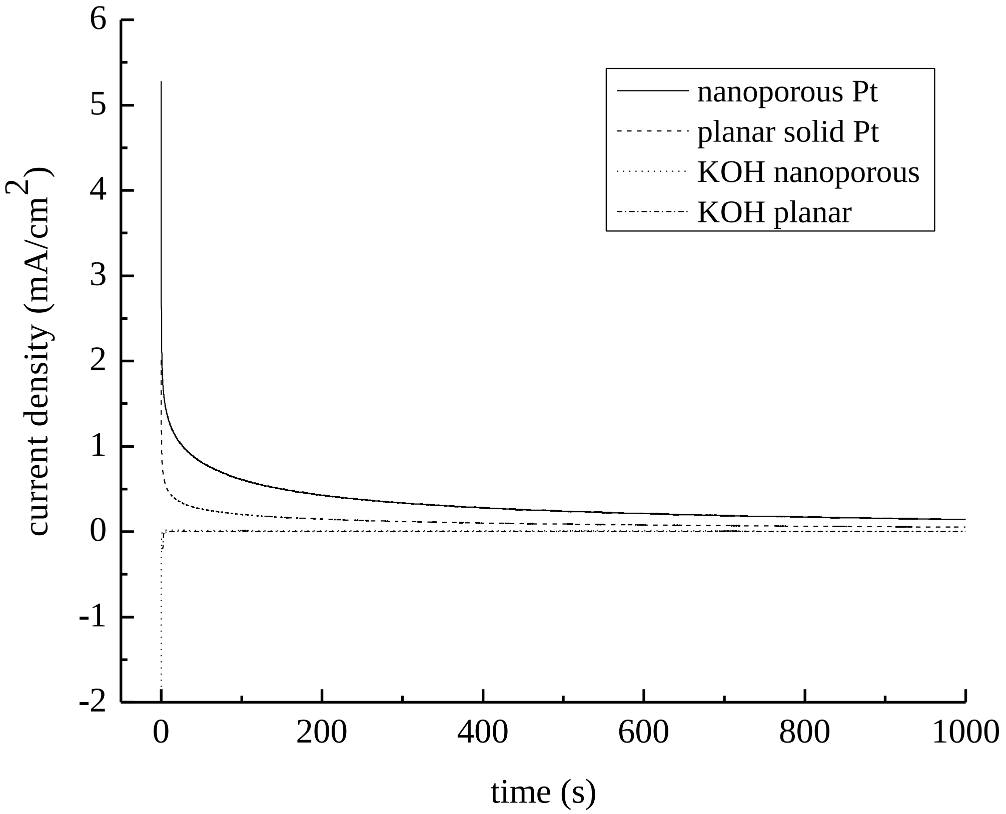

Figure 4.3: Chronoamperometric scans using nanoporous Pt (solid line) and planar solid Pt (dashed line) of 1.0 M 1,2-propanediol/1.0 M KOH acquired at a potential of -0.355 V vs Ag/AgCl.

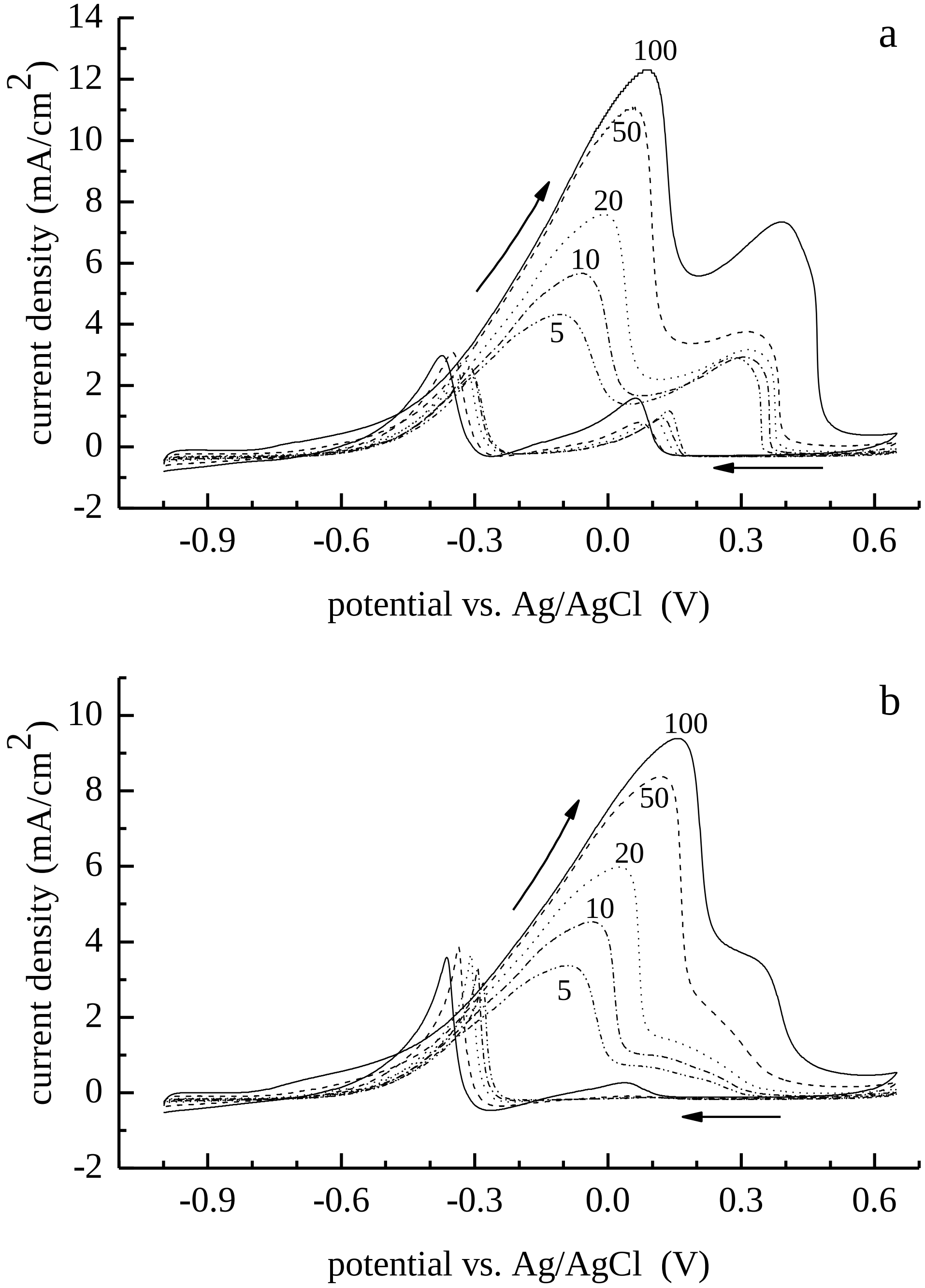

Figure 4.4: Effect of CV scan rate on oxidation waves for 1.0 M 1,2-propanediol/1.0 M KOH at scan rates as indicated for (a) nanoporous Pt and (b) planar solid Pt electrodes. Arrows indicate potential scan direction.

density (Figure 4.5). This finding is consistent with earlier reports on 1,2-propanediol oxidation under acidic conditions,[68] where a rate determining step that mediates electron transfer involves both diffusion and adsorption.

Sequential Scans. The oxidation of 1,2-propanediol and its reaction products was examined by performing sequential CVs (Figure 4.6) for both the nanoporous and planar solid Pt electrodes. These data were acquired at a scan rate of 10 mV/s. For the nanoporous Pt electrode, (Figure 4.6a) there is a slight negative shift of the peak potentials and a decrease in the current density of the forward oxidation scans, but the functional form of the CV remains largely unchanged with sequential scans. The decrease in current density may be due to a slight poisoning of the surface by reaction products that accumulate with additional scans. The potential shift for planar solid Pt (Figure 4.6b) is also seen to be slightly negative, and with a small increase in current density, suggesting that the surface is not experiencing the same catalytic poisoning as is seen for the nanoporous solid. The difference in behavior for the two substrates is consistent with these two forms of Pt being characterized by a different distribution of crystalline metal faces.[72-74] It is interesting to note that the peak potential of the first forward oxidation peak stabilizes after 10 consecutive scans for planar solid Pt, but *ca.* 20 scans are required for the same stabilization to occur for nanoporous Pt. For both the nanoporous and planar solid Pt reverse scan peak at -0.30 V, neither the peak potential nor current density depend on the number of CV cycles. This finding indicates that the surface interaction of the oxidation product responsible for this peak does not depend on Pt surface organization as sensitively as 1,2-propanediol, and that the amount present is

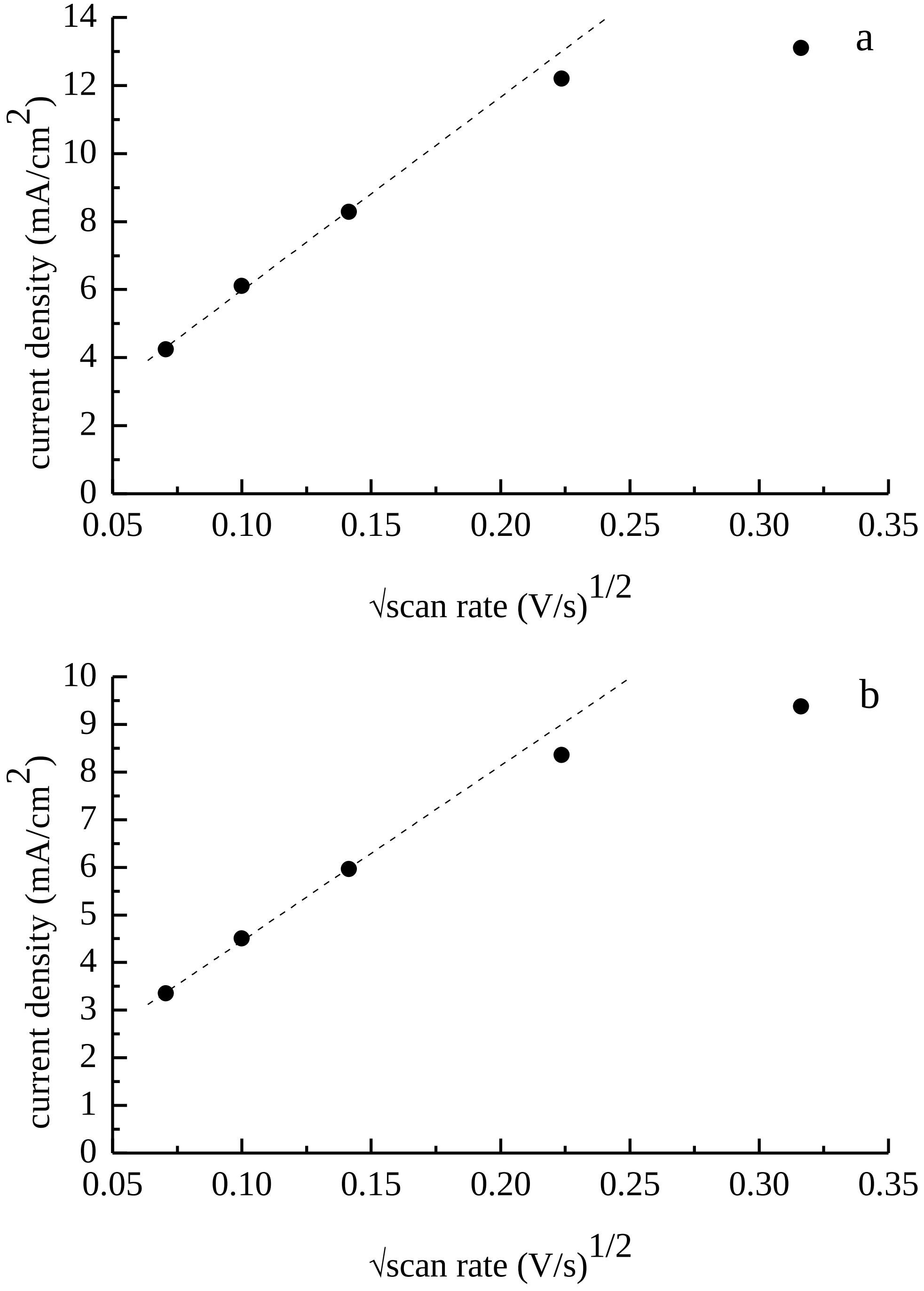

Figure 4.5: Current density *vs.* (scan rate)$^{1/2}$ for (a) nanoporous Pt and (b) planar solid Pt electrodes. The dashed lines are presented as guides to the eye.

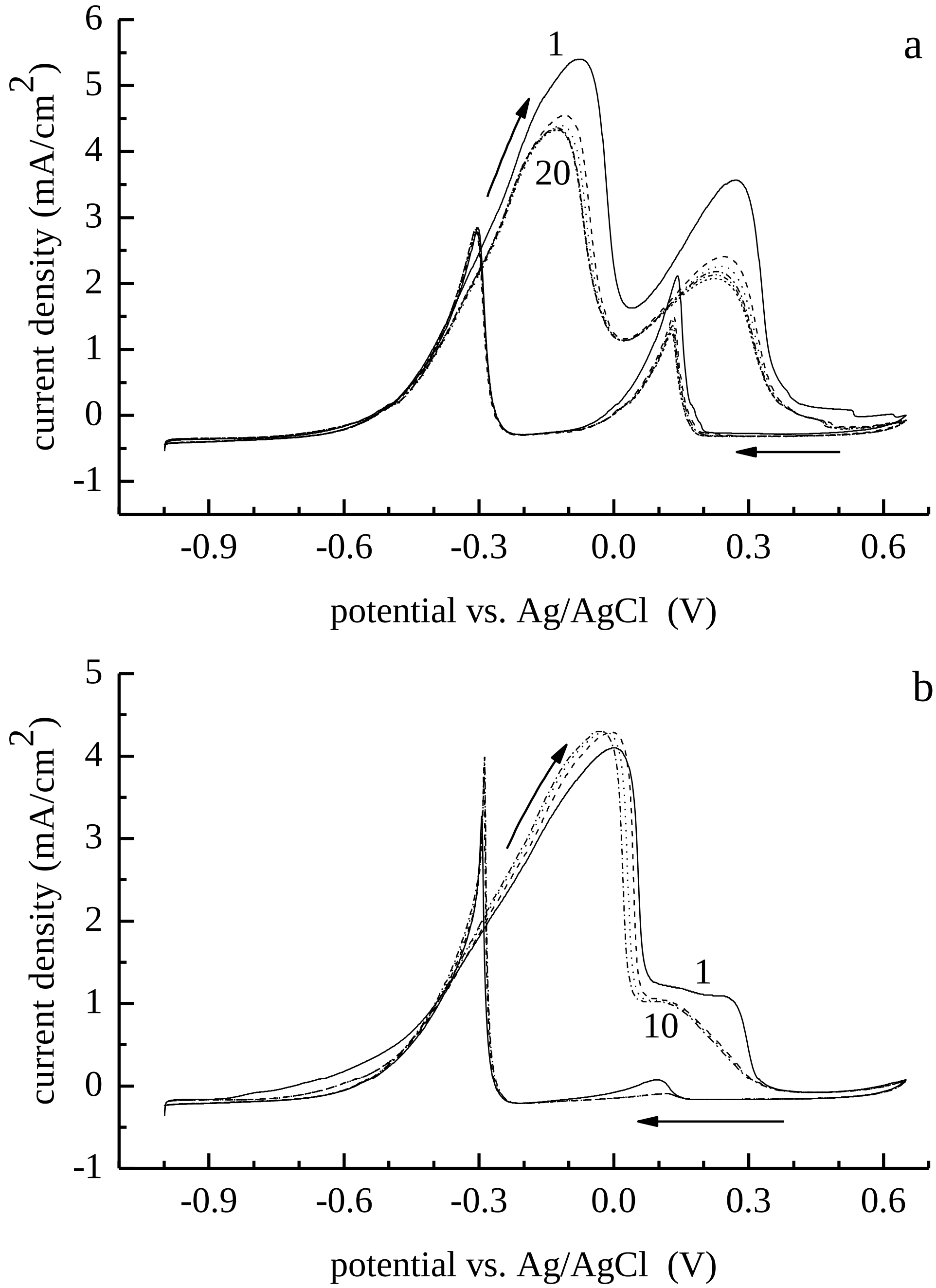

Figure 4.6: Consecutive scans of 1.0 M 1,2-propanediol/1.0 M KOH at a scan rate of 10 mV/s for (a) nanoporous Pt and (b) planar solid Pt. Arrows indicate potential scan direction.

comparatively constant. We assert that the initial reaction products adsorb onto the Pt surface, a hypothesis in agreement with the oxidation of these species not being diffusion limited. It has been determined previously that during continuous potential cycling, the number of available catalytic sites on Pt diminishes, and this finding is consistent with our forward scan cycling dependence.[54] The fact that the forward oxidation scans show a decreasing current density with number of scans while the reverse scans show an essentially constant concentration of reaction products suggests that the surface sites occupied by this reaction product are not the surface sites that are catalytic for 1,2-propanediol.

One point that is abundantly clear from the data presented in Figure 4.6 is that the form of the CVs is different for nanoporous and planar Pt. This difference remains to be explained fully but it is consistent with a different distribution of oxidation events at the electrode surface, possibly as a consequence of a different distribution of crystalline metal faces.[72-74]

Adsorption and Product Catalysis. The propensity of nanoporous and planar solid Pt to adsorb the reactant was evaluated electrochemically. Each substrate was cycled 10 times in a fresh solution of deoxygenated 1.0 M KOH after first being immersed in a solution of 1.0 M 1,2-propanediol for 30 seconds, and subsequently dipped in KOH solution. In comparing the first cycle from both nanoporous and planar solid Pt, there is a characteristic difference in reactant adsorption on the two surfaces (Figure 4.7). Although both electrodes exhibit a peak at *ca*. -0.4 V, the nanoporous Pt continues to exhibit a broad shoulder while the planar solid Pt produces a narrow peak. In addition,

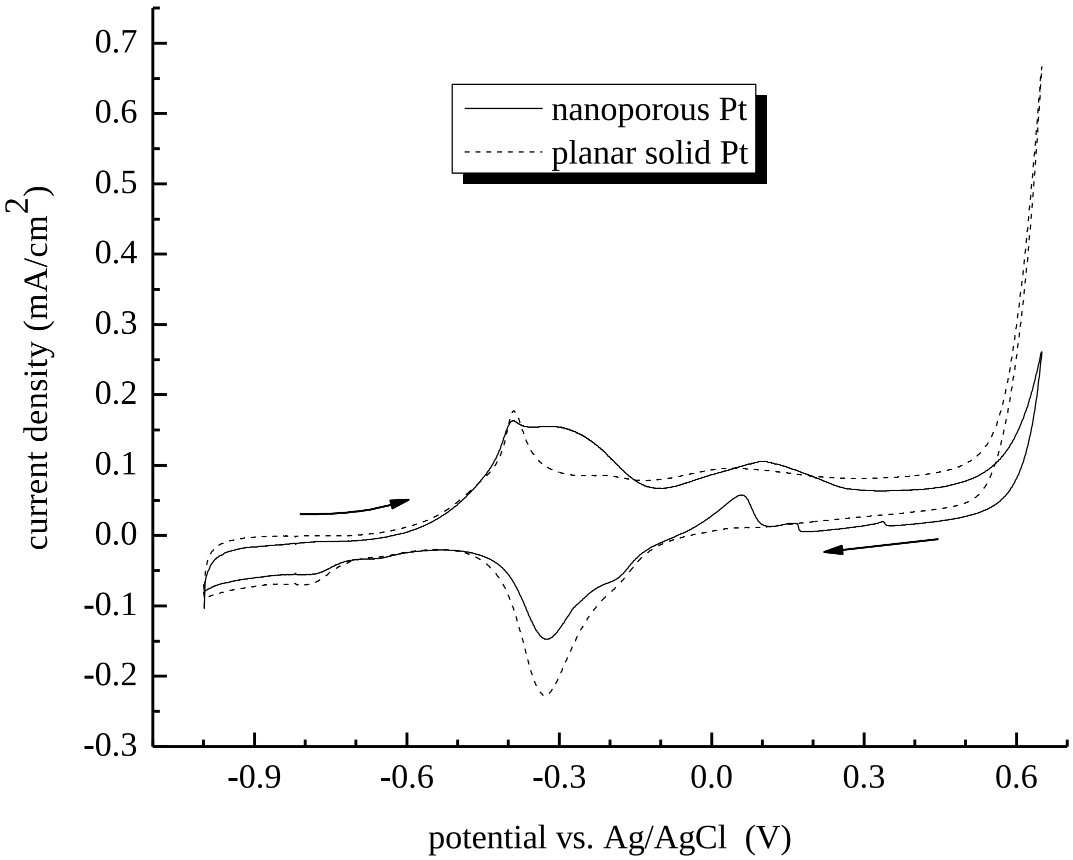

Figure 4.7: Single scan cyclic voltammograms of 1,2-propanediol at nanoporous Pt (solid line) and planar solid Pt (dashed line). CVs of the adsorbed reactant were acquired at a scan rate of 10 mV/s in solutions of 1.0 M KOH(*aq*). Arrows indicate potential scan direction.

the second forward oxidation peak is seen for the nanoporous Pt but not for the planar solid Pt. There are also reverse oxidation peaks seen for the nanoporous substrate but absent in CVs recorded for the planar solid Pt electrode. The reason for the different peak potentials for the two surface morphologies may be related to the catalytic activity of the surfaces, as has been seen with other alcohol catalysis on Pt.[52-54] Another point of interest is how the current density rises rapidly at *ca*. 0.46 V for the planar solid Pt electrode. Although there is a corresponding increase with the nanoporous Pt electrode, it occurs at *ca*. 0.496 V and is not as prominent as that seen for the planar solid Pt. This feature may be due to the presence of hydroxide from the electrolyte solution and is seen more prominently with the planar solid Pt, which may be the result of the morphological differences between the planar solid Pt and nanoporous Pt.

Examining the sequential CV scans for the samples used in Figure 8 for both the nanoporous and planar solid Pt substrates can provide insight into the evolution of the adsorbed reaction products (Figure 4.8). To aid in the assignment of the oxidation peaks observed with the sequential cycles of adsorbed 1,2-propanediol, some of the putative electro-catalytic reaction products[77] were subjected to CV cycling after adsorption onto a nanoporous Pt electrode (Figure 4.9). For most of the reaction products there are two forward oxidation peaks, but adsorption of these species onto the nanoporous Pt yields current densities somewhat lower than that measured for 1,2-propanediol. This finding is consistent with the presence of two hydroxyl groups on the reactant giving rise to stronger interactions with selected faces of the platinum surface. The peak potentials we record for hydroxyacetone are more negative than those observed for 1,2-propanediol,

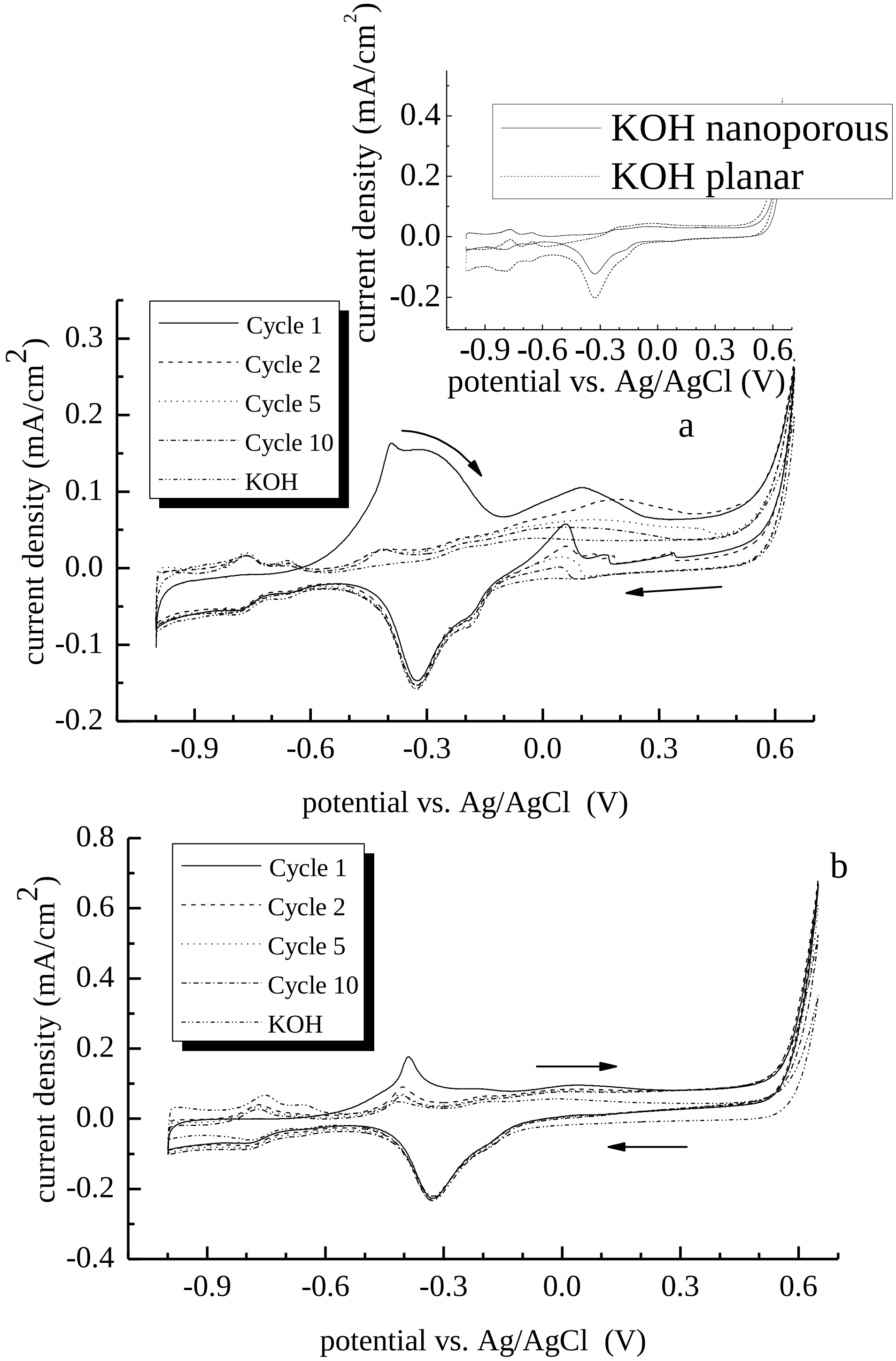

Figure 4.8: Sequential CV scans of the electrodes containing adsorbed 1,2-propanediol, acquired under the same conditions as the CV scans shown in Figure 4.7. (a) nanoporous Pt and (b) planar solid Pt. Arrows indicate potential scan direction. Inset: CV scans after 10 cycles in solely KOH for both nanoporous Pt and planar solid Pt.

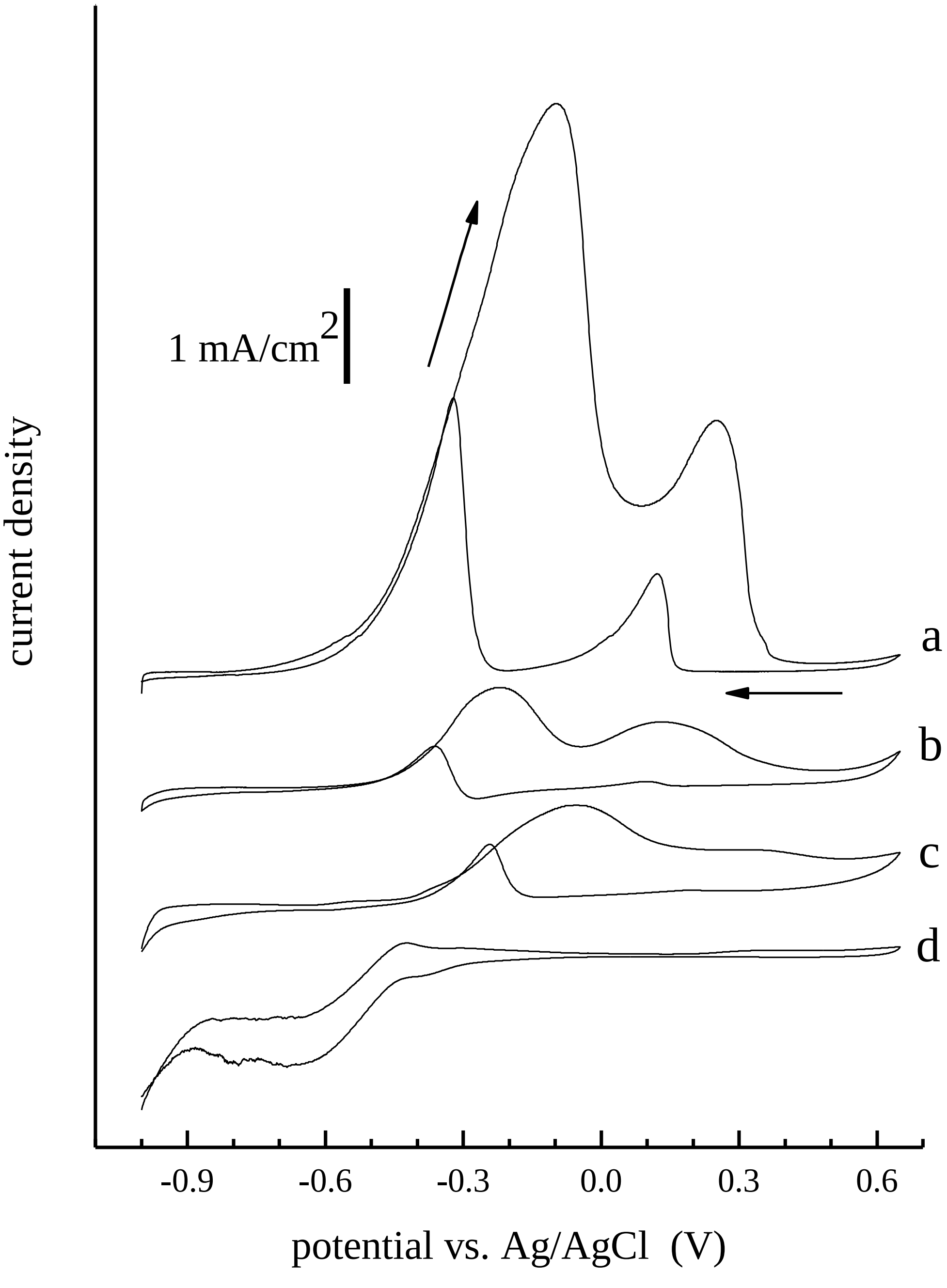

Figure 4.9: Cyclic voltammograms of putative reaction products. (a) 1.0 M 1,2-propanediol/1.0 M KOH, (b) 1.0 M hydroxyacetone/1.0 M KOH, (c) 1.0 M methylglyoxal/1.0 M KOH and (d) 1.0 M pyruvic acid/1.0 M KOH. All CVs were recorded at a scan rate of 10 mV/s using nanoporous Pt solid. Arrows indicate potential scan direction.

while those of the methylglyoxal are more positive. These observations, along with the positions of the reverse oxidation peaks, indicate that the initial products of diol oxidation (hydroxyacetone and methylglyoxal, Scheme 4.1) are responsible for the peaks observed with the Pt nanoporous solid on sequential CV scans (*e.g.* Figure 4.6).

When examining sequential scans, the greatest difference between cycles is observed between the first and second cycle with the nanoporous Pt electrode. The shifting of the peak at -0.086 V to 0.185 V from the first to the second cycle indicates the presence of a product from the initial 1,2-propanediol oxidation (*i.e.* hydroxyacetone) that is subsequently oxidized. The presence of different species on the surface of the nanoporous Pt resulting from different reaction pathways would also explain the form of the reverse scan, with oxidation peaks that only occur in the CVs recorded with the nanoporous Pt electrode. The fact that the different electrode morphologies give rise to a different distribution of reaction products underscores the importance of the distribution of crystalline facets present on the different electrodes. It is tempting to speculate on the crystal face(s) that give rise to our findings based on the presence and spacing of the diol OH groups and geometric correspondence with various Pt crystal lattice site spacings. In principle, the lattice spacings that are characteristic of a given crystal face would allow for more or less efficient binding of the reactant on geometric grounds. Unfortunately, the details of the initial reactant binding step remain to be understood fully, and the reactant itself possesses sufficient degrees of freedom[80] to preclude a simple correspondence with a geometric model. For these reasons, we do not yet have a sufficient body of information to be able to evaluate the atomic-scale morphological differences between nanoporous and planar solid Pt. For both the nanoporous and planar solid Pt, the peak observed at *ca*. 0.40 V decreases over time, likely due to the depletion of 1,2-propanediol from the surface. This finding is consistent with the recovery of hydrogen adsorption region peaks on Pt with the loss of 1,2-propanediol.

Conclusions

Platinum nanoporous solids made from the electrodeposition of the metal around a silica nanosphere template offer a catalytic advantage over planar solid Pt for the electro-oxidation of 1,2-propanediol. While this enhanced catalytic behavior is somewhat less than that seen for the electro-catalytic oxidation of methanol under basic conditions,[65] the use of a vicinal diol and the difference in CV scans for the nanoporous and planar solid Pt electrodes indicate that these two electrodes are characterized by a different distribution of crystalline faces, with each crystalline face being characterized by a different electro-catalytic efficiency.[52-54,72-74] Comparing the oxidation of 1,2-propanediol and its reaction products shows that some products bind to Pt, with the binding efficiency depending on the morphology of the Pt. These data point collectively to the central role of metal morphology in mediating electro-catalytic efficiency and to the fact that the distribution of crystalline faces present in the nanoporous Pt is different than that of planar solid Pt. Future work will focus on the dependence of electro-catalytic activity of nanoporous solid Pt as a function of the size of the nanospheres used in the formation of the nanoporous metal.

CHAPTER 5

EXAMINING THE ELECTRO-CATALYTIC OXIDATION OF SELECTED DIOLS AT NANOPOROUS AND PLANAR PT ELECTRODES: PART I: REACTION MECHANISM(S)

Introduction

The electrocatalytic oxidation of small organic molecules, especially those derived from biomass, is taking on increasing significance, especially with regard to the operation of fuel cells. Although much of the work in this area focuses on methanol and ethanol, there is also a substantial effort aimed at understanding more complex species such as diols, because many diol species exist that could potentially be useful as energy sources. We are interested in diols because of their potential for interrogating chemical reaction processes at and near electrode surfaces. We have studied the electrocatalysis of 1,2-propanediol using nanoporous and planar solid Pt electrodes.[81] We found that the presence of two hydroxyl moieties gave rise to cyclic voltammograms that were different for the nanoporous and planar solid electrodes, suggesting a role for diols in probing electrode morphology. In this work we focus on a series of diols with a goal of understanding how the positions of the hydroxyl groups on the diols influence the electrocatalytic reaction pathways used as a function of electrode morphology. A key step in understanding the potential utility of diols for this purpose is to first resolve which reactions proceed under our experimental conditions. We compare cyclic voltammetry (CV) data for several diols at nanoporous and planar Pt electrodes. The oxidation waves we observe can be assigned based on literature precedent.

We have focused on nanoporous electrode materials because of their combined mechanical robustness and unique catalytic properties. Nanoporous metal structures are not new, and such materials have been investigated for their utility in chemical separations[16-18] and selected electrochemical applications.[19-20] We have used Pt as the metal of choice for our studies because of its ability to function as a catalyst for the electrochemical oxidation of alcohols under basic conditions.[65] It is known that the length of alcohol carbon chains and the position of the hydroxyl functionality have an influence on the efficiency of electrocatalytic oxidation. We are interested in understanding the interplay between electrode morphology and reactant structure in mediating the electrocatalytic oxidation of alcohols.[82-85]

In this work we have examined 1,2-butanediol, 2,3-butanediol, 1,3-propanediol, 1,3-butanediol and 1,4-butanediol. Our choice of reactants was based on the positions of the hydroxyl moieties, with a goal of elucidating the role of functional group position in determining reaction pathway(s). Our data point to the importance of hydroxyl group proximity and electrode morphology in determining the reaction(s) that proceed under basic conditions.

Experimental

Nanoporous Solid Fabrication: The fabrication of the nanoporous Pt electrodes used in this work has been described previously.[65] Briefly, silica spheres of *ca.* 450 nm diameter were synthesized in-house using a modified Stöber method.[13,27-28] The silica spheres were deposited on a gold substrate by vertical withdrawal at a rate of 0.34 µm/s from an ethanolic suspension (SDI Nanodip Coater). The resulting nanosphere assembly was sintered at 200°C for two hours to enhance the integrity of the colloidal crystal structure.

Platinum electrodeposition onto/into the nanosphere assembly was performed using a CHI604A electrochemical bench in a three electrode configuration with a Ag/AgCl 3M KCl reference electrode (E_0 = 0.210 V *vs.* NHE), a Pt counter electrode, and the silica nanosphere/gold substrate as the working electrode. Pt deposition was performed using a 10% w/w solution of H_4PtCl_6 (Fluka) and cycling the potential from -0.4 to 1.6 V ten times at a scan rate of 50 mV/s.[22] The physical region of deposition on the nanosphere assembly was controlled using an insulating mask. Subsequent to Pt deposition, the nanosphere assembly was immersed in a 10% (v/v) HF solution for *ca.* 15 min. to remove the silica nanosphere template. The same electrodeposition methodology was used to deposit Pt on bare gold to produce the planar solid Pt electrode.

Characterization: The resulting Pt nanoporous solid was examined by scanning electron microscopy (SEM, JEOL 6400). The SEM images (Figure 5.1) show the expected structure for a multi-layer inverse opal material. Cyclic voltammetry of a solution of 1.0 M H_2SO_4 (Sigma-Aldrich) was used to determine the electro-active

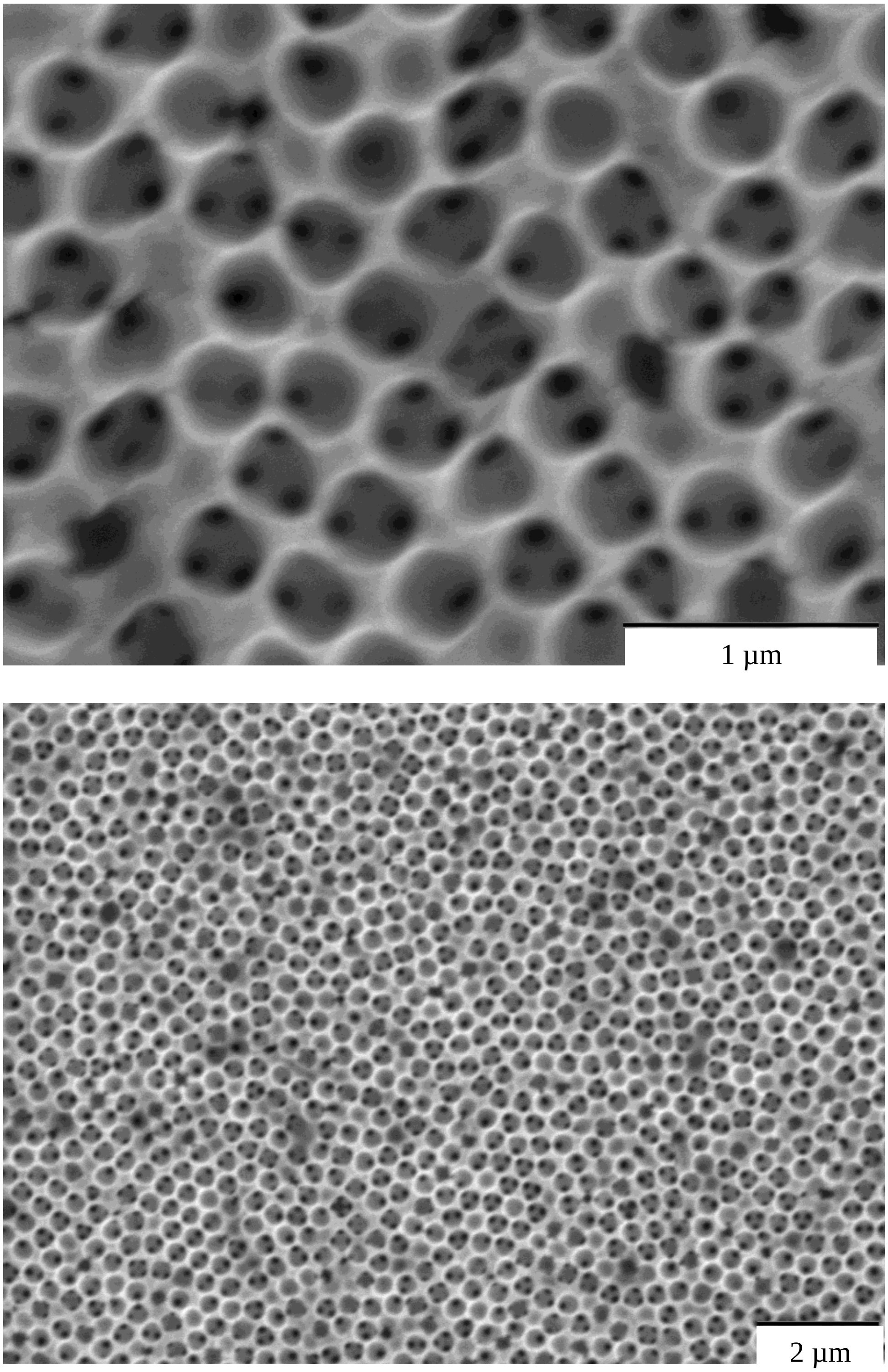

Figure 5.1: SEM micrographs of nanoporous Pt at two different magnifications. 450 nm diameter silica nanospheres were used in the construction of the nanoporous structure. Top panel 40,000X magnification, bottom panel 9500X magnification.

surface areas of both the nanoporous and planar substrates. For this determination, the potential was cycled between 0.25 V and 1.25 V (vs. Ag/AgCl 3M KCl), using the planar solid or nanoporous Pt as the working electrode and Pt wire as the counter electrode. The electrochemically active surface area (A) can be determined using the area of the hydrogen adsorption/desorption peaks (the Coulombic charge of hydrogen desorption, Q_H), along with the charge associated with the adsorption of a monolayer of hydrogen, so that $A = Q_H/210\ \mu C\ cm^{-2}$.[26,49-50]

Diol Oxidation: All reagents used were purchased in the highest purity grade available and used as received. All electrochemical measurements were made at 20°C. Aqueous solutions of 1.0 M 1,3-propanediol (Aldrich, 99.6%), 1.0 M 1,2-butanediol (Fluka, ≥98%), 1.0 M 1,3-butanediol (Sigma-Aldrich, ≥99%), 1.0 M 1,4-butanediol (Sigma-Aldrich, ≥99%), and 1.0 M 2,3-butanediol (Aldrich, 98%) were made with 1.0 M KOH (*aq*). All solutions were deoxygenated with nitrogen gas before use. The potential for the cyclic voltammetry experiments was cycled between -1.0 and 0.65 V (vs. Ag/AgCl 3M KCl) at a scan rate of 10 mV/s unless specified otherwise.

Results and Discussion

As noted in the Introduction, the electrocatalytic oxidation reaction(s) of selected alcohols and diols depend on the electrode morphology as well as the reactant identity. Because of the potential importance of this type of chemical process, we must understand the factors that influence the reaction pathway(s) and efficiency for compounds that may be derived from biomass. In this manuscript we focus on the reactions seen at nanoporous and planar Pt electrodes when electrocatalytic oxidation is carried out under basic conditions. Our data demonstrate that the proximity of diol hydroxyl groups to one another is an important factor in determining the reaction pathway. We have also shown (*vide infra*) that the morphology of the Pt electrode can serve to mediate the reaction pathway for certain reactants. We discuss below our findings for 1,3-propanediol and the four butanediols before considering broader conclusions that can be drawn from these data. We have organized the data according to the proximity of the reactant hydroxyl groups, because this structural feature appears to be an important factor in mediating the reaction pathway.

1,2-Butanediol and 2,3-Butanediol: The cyclic voltammograms of 1,2-butanediol (Figure 5.2a) and 2,3-butanediol (Figure 5.2b) in KOH exhibit substantial similarities. For both reactants, there are forward oxidation peaks at *ca.* -0.25 V and +0.25 V, with corresponding product oxidation waves seen at *ca.* 0.1 and -0.4 V on the reverse scans. We first consider the assignment of the peaks in terms of the relevant reactions. We show in Scheme 5.1 a reaction schematic consistent with the data. There are two primary reaction pathways; the first is sequential, step-wise oxidation of the two hydroxyl functionalities to produce a dione and the second is bond cleavage to produce two

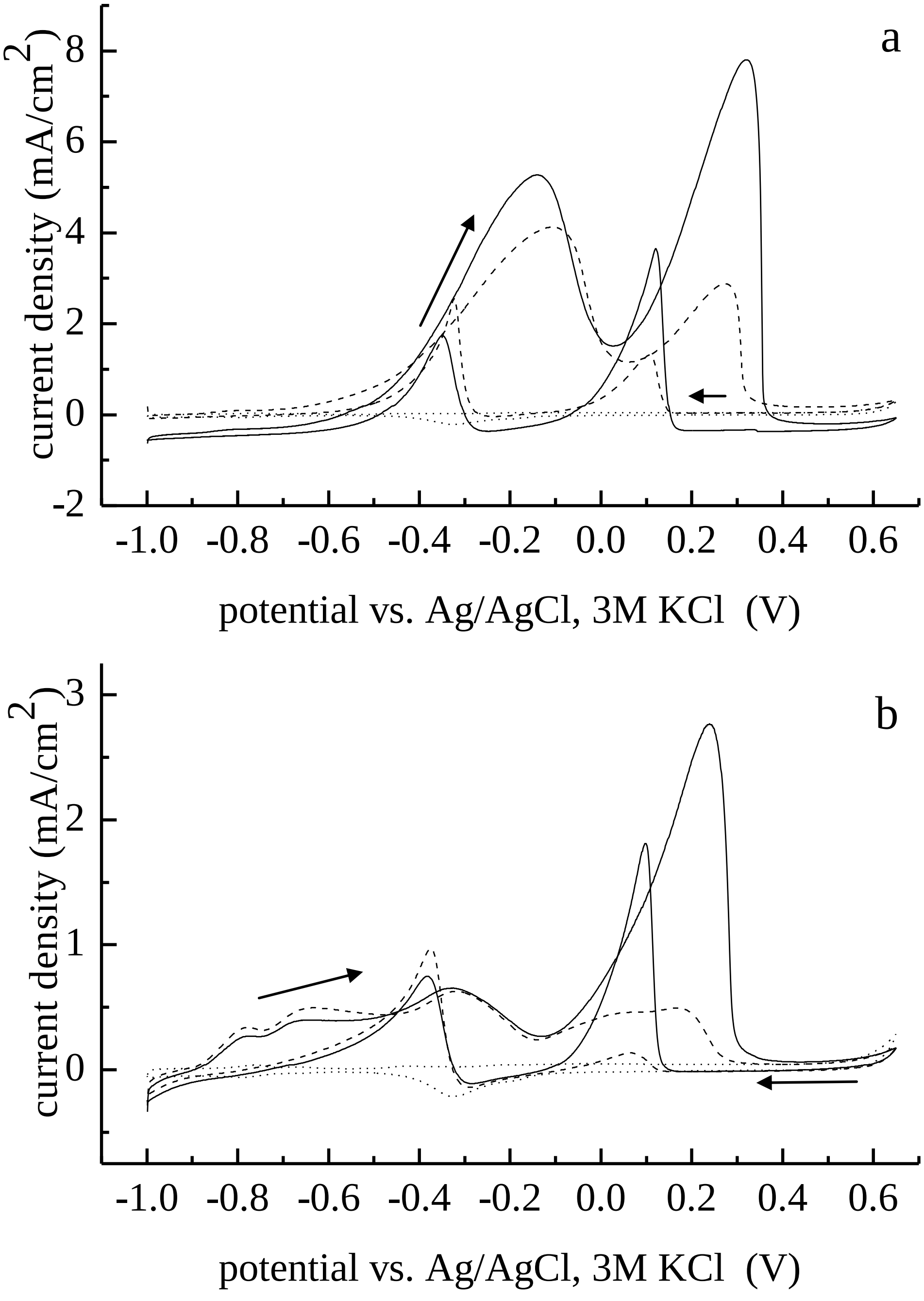

Figure 5.2: Cyclic voltammograms of (a) 1.0 M 1,2-butanediol and (b)1.0 M 2,3-butanediol in 1.0 M KOH, acquired at a scan rate of 10 mV/s. Solid line data were acquired at a nanoporous Pt electrode, dashed line data were acquired at a planar solid Pt electrode, and dotted line data are the background, 1.0 M KOH(*aq*).

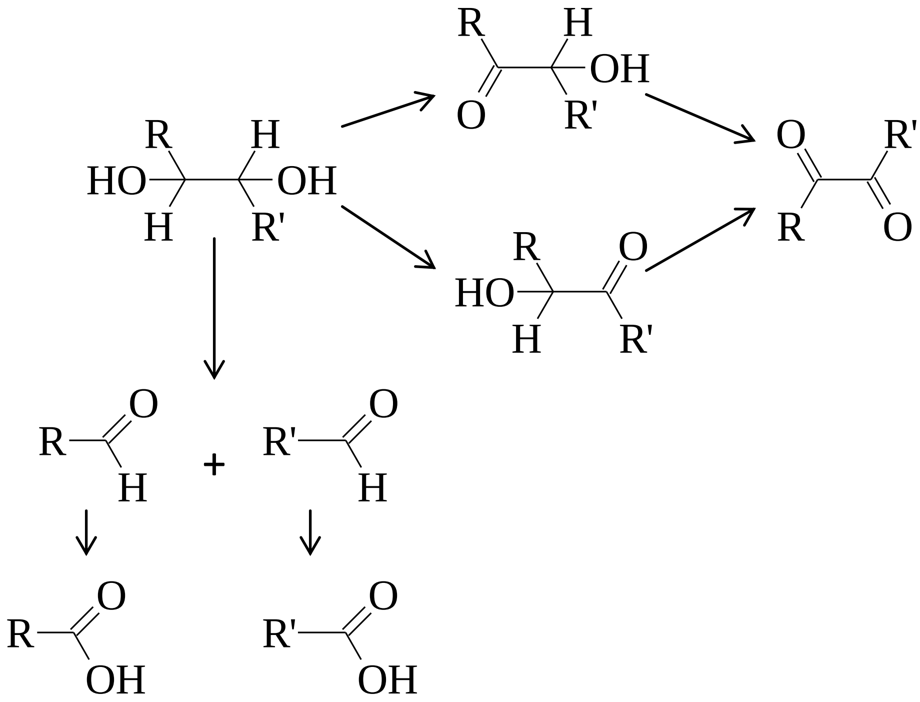

Scheme 5.1: Reaction schematic for the electrocatalytic oxidation of 1,2-butanediol and 2,3-butanediol

aldehydes, with subsequent oxidation to the corresponding carboxylic acid. Based on literature data showing the oxidation of 1- and 2-propanol to occur at *ca*. -0.3 V vs. SCE under basic conditions at a Pt electrode, we assign the forward oxidation wave at *ca*. -0.25 V in Figures 5.2a and 5.2b to alcohol oxidation and the reverse wave at *ca*. -0.4 V to be associated with oxidation to the dione.[86] We assert that the second forward oxidation wave corresponds to bond cleavage of the diol to form two aldehydes, with the oxidation wave on the reverse scan at *ca*. 0.1 V to be oxidation of the aldehydes to carboxylic acids (Scheme 5.1)[87] We note that the forward wave at -0.25 V is broader and more prominent for 1,2-butanediol than it is for 2,3-butanediol. We ascribe this width to be the result of two different unresolved species, 1-hydroxy-2-butanone and 2-hydroxybutanaldehyde, resulting from 1,2-butanediol oxidation[84] (Scheme 5.1), and only one α-hydroxyketone formed in the initial oxidation of 2,3-butanediol. The relative intensities of the initial oxidation waves for each diol may indicate a kinetic advantage in the formation of one of the products from 1,2-butanediol (likely the aldehyde).

Examination of the second forward oxidation wave for both diols indicates relatively facile bond cleavage at the Pt surface. It is known that bond cleavage can proceed efficiently at Pt electrode surfaces.[88] The current density for this wave is a factor of *ca*. 2.5 higher for 1,2-butanediol than it is for 2,3-butanediol, suggesting that cleavage between the 1 and 2 carbons is more efficient than cleavage between the 2 and 3 carbons.

An important feature in the data in Figure 5.2 is that the oxidation waves for nanoporous Pt are shifted to negative potentials relative to those seen for the planar solid electrode. This finding suggests enhanced electrocatalytic efficiency for the nanoporous solid, consistent with higher current densities for the nanoporous electrode. We note that there is a substantial difference between the nanoporous electrode second oxidation wave and that seen for the planar solid. Based on our assignment of this wave as C-C bond cleavage, it appears that the nanoporous Pt enhances the efficiency of this reaction beyond the enhancement expected for the confined geometry of this structural motif. These data are consistent with the distribution of crystal faces being different for the nanoporous Pt than for the planar solid, and the adjacent hydroxyl groups on 1,2- and 2,3-butanediol preferentially interact with one of the exposed Pt crystal faces in the nanoporous material. [53-54]

1,3-Propanediol and 1,3-Butanediol: The CV data for 1,3-propanediol and 1,3-butanediol are similar to one another (Figure 5.3) and are significantly different than those seen for 1,2- and 2,3-butanediol. We believe the fundamental differences in these data are associated with the 1,3 (non-vicinal) positions of the hydroxyl groups. As a result of this structural difference, the second oxidation wave on the forward scan that is prominent for the vicinal diols is much less pronounced for the 1,3-diols. The assignment of the oxidation wave at *ca*. -0.25 V as the initial oxidation step(s) taking the diol to the β-hydroxy aldehyde (1,3-propanediol) or ketone (1,3-butanediol) is consistent with these data (Scheme 5.2). If the forward scan oxidation wave at *ca*. 0.3 V is associated with bond cleavage, the operative mechanism for the cleavage step must rely to a significant extent on the proximity of the diol hydroxyl moieties, and thus the greater distance between the these moieties in the 1,3-diols leads to inefficient bond cleavage. It is this difference in bond cleavage that results in the differences from the vicinal diols.

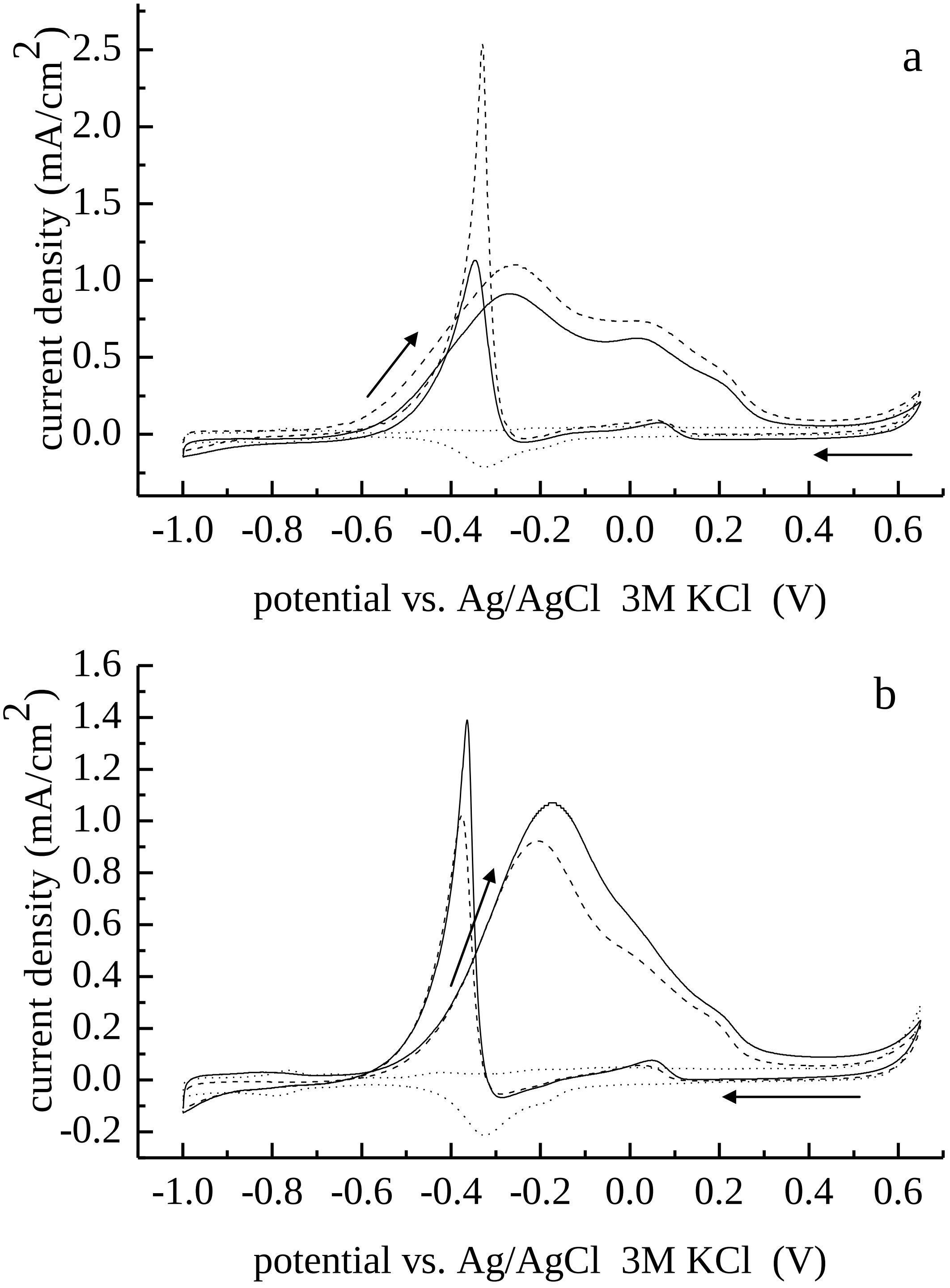

Figure 5.3: Cyclic voltammograms of (a) 1.0 M 1,3-propanediol and (b) 1.0 M 1,3-butanediol in 1.0 M KOH, acquired at a scan rate of 10 mV/s. Solid line data were acquired at a nanoporous Pt electrode, dashed line data were acquired at a planar solid Pt electrode, and dotted line data are the background, 1.0 M KOH(*aq*).

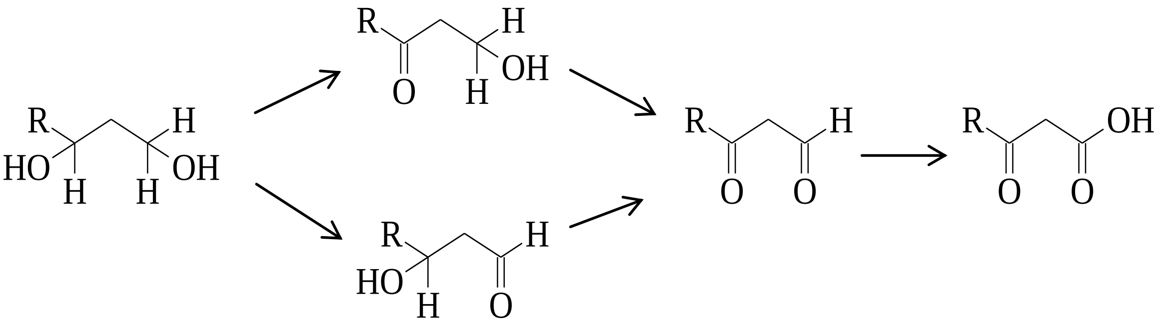

Scheme 5.2: Reaction schematic for the electrocatalytic oxidation of 1,3-propanediol and 1,3-butanediol

The electrocatalytic oxidation of 1,3-propanediol at Pt has been reported before.[67,83,89-90] The data we report here appear to manifest slight differences compared to those reported before and we understand this difference to be due to our experimental conditions. The broad features of our data are fully consistent with previous reports.[83,90] The primary issue is that there are typically two peaks on the forward oxidation scan, and for both the nanoporous Pt and the planar solid Pt electrodes we use, there is an indication of a third wave in the vicinity of 0.05 V. We cannot at this time offer a chemical structure to associate with this wave, but it is possibly the result of a dehydration reaction that operates with comparatively low efficiency. Further investigation under a variety of reaction conditions will be required to resolve this issue.

The oxidation products seen in the reverse scans are typical for alcohol oxidations. As for the vicinal diols, we believe that the reverse scan oxidation wave at *ca*. 0.2 V is associated with the oxidation of cleavage reaction products, resulting in the formation of carboxylic acids. The oxidation wave seen in the vicinity of -0.4 V is reflective of the β-hydroxy aldehyde or ketone being oxidized to the dialdehyde or β -ketoaldehyde, respectively.

It is also important to note that, in contrast to the data for the vicinal diols (Figure 5.2), the data for the 1,3-diols exhibit substantially the same current density profiles for both nanoporous and planar solid Pt electrodes. For the 1,3-diols there appears to be no enhancement in current density with nanoporous Pt electrodes. Thus neither geometric enhancement nor differences associated with the distribution of Pt crystal faces play a role in the data for these reactants. The fact that the CV data are essentially indistinguishable for these reactants points to the comparatively minor role the geometrically-derived enhancements play in the electrocatalytic process for these electrodes, and the comparative importance of the Pt electrode morphology. If a geometrically-derived enhancement in current density were operative for the nanoporous electrode, it should be seen for all reactants and its absence here is important to understanding the dominant factors in the enhancements seen for electrocatalysis of alcohols we have reported previously.[65]

1,4-Butanediol: The CVs of 1,4-butanediol are shown in Figure 5.4. In contrast to the data presented for the other diols, there is a single, asymmetric oxidation wave seen for the forward scan. The maximum for this wave is at *ca*. -0.05 V and, significantly, there is no component of the wave that extends beyond 0.3 V. These data suggest that multiple oxidation processes are responsible for the oxidation wave, but none of these appear to involve C-C bond cleavage. The absence of cleavage is not surprising given the data for the 1,3-diols and the distance between the 1- and 4- hydroxyl groups in 1,4-butanediol. It appears from these data that any C-C bond cleaving mechanism must involve contributions from both hydroxyl groups. The schematic of the oxidation steps for 1,4-butanediol is shown in Scheme 5.3, and the CV data are consistent with this schematic. The reverse waves seen for 1,4-butanediol are in the -0.05 to -0.2 V and -0.4 V regions. The broad wave in the -0.05 to -0.2 V window is weak and the wave at -0.4 V is more prominent and typical of the reverse waves seen for the other diols.

In contrast to the data on the 1,3-diols, we find that the nanoporous Pt electrode produces a higher current density than the planar solid Pt electrode for 1,4-butanediol. As noted above for the 1,3-diols, it appears that any diffusion-related enhancement in current density does not appear to be operative for the diols, leaving Pt surface

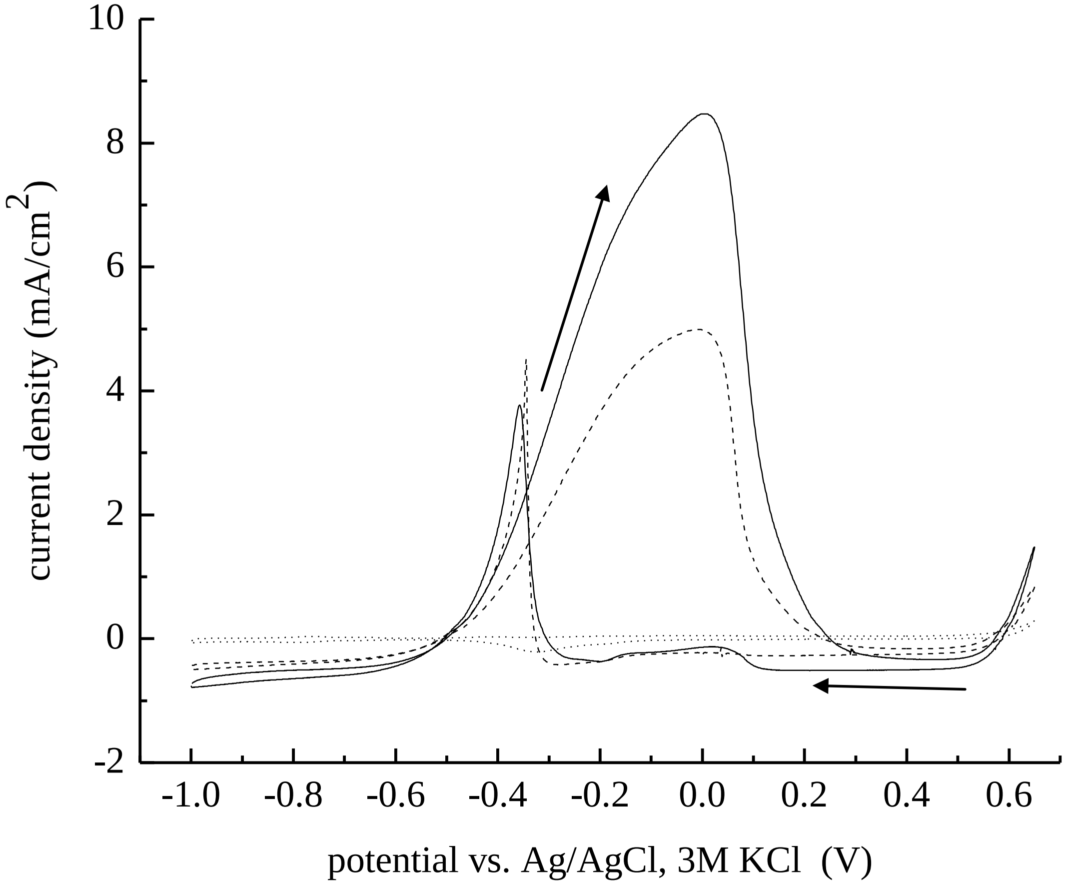

Figure 5.4: Cyclic voltammograms of 1.0 M 1,4-butanediol in 1.0 M KOH, acquired at a scan rate of 10 mV/s. Solid line data were acquired at a nanoporous Pt electrode, dashed line data were acquired at a planar solid Pt electrode, and dotted line data are the background, 1.0 M KOH(*aq*).

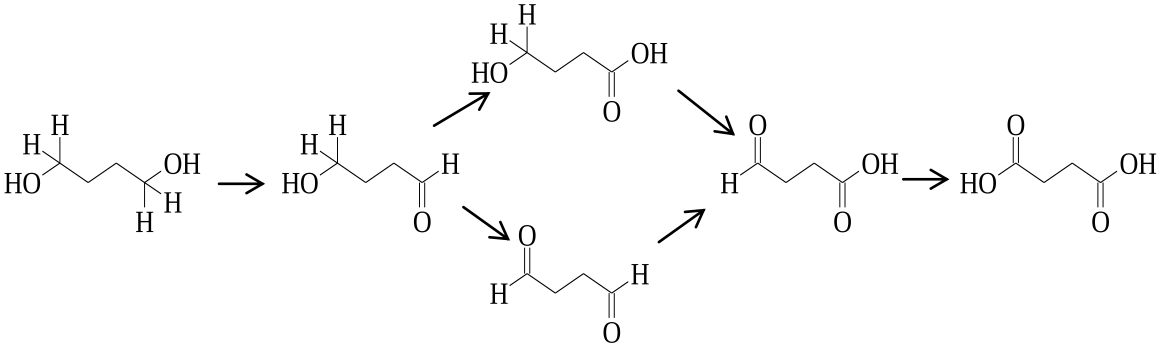

Scheme 5.3: Reaction schematic for the electrocatalytic oxidation of 1,4-butanediol

morphology as the dominant factor in determining current density. We also note a slight negative shift of the oxidation waves on nanoporous Pt relative to that seen for the planar solid. These findings are suggestive of a structural selectivity on the part of the Pt for specific diols.

It is tempting to compare the data for 1,4-butanediol to that for 1,3-propanediol because of the alcohol functionalities being present on the terminal carbons. We find that there is a limited resemblance between these two CVs (Figures 5.3a, 5.4), and this finding is significant in the context of determining the dominant reaction pathways. Where there is some oxidation process operating in the vicinity of 0.3 V for 1,3-propanediol, which we attribute to C-C cleavage, there is no corresponding wave seen for 1,4-butanediol. This comparison indicates that it is the proximity of the hydroxyl groups rather than their position(s) as primary alcohols that dominates the cleavage process. This finding is reinforced by the similarity of the CV data for the vicinal diols, where 1,2-butanediol contains a primary alcohol and 2,3-butanediol does not. Interestingly, the current density obtained for 1,4-butanediol (Figure 5.4) is higher than that for 1,3-propanediol at the nanoporous Pt electrode. This finding suggests that the Pt morphology plays a significant role in accommodating different diols selectively. The expected result, in the absence of any structurally-mediated Pt-diol interactions would be that the current density should decrease as the number of carbons in the diol chain increases.[83]

Conclusion

We have investigated the electrocatalytic oxidation of selected diols on nanoporous and planar solid Pt electrode surfaces under basic conditions. Our CV data show that the dominant factor in mediating the oxidation pathway is the proximity of the hydroxyl groups on the diol. Vicinal diols exhibit primarily C-C bond cleavage between the alcohol carbons. The propensity for this reaction to proceed diminishes as the distance between the hydroxyl moieties increases. It is thus clear that the hydroxyl groups play a major role in the bond cleavage mechanism.

In addition to the reactant-dependent reaction pathway, we find that for the vicinal diols and 1,4-butanediol, the nanoporous Pt electrode produces a higher current density than the planar solid electrode. For the 1,3-diols, this is not the case, and both Pt electrodes produce essentially the same current densities. These findings point to the importance of the reactant structure relative to Pt morphology in mediating the reaction efficiency. It is also clear from these data that the morphology of the nanoporous Pt is different than the planar solid Pt. Resolving the details of the difference in Pt surface morphology for the two types of electrodes is not trivial because traditional high vacuum surface techniques are incapable of accessing all surface sites in the nanoporous Pt. Underpotential deposition of selected metals onto the Pt surface may assist in resolving these surface morphological issues.

CHAPTER 6

EXAMINING THE ELECTRO-CATALYTIC OXIDATION OF SELECTED DIOLS AT NANOPOROUS AND PLANAR PT ELECTRODES: PART II: SCAN RATE DEPENDENCE

Introduction

We are interested in understanding from a fundamental perspective the electrocatalytic oxidation behavior of nanoporous and planar solid Pt electrodes for oxidation of diols under basic conditions. Our reasons for interest in these systems are that the feedstock(s) for such reactions are simple organic compounds that in principle, can be derived from biomass, and based on our previous work, nanoporous Pt structures appear to hold promise as relatively efficient electrode materials for fuel cell applications. At the present time, catalyst nanoparticles of Pt and mixed metals show promise for such applications.[19-20] These materials are not without limitation, however. The physical robustness and long-term stability of this type of catalyst are significant issues that are related intrinsically to their design. We have chosen to examine nanoporous solids formed by the electrodeposition of metal (*i.e.* Pt or Pd) around a silica sphere colloidal crystal template, to form inverse opal structures. These structures afford facile control over pore size and possess physical properties that should compete effectively with nanoparticle/polymer matrix catalysts. We have demonstrated increased catalytic activity for methanol and ethanol using these nanoporous Pt structures.[65] In the Chapter 5 we examined the electrocatalytic oxidation of a series of diols to understand the role of reactant structure in mediating the reaction pathway(s) of the oxidation process. We found that the reaction pathway for these processes depends on both the reactant structure and Pt morphology. In this Chapter we report on the scan-rate dependence of these reactions at nanoporous and planar solid Pt electrodes. Our data indicate that for fast scan rates, there can be a competition between oxidation of reaction products and reduction of transient intermediate species, and this behavior depends sensitively on the diol reactant and the resulting reaction pathway.

In the work we present here, we focus on the scan-rate dependence of cyclic voltammograms acquired for the reactants. In all cases the measured current densities scale with the scan rate, as expected. The functional shapes of the CVs as well as scan rate-dependent shifts in peak potentials provide insight into the kinetics of the reactions proceeding at the electrodes.

Experimental

Nanoporous Solid Fabrication: The fabrication of the nanoporous Pt electrodes used in this work has been described in Chapter 2.[65] 450 nm Diameter silica spheres were synthesized using a modified Stöber method,[13,27-28] and deposited on a gold substrate by vertical withdrawal from an ethanolic suspension at a rate of 0.34 µm/s (SDI Nanodip Coater). The resulting nanosphere assembly was sintered at 200°C for two hours.

Pt electrodeposition onto/into the nanosphere assembly was performed using a CHI604A electrochemical bench in a three electrode configuration with a Ag/AgCl 3M KCl reference electrode (E_0 = 0.210 V *vs.* NHE), a Pt counter electrode, and the silica nanosphere/gold substrate as the working electrode. Pt deposition was performed using a 10% w/w H_4PtCl_6 solution (Fluka) and cycling the potential between -0.4 and 1.6 V ten times at a scan rate of 50 mV/s.[22] The physical region of deposition on the nanosphere assembly was determined by masking the substrate. Following Pt deposition, the nanosphere assembly was immersed in a 10% (v/v) HF solution for *ca.* 15 min. to remove the silica nanosphere template. The same electrodeposition was used to deposit Pt on Au to produce the planar solid Pt electrode.

Characterization: The resulting Pt nanoporous solid was examined by scanning electron microscopy (SEM, JEOL 6400). Cyclic voltammetry of a solution of 1.0 M H_2SO_4 (Sigma-Aldrich) was used to determine the electro-active surface areas of both the nanoporous and planar substrates. For this determination, the potential was cycled between 0.25 V and 1.25 V (*vs.* Ag/AgCl 3M KCl), using the planar solid or nanoporous Pt as the working electrode and Pt wire as the counter electrode. The electrochemically active surface area (A) can be determined using the area of the hydrogen adsorption/desorption peaks (the Coulombic charge of hydrogen desorption, Q_H), along with the charge associated with the adsorption of a monolayer of hydrogen, so that A = Q_H/210 μC cm^{-2}.[26,49-50]

Diol Oxidation: All reagents used were purchased in the highest purity grade available and used as received. All electrochemical measurements were made at 20°C. Aqueous solutions of 1.0 M 1,3-propanediol (Aldrich, 99.6%), 1.0 M 1,2-butanediol (Fluka, ≥98%), 1.0 M 1,3-butanediol (Sigma-Aldrich, ≥99%), 1.0 M 1,4-butanediol (Sigma-Aldrich, ≥99%), and 1.0 M 2,3-butanediol (Aldrich, 98%) were made with 1.0 M KOH (*aq*). All solutions were deoxygenated with nitrogen gas before use. The potential for the cyclic voltammetry experiments was cycled between -1.0 and 0.65 V (vs. Ag/AgCl 3M KCl) at a series of scan rates ranging from 1 mV/s to 100 mV/s.

Results and Discussion

We have investigated the use of nanoporous Pt electrodes previously for the electrocatalytic oxidation of methanol, ethanol (Chapter 3) and 1,2-propanediol (Chapter 4).[65,81] We found that nanoporous Pt electrodes produced enhanced oxidation current densities relative to planar solid Pt for these reactants. There are, in principle, two possible factors that could account for this finding. One factor is based on an intrinsic geometric enhancement associated with the nano-confinement that results from the electrode structure, and the other factor is the possibility that a different distribution of crystal faces are produced in the formation of nanoporous and planar solid electrodes. The findings we report in the Chapter 5 indicate that the morphology of the Pt electrode plays a dominant role in mediating the extent of current density enhancement, and it is the purpose of this Chapter to provide information on the scan rate dependence of electrocatalytic oxidation at nanoporous and planar solid Pt electrodes. We consider the results for the diols we have examined according to the proximity of their hydroxyl groups because it is this reactant property that is related most closely to the reaction pathway. For all of the diols, we note that the position of the oxidation waves is scan rate dependent, for both forward and reverse scanning directions. While it is tempting to try to extract electron transfer rate constants from these data, the fact that the peaks are comprised of multiple, unresolved features, as reflected in the scan rate dependencies (*vide infra*) precludes this possibility. Any determination of an average rate constant would not be useful because such information could not be associated unambiguously with a specific reaction.

1,2-butanediol and 2,3-butanediol. The vicinal diols 1,2-butanediol and 2,3-butanediol exhibit qualitatively similar cyclic voltammograms, as discussed in Chapter 5. The presence of two forward oxidation waves points to the existence of competing oxidation reactions. It is known that Pt facilitates bond cleavage for certain reactants, and Scheme 5.1 shows two putative reaction pathways. We show the scan rate dependence of the cyclic voltammograms of 1,2-butanediol in Figure 6.1 and of 2,3-butanediol in Figure 6.2 for both nanoporous and planar solid Pt electrodes. The CV data for both diols exhibits scan rate dependencies that are useful in understanding the reactions proceeding at the electrodes. For 1,2-butanediol, the first forward oxidative wave at *ca*. 0 V exhibits a scan rate dependence different from that seen for the second oxidative wave (see insets to Figure 6.1). The log j vs. log v plots for both nanoporous and planar solid electrodes show that there is an approximately linear scan rate dependence for the first oxidative wave, with slopes of 0.50 for nanoporous Pt and 0.57 for planar solid Pt. The observation of slopes in the range of 0.5 indicates that there are multiple processes operating at the electrode and possibly also that there are multiple unresolved oxidation reactions contributing to the observed wave.[84] The corresponding slopes for 2,3-butanediol are 0.65 for both nanoporous and planar solid Pt. Despite the modest difference in slope for 1,2-butanediol and 2,3-butanediol, the conclusion that the first oxidation wave is dominated by multiple redox processes and/or several moderately slow kinetic steps is equally applicable to both reactants.

The scan rate dependence (log j vs. log v) for the second forward oxidation wave for both 1,2- and 2,3-butanediol exhibits curvilinear behavior. While the explanation of such behavior requires that there are multiple, perhaps competing or sequential processes

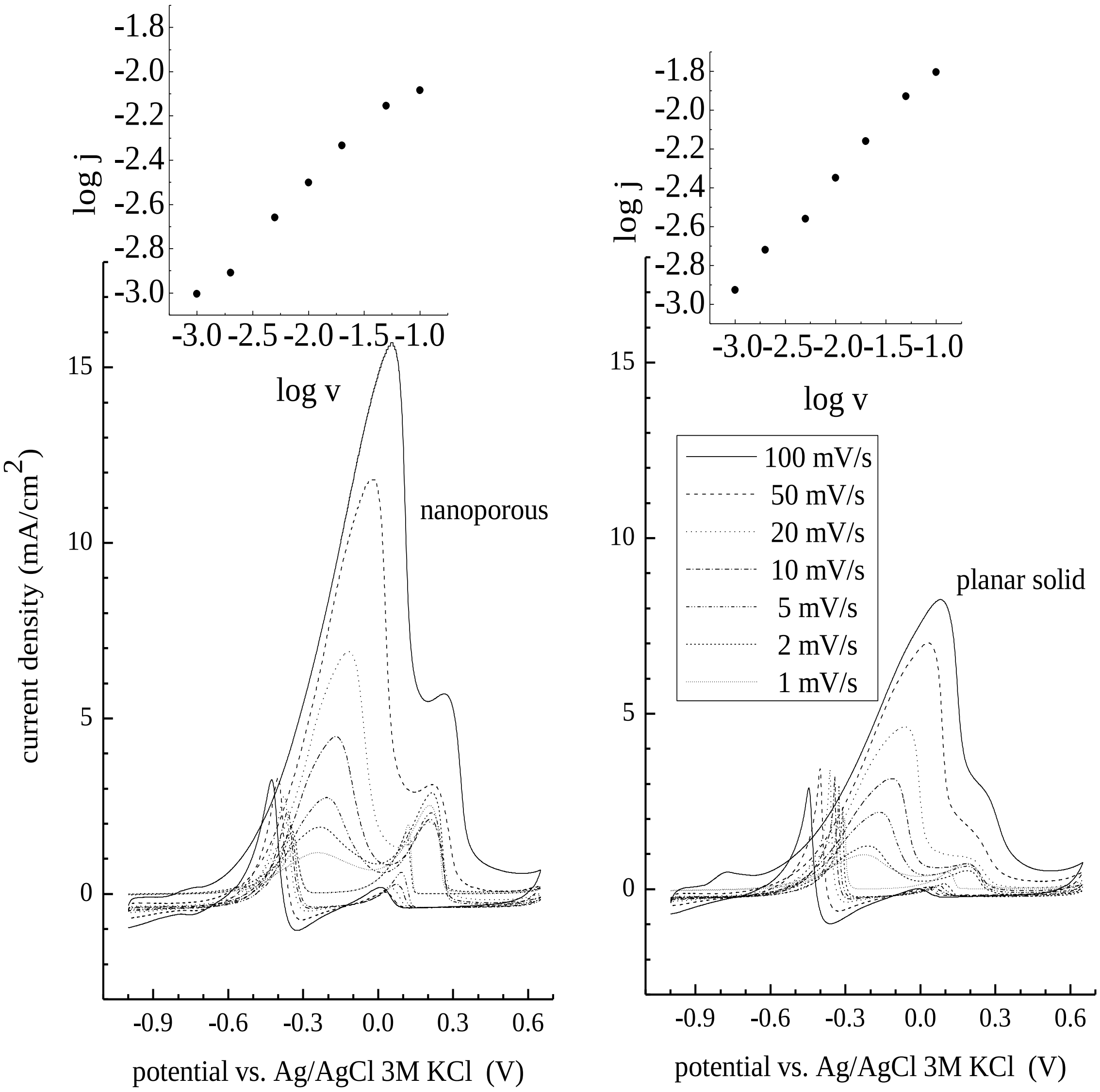

Figure 6.1. 1,2-Butanediol oxidation at nanoporous (left) and planar solid (right) Pt electrodes, as a function of scan rate. Insets for each data set show the dependence of the measured current density of the first (•) and second (o) forward oxidation waves. For nanoporous Pt, the first oxidation wave, the slope is 0.50 and for planar solid Pt the slope is 0.57. For the second forward oxidation wave, the current density does not vary linearly with the scan rate.

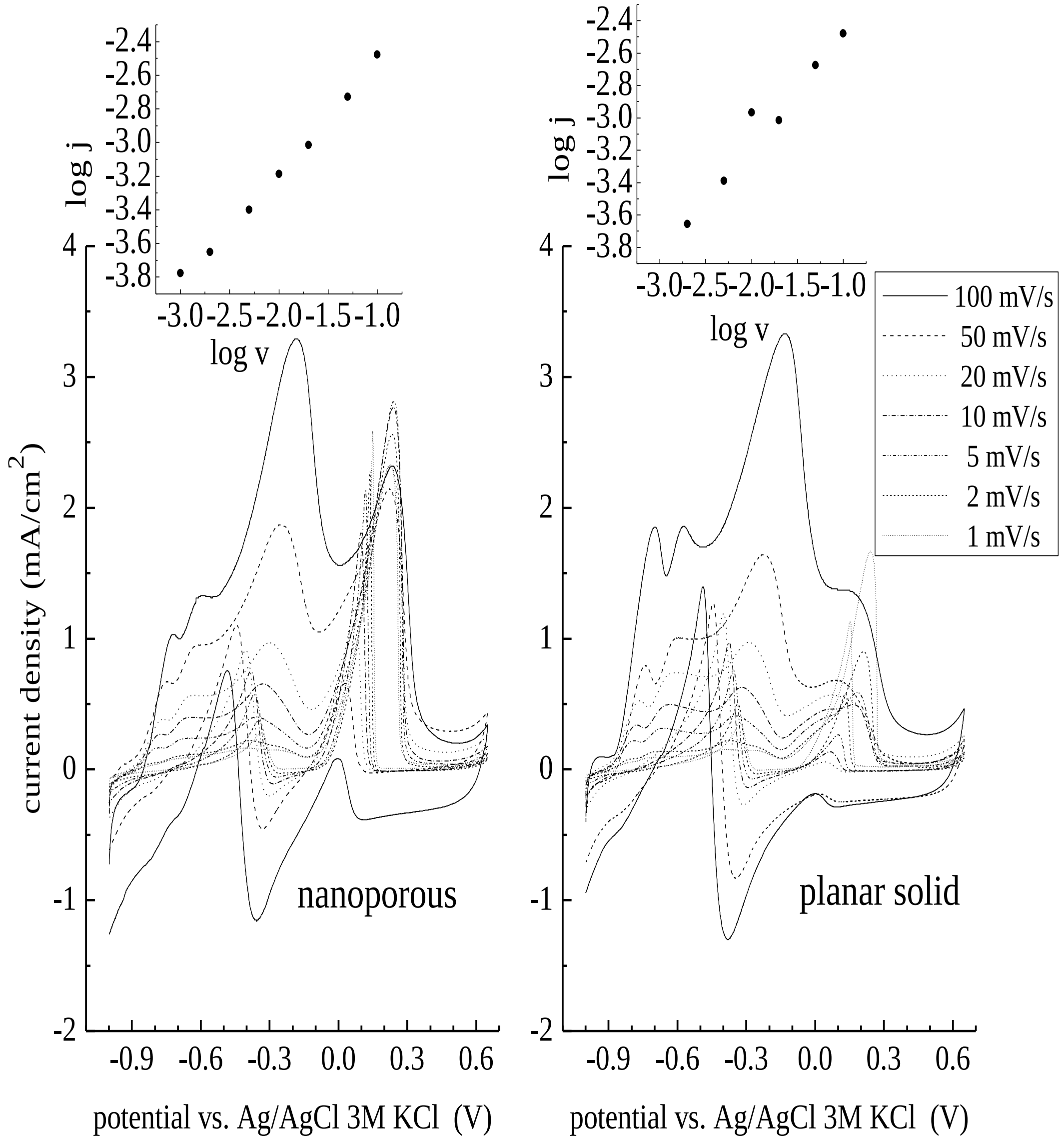

Figure 6.2. 2,3-Butanediol oxidation at nanoporous (left) and planar solid (right) Pt electrodes, as a function of scan rate. Insets for each data set show the dependence of the measured current density of the first (•) and second (o) forward oxidation waves. For both Pt electrodes, the first oxidation wave, the slope is 0.65. For the second forward oxidation wave, the current density does not vary linearly with the scan rate.

operating for this oxidation step, these data do contain some useful information. Specifically, comparison of the scan rate dependence for the second oxidation wave in 1,2- and 2,3-butanediol (Figures 6.1 and 6.2) shows the same functional form for both diols at the nanoporous Pt electrode. The same functional form is also seen for both diols at the planar solid Pt electrode, but the scan rate dependence is substantially different for the nanoporous and planar solid Pt electrodes. These data demonstrate that the reaction pathway(s) for both vicinal diols are the same at a given electrode type, but the pathways differ in detail at the two different types of electrode surface.

The reaction pathways indicated in Scheme 5.1 of the preceding chapter indicate a bond cleavage process as well as an oxidation from the diol to the dione, proceeding through two possible intermediates. The bond cleavage pathway is irreversible while the diol/ketone or diol/aldehyde couple should exhibit at least partial reversibility, and this is seen in the scan rate dependent data in Figures 6.1 and 6.2. The first oxidative wave near 0 V exhibits a corresponding reduction wave (much more prominent for 2,3-butanediol) for fast scan rates, while the second oxidation wave at *ca*. 0.25 V for both diols does not manifest a reduction wave on the reverse scan. The first wave behavior is consistent with the diol oxidation and the second wave is consistent with the bond cleavage reaction to produce the corresponding acid(s). We note that the reduction wave seen for fast scan rates competes with the oxidation wave in the reverse scan, but due to the different scan rate dependencies, the appearance of the peak (*ca*. -0.4V) changes from being predominantly oxidative at slow scan rates to what appears to be “dispersive” at faster scan rates. The oxidation reaction seen in the reverse wave thus originates from a surface-bound species while the reduction reaction proceeds with a solution phase species. In the preceding chapter, we suggested that the oxidation wave seen in the reverse scan at *ca*. -0.5 V was from a surface bound reaction product, producing the dione. The implication of these data is that the reaction intermediate(s) for this two-step oxidation from diol to dione bind with modest efficiency to the Pt surface and the scan rate dependence in this wave reflects that equilibrium.

1,3-propanediol and 1,3-butanediol. The data for 1,3-propanediol (Figure 6.3) and for 1,3-butanediol (Figure 6.4) exhibit less well-resolved oxidation waves for their forward scans than do the vicinal diols. We asserted in the preceding chapter that this difference is due to the comparatively lower efficiency for C-C bond cleavage to occur with the 1,3-diols. The forward oxidation wave(s) for the 1,3-diols are clearly comprised of several overlapped peaks and, as noted previously, the responses of these two diols are remarkably similar for both electrode morphologies. Such similarity indicates that geometric confinement plays a secondary role to surface morphology and reactant structure in mediating the electro-oxidative reaction efficiency. For the 1,3-diols, we note that the scan rate dependence (insets to Figures 6.3 and 6.4) is approximately linear for the maximum of the first forward oxidation wave, and in all cases the slope of the scan rate dependence is *ca*. 0.6. This value is consistent with there being multiple processes and/or unresolved species present. The presence of multiple reactive species in these systems is apparent at slower scan rates (Figures 6.3 and 6.4). As indicated in Scheme 5.2 of Chapter 5, the first oxidation reaction forms either an aldehyde or a ketone. For 1,3-propanediol, there is only one reaction intermediate (3-hydroxypropanaldehyde) and for 1,3-butanediol the reaction intermediates are methyl-2-hydroxyethyl ketone and 3-hydroxybutaraldehyde. The presence of multiple resolvable

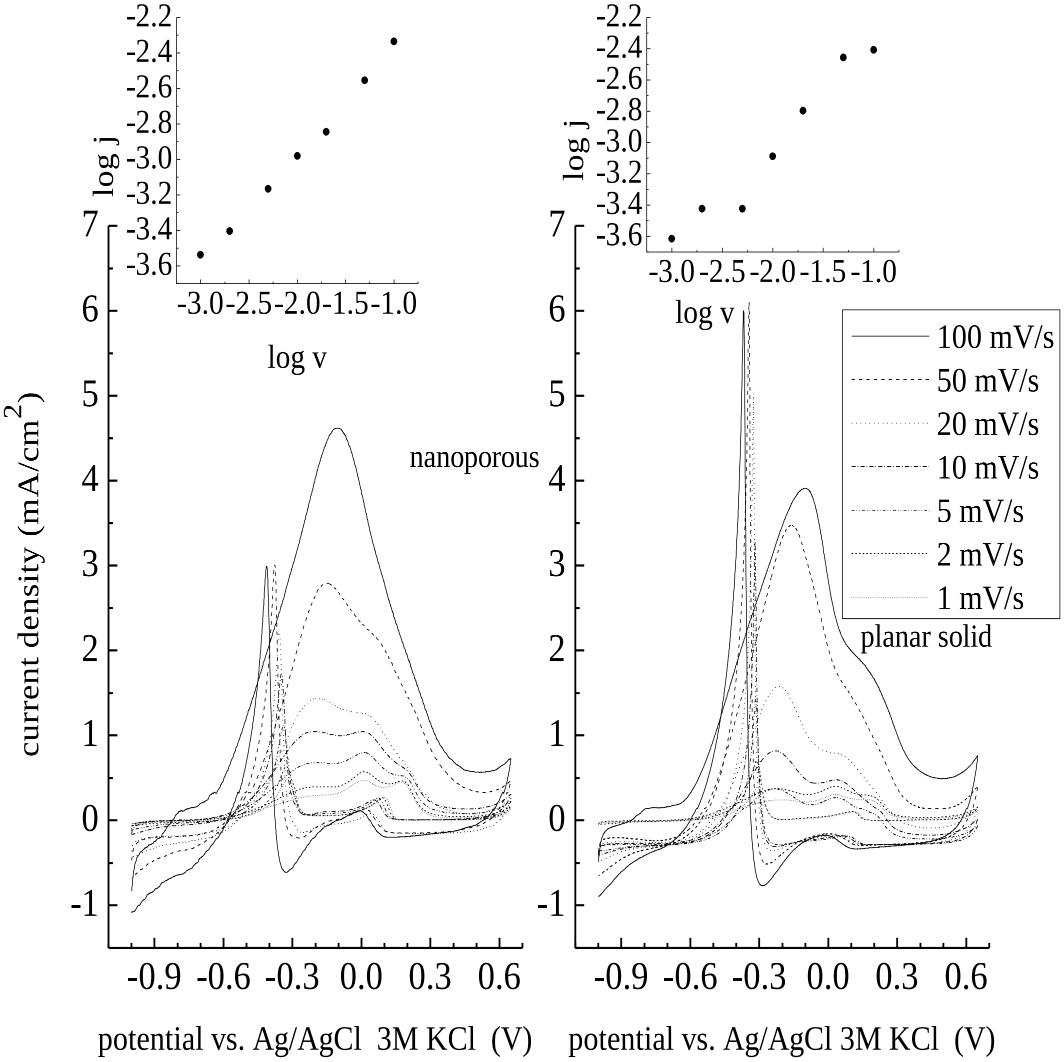

Figure 6.3. 1,3-Propanediol oxidation at nanoporous (left) and planar solid (right) Pt electrodes, as a function of scan rate. Insets for each data set show the dependence of the measured current density of the first (•) and second (o) forward oxidation waves. For nanoporous Pt, the first oxidation wave, the slope is 0.60 and for planar solid Pt the slope is 0.66. The second forward oxidation wave cannot be resolved sufficiently to determine its scan rate dependence.

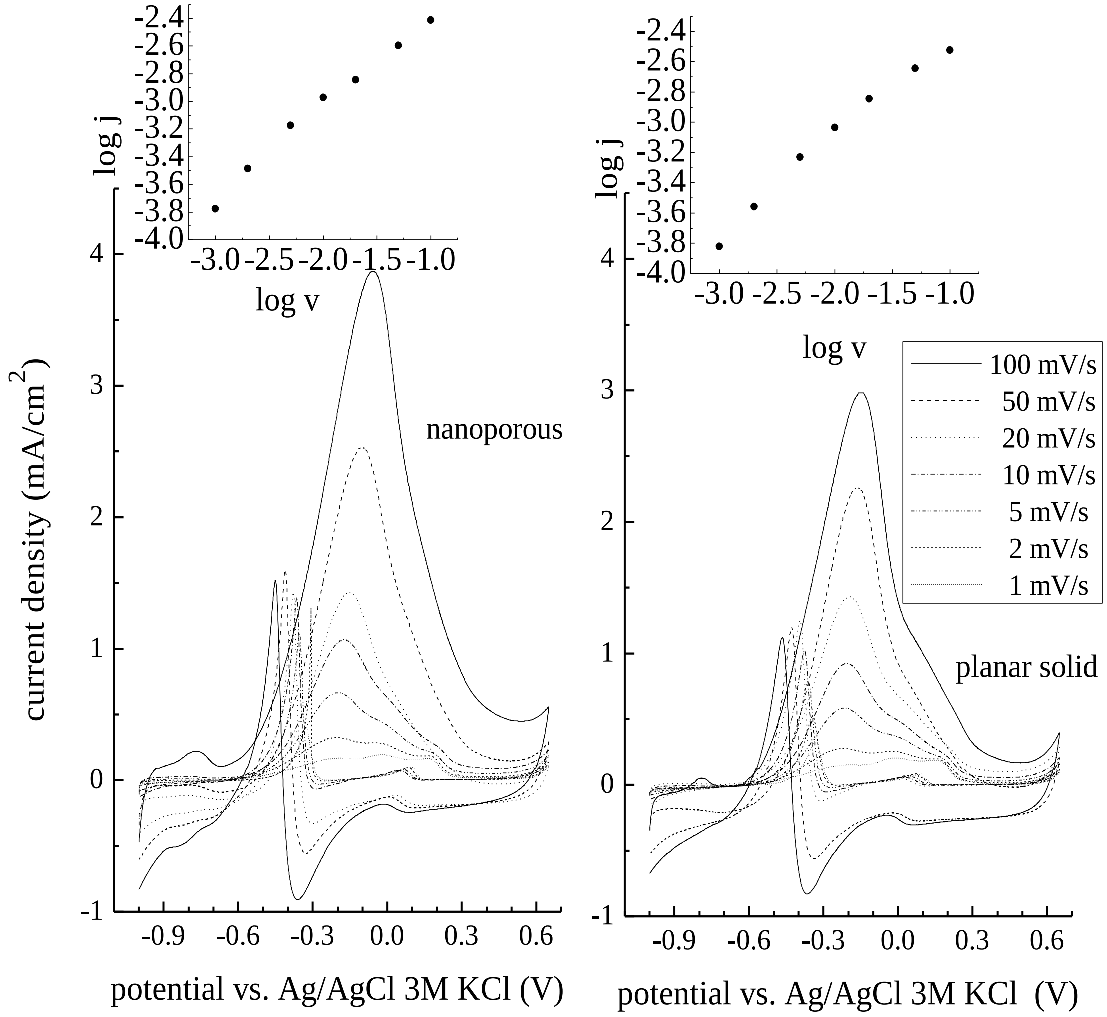

Figure 6.4. 1,3-Butanediol oxidation at nanoporous (left) and planar solid (right) Pt electrodes, as a function of scan rate. Insets for each data set show the dependence of the measured current density of the first (•) and second (o) forward oxidation waves. For nanoporous Pt, the first oxidation wave, the slope is 0.66 and for planar solid Pt the slope is 0.65. The second forward oxidation wave cannot be resolved sufficiently to determine its scan rate dependence.

peaks at low scan rate is most likely associated with a comparatively inefficient, Pt-mediated cleavage reaction, analogous to that seen prominently for the vicinal diols.

As was seen for the vicinal diols, the reverse scans reveal a scan-rate dependent competition between a reduction reaction and an oxidation process. We assert that the most likely assignment for the reduction wave is the reversible reduction of the initial reaction products back to the 1,3-diols. The oxidation at *ca*. -0.5 V exhibits a scan rate dependence and is likely the oxidation product of the intermediates to the 1,3-dione. We note that this oxidation reaction is especially efficient for 1,3-propanediol at planar Pt. It is likely that an equilibrium exists between adsorbed and solution phase reaction products and the scan rate dependence manifested for the reverse wave oxidation reflects this equilibrium.

1,4-butanediol. For 1,4-butanediol there is only one resolvable forward oxidation wave for high scan rates (Figure 6.5), and several unresolved peaks at low scan rates. The functional form of these data is the same for both nanoporous and planar Pt, with notably higher current density for the nanoporous electrode. The scan rate dependence for the two electrode morphologies is shown in the insets to Figure 6.5. The slope of the scan rate dependence is 0.59 for nanoporous Pt and 0.54 for planar Pt, indicating, as before, the operation of multiple processes. Because of the symmetry of the molecule, there is only one initial reaction product, 4-hydroxybutaraldehyde, with subsequent reactions producing either 4-hydroxybutyric acid or 1,4-butanedialdehyde. The reverse scans reveal little propensity for reversible reduction reactions, with the dominant reverse scan oxidation wave being assigned to 1,4-butanedioic acid. Because of the positions of

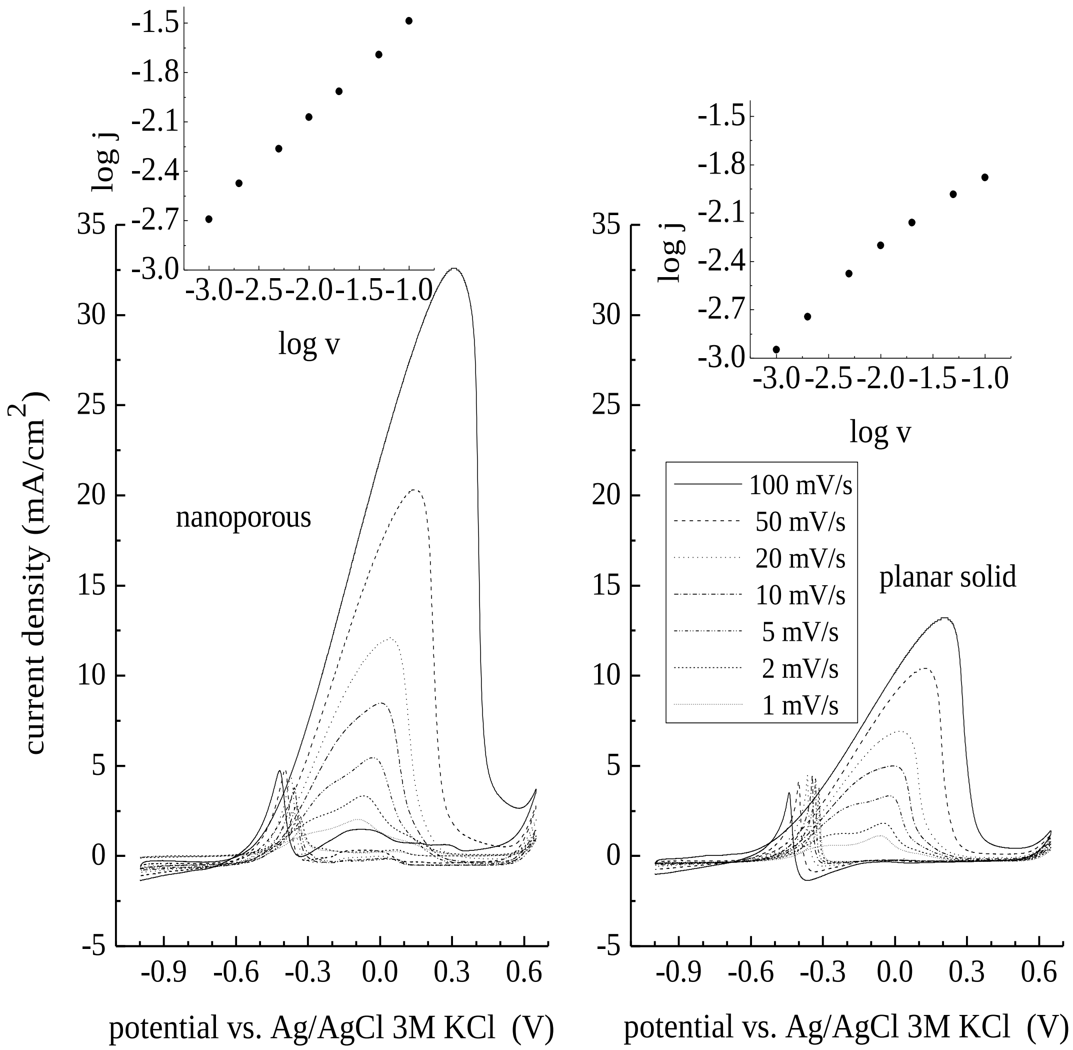

Figure 6.5. 1,4-Butanediol oxidation at nanoporous (left) and planar solid (right) Pt electrodes, as a function of scan rate. Insets for each data set show the dependence of the measured current density of the first (•) and second (o) forward oxidation waves. For nanoporous Pt, the first oxidation wave, the slope is 0.59 and for planar solid Pt the slope is 0.54. The second forward oxidation wave cannot be resolved sufficiently to determine its scan rate dependence.

the hydroxyl moieties in the reactant, we anticipate that the efficiency of the Pt-mediated bond cleavage will be low for this diol.

Nanoporous vs. Planar Pt. One way to evaluate these data is to compare the onset potentials for oxidation with the nanoporous Pt and planar solid Pt electrodes (Table 6.1).[7,25] Comparing the five diols at a scan rate of 10 mV/s shows that 1,3-propanediol and 1,3-butanediol exhibit more negative onset potentials with the nanoporous Pt electrode, while the onset potential of the electrocatalytic oxidation of 2,3-butanediol and 1,4-butanediol is seen to be somewhat smaller. The only diol of those studied here that exhibited a more positive onset potential with the nanoporous Pt was the 1,2-butanediol. While the onset potential is sometimes used to gauge relative catalytic efficiency, we note that these onset potential data do not appear to correlate with current density data (Table 6.1). We observe enhanced current densities for the nanoporous Pt electrodes for the vicinal diols and for 1,4-butanediol. The 1,3-diols do not exhibit any enhancement in current density with the nanoporous Pt electrode. In considering onset potential data, it is useful to keep in mind that the CV peaks we report in Figures 6.1-6.5 are not comprised of well resolved, discrete features. Rather, there are multiple contributions to each peak, as can be seen through the scan rate dependence date. For systems characterized by such complexity, the onset potential may not necessarily correlate with catalytic activity.

A gauge of catalytic efficiency is the current density achievable with these electrode structures. Our current density data are based on the electrochemical determination of the electrode surface area.[65,81] In the discussion that follows, we compare our CV current density data for 10 mV/s scans. We note that the enhancement

Table 6.1: Comparison of Electrochemical Performance

1,2-Butanediol

Platinum Substrate	Onset Potential (V)	Peak Potential I (V)	Peak Potential II (V)	Current Density PI (mA/cm^2)	Current Density PII (mA/cm^2)
Nanopor.	-0.668	-0.141	0.320	5.265	7.802
Planar	-0.690	-0.108	0.273	4.118	2.883

2,3-Butanediol

Platinum Substrate	Onset Potential (V)	Peak Potential I (V)	Peak Potential II (V)	Current Density PI (mA/cm^2)	Current Density PII (mA/cm^2)
Nanopor.	-0.529	-0.325	0.239	0.653	2.765
Planar	-0.522	-0.319	0.167	0.627	0.495

1,3-Propanediol

Platinum Substrate	Onset Potential (V)	Peak Potential I (V)	Peak Potential II (V)	Peak Potential III (V)	Current Density PI (mA/cm^2)	Current Density PII (mA/cm^2)	Current Density PIII (mA/cm^2)
Nanopor.	-0.666	-0.269	0.015	0.196	0.913	0.625	0.348
Planar	-0.655	-0.262	0.024	0.205	1.108	0.736	0.416

1,3-Butanediol

Platinum Substrate	Onset Potential (V)	Peak Potential I (V)	Peak Potential II (V)	Current Density PI (mA/cm^2)	Current Density PII (mA/cm^2)
Nanoporous	-0.682	-0.173	0.196	1.067	0.265
Planar	-0.653	-0.207	0.179	0.922	0.244

1,4-Butanediol

Platinum Substrate	Onset Potential (V)	Peak Potential I (V)	Current Density PI (mA/cm^2)
Nanoporous	-0.573	0.004	8.472
Planar	-0.578	-0.008	4.993

factors vary with scan rate, but the qualitative relationship between the electrode responses remains the same for a given diol. For the vicinal diols, the first forward oxidation wave is a factor of 1.3 times greater at the nanoporous Pt electrode for 1,2-butanediol and a factor of 1.1 for 2,3-butanediol. The comparison of the first oxidation wave does not provide a complete picture of the enhancement, however. For the second oxidative wave, corresponding to Pt-mediated bond cleavage for the vicinal diols (*vide infra*),[81] we observe a current density enhancement of a factor of 2.7 for 1,2-butanediol and a factor of 5.6 for 2,3-butanediol. In contrast to the vicinal diols and as noted above, there appears to be essentially no enhancement associated with the use of nanoporous Pt electrodes for the 1,3-diols at a scan rate of 10 mV/s. We do note differences in the reverse wave for 1,3-propanediol and it is clear from the data in Figures 6.3 and 6.4 that there is a modest current density enhancement seen for nanoporous Pt electrodes at higher scan rates. The current density enhancement seen for 1,4-butanediol at nanoporous Pt is *ca*. 1.7 at a 10 mV/s scan rate, with an increased enhancement to *ca*. 2.2 for a 100 mV/s scan rate. We note that 1,4-butanediol exhibits the highest absolute current density for the diols examined.

Sequential Scans. The oxidation of the five diols and their reaction products were examined by performing sequential cyclic voltammetry scans acquired at a scan rate of 10 mV/s. These data, shown in Figures 6.6-6.10, can provide insight into which species bind to the electrode surface and which reside in the solution phase. For 1,2-butanediol and 2,3-butanediol (Figures. 6.6 and 6.7), we find that the first oxidation wave, in the region of -0.2 V, the loss of signal with increasing number of scans is modest, consistent with this wave being associated with the initial oxidation of the reactant diol. For both

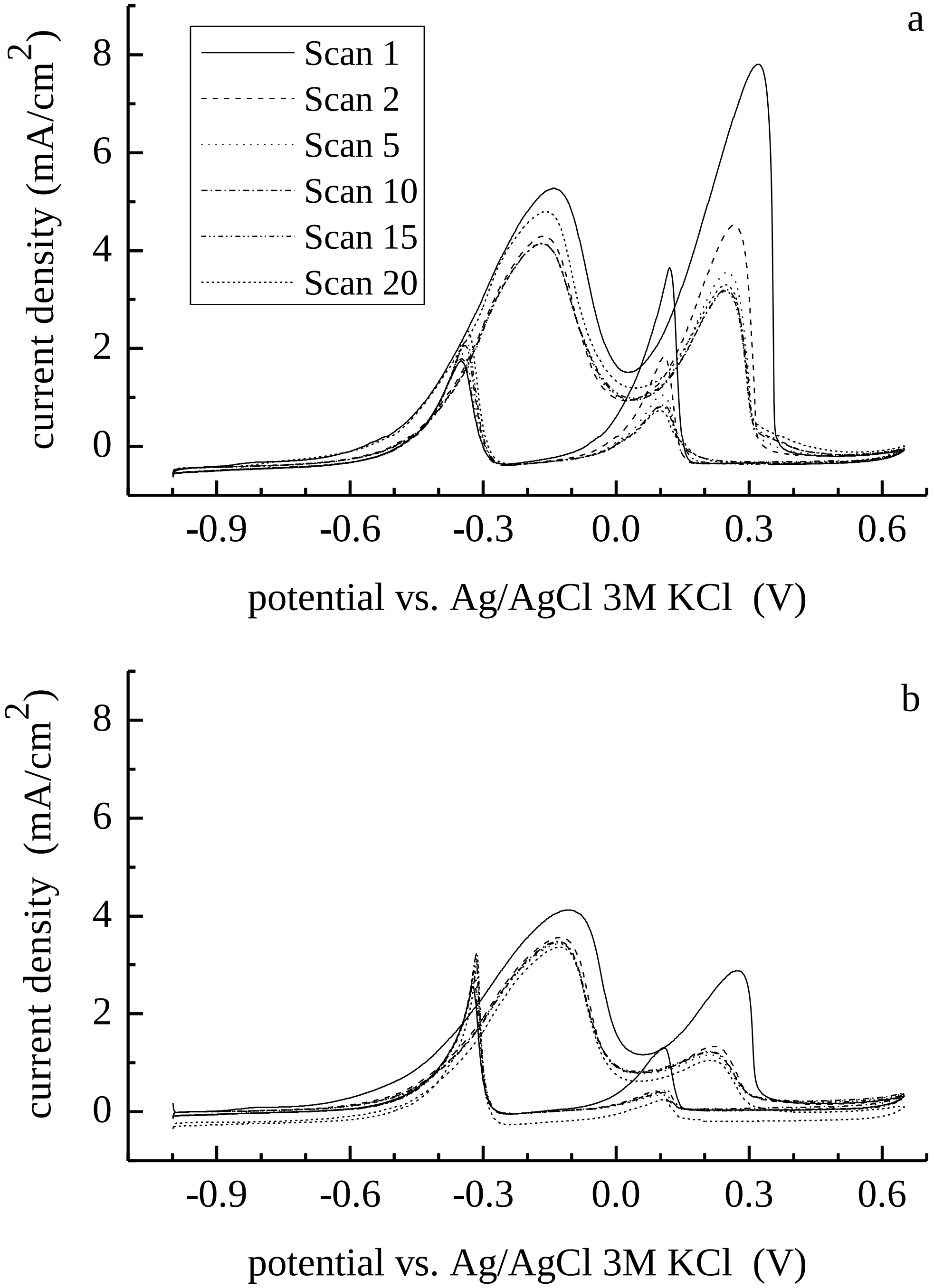

Figure 6.6. Cyclic voltammograms of 1,2-butanediol as a function of number of cycles. (a) Data acquired at a nanoporous Pt electrode. (b) Data acquired at a planar solid Pt electrode.

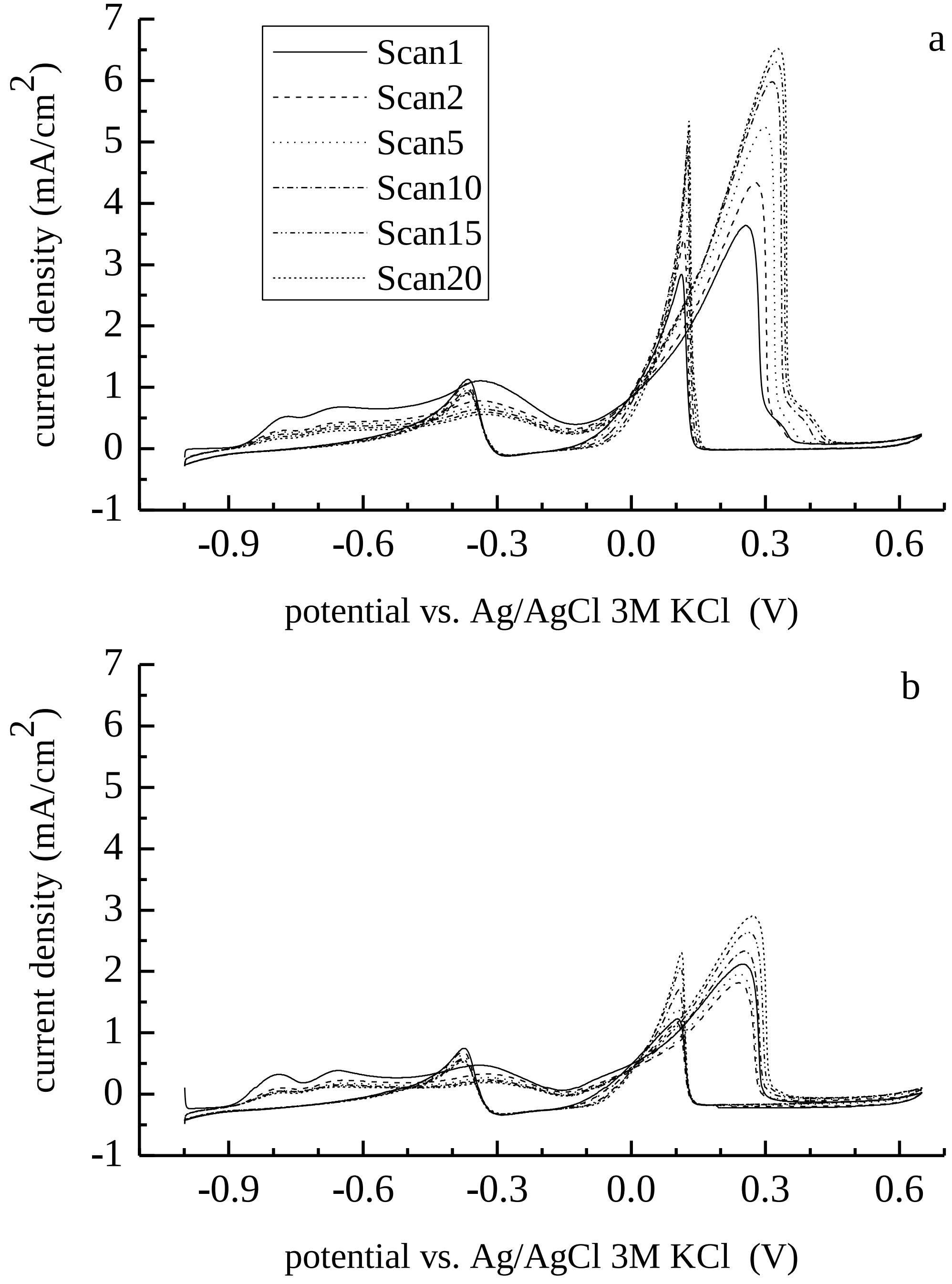

Figure 6.7. Cyclic voltammograms of 2,3-butanediol as a function of number of cycles. (a) Data acquired at a nanoporous Pt electrode. (b) Data acquired at a planar solid Pt electrode.

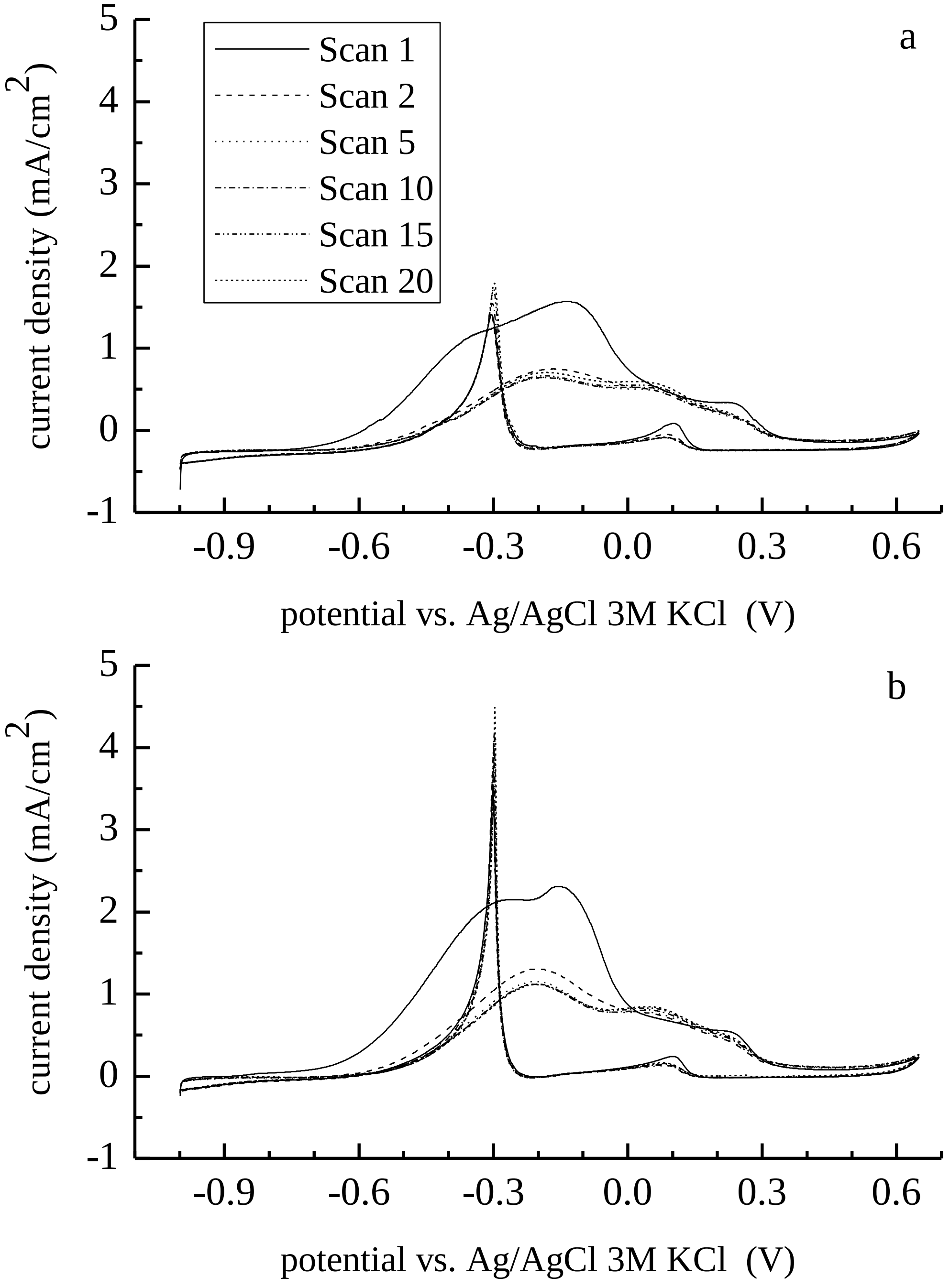

Figure 6.8. Cyclic voltammograms of 1,3-propanediol as a function of number of cycles. (a) Data acquired at a nanoporous Pt electrode. (b) Data acquired at a planar solid Pt electrode.

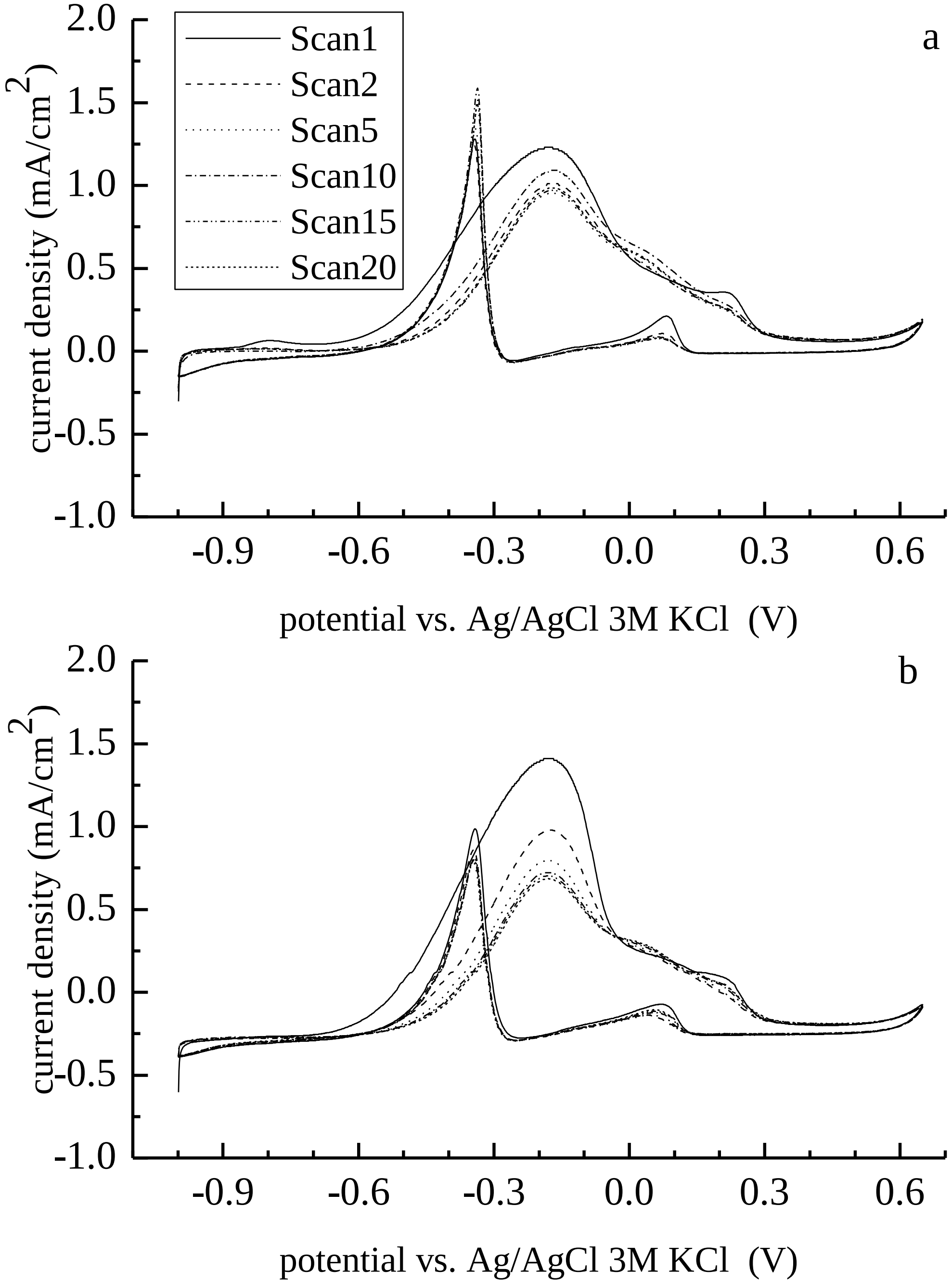

Figure 6.9. Cyclic voltammograms of 1,3-butanediol as a function of number of cycles. (a) Data acquired at a nanoporous Pt electrode. (b) Data acquired at a planar solid Pt electrode.

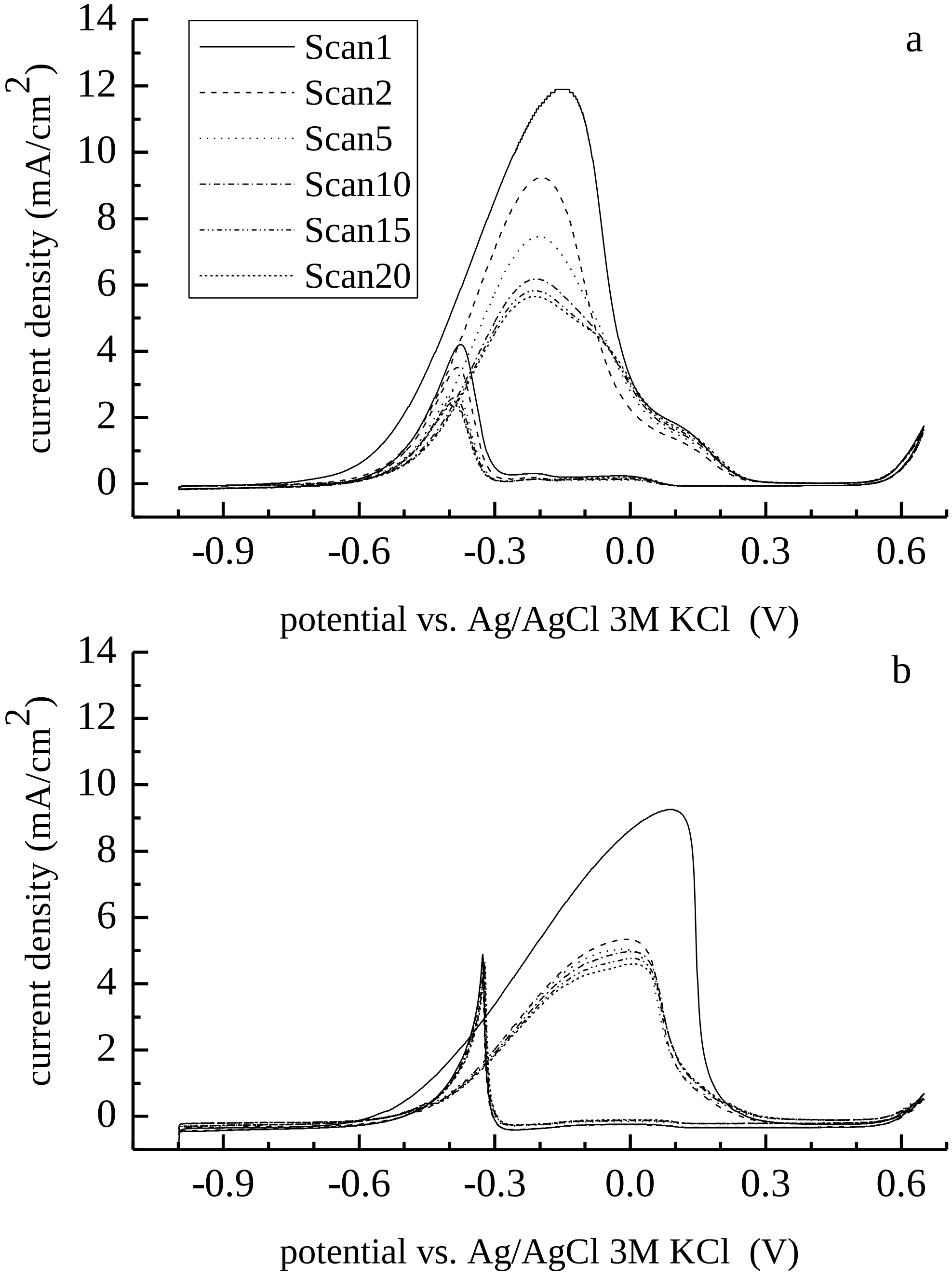

Figure 6.10. Cyclic voltammograms of 1,4-butanediol as a function of number of cycles. (a) Data acquired at a nanoporous Pt electrode. (b) Data acquired at a planar solid Pt electrode.

diols, the loss of current density for the second oxidation wave is more pronounced, suggesting that the oxidizing species interacts significantly with the Pt electrode surface, and this is true for both Pt morphologies. The species involved in the reverse scan oxidations also exhibit a dependence on the number of scans taken, suggesting that these species exhibit binding to some extent to the electrode surface(s). For the 1,3-diols (Figures 6.8 and 6.9), it is the first oxidation wave(s), between -0.3 and 0.0 V that exhibit the most pronounced scan dependence, at least for the first scan. The loss of signal after the first scan, followed by a plateauing behavior for subsequent scans suggests that after initial depletion of reactant in the first several cycles, a mass-transport-mediated equilibrium is established. Interestingly, for both 1,3-diols the second oxidation waves, in the region of 0.1V exhibit little dependence on the number of scans. This finding suggests that these reaction intermediates establish an equilibrium between being surface-bound and in the solution phase, and the kinetics of adsorption and desorption are fast relative to the scan rate we use. For 1,4-butanediol (Figure 6.10), the forward oxidation peak of the oxidation using the planar Pt resembles that observed for the first oxidation wave of the 1,3-diols. This mass-transport-mediated equilibrium takes longer to establish with the nanoporous Pt morphology, as it is not until after 10 consecutive scans that the initial reactants are depleted and the plateau seen with the planar Pt is observed. These results suggest that there is an intrinsic interaction between the surface-bound and solution phase intermediates that differs with each diol and, in some cases, with the Pt morphology.

Conclusions

We have examined the electrocatalytic oxidation of several diols at planar and nanoporous Pt electrodes as a function of cyclic voltammetric scan rate. These data show that the first forward oxidation waves for the diols are characterized by either multiple unresolved species or multiple reaction processes proceeding in parallel. Subsequent oxidation processes exhibit scan rate dependences that are also consistent with complex reaction(s), and in these cases the scan rate does not correlate linearly with the measured peak current density. Such findings suggest significant interaction(s) between the reactant(s) and the electrode surface, and these findings are corroborated by the dependence of the CV data on the number of sequential scans.

In the comparison of nanoporous and planar solid Pt electrodes, it is possible, in principle, to observe signal enhancements derived from geometric considerations (the formation of nanoscale "reactor" volumes) and from electrode morphology issues. The data we present here for the 1,3-diols suggest that, at least for these species, it is the electrode morphology (*i.e.* distribution of different metal crystal facets for the two types of Pt electrodes) that appears to be the dominant factor. We also note that Pt-mediated bond cleavage appears to be favored for vicinal diols, with this mechanism becoming less dominant with increasing distance between –OH moieties. Taken collectively, these data point to a novel electrode morphology that can give rise to enhancements in electrocatalytic current densities, depending on the reactants used.

CHAPTER 7

CONCLUSIONS

The long-term goal for this work is to develop flow-through catalytic nanoporous solids. Such materials can be useful in a number of applications, including their incorporation in fuel cells, for example. Before nanoporous solid materials can be utilized, however, there needs to be a thorough understanding of the catalytic reactions being performed and the advantages that the nanoporous solid material format can provide. In the work reported in this dissertation, we focused on comparing nanoporous solids on a solid substrate to the corresponding planar metal electrodes. One of the primary purposes of this work has been to understand the underlying causes for the catalytic enhancement that was seen for electrocatalytic oxidation of alcohols using nanoporous solids. Information on how the observed electrocatalytic enhancement varies with reactant identity can be assistance in understanding the factors that contribute to the effect. The chapters of this dissertation report on several investigations that serve collectively to initiate our effort in understanding this effect.

Gaining the ability to synthesize nanoporous solids reproducibly was a substantial experimental challenge, as detailed in Chapter 2. The issues included the identification of a compatible solid support, synthesis of the silica nanospheres and the colloidal crystal template required for nanoporous solid construction, and electrodeposition of the metal framework. All were critical steps in the formation of a nanoporous solid catalyst material. The solution of each problem lead to the reproducible formation of nanoporous solid catalyst materials made of Pt and Pd. The characterization of these materials has proven to be as challenging as their synthesis was.

As discussed in Chapter 3, we used Pt and Pd nanoporous solids to examine the electrocatalytic oxidation of methanol and ethanol, under acidic and basic conditions, primarily using cyclic voltammetry (CV) and chronoamperometry.[65] These results were then compared to planar Pt and Pd solid electrodes which were made using the same electrodeposition technique. It was found that, for certain conditions, the nanoporous solids offered greater electrocatalytic current density and greater stability than the planar solid electrodes. In comparing the Pt and Pd nanoporous solids, it was found that the platinum nanoporous solids offered greater electrocatalytic current density for the electrocatalytic oxidation of methanol, while the palladium nanoporous solids were a better catalyst for the electrocatalytic oxidation of ethanol. It was also determined that there is more than a simple surface area advantage to the use of nanoporous solids, as comparisons of the nanoporous and planar solids were made using current density. This finding, in concert with literature reports indicating that the electrocatalytic oxidation of methanol occurs with different efficiency depending on the Pt crystal facet used,[23,52-55] lend to the conclusion that there may be a metal morphology based contribution to the observed enhancement.

The examination of the factors that likely contribute to the advantages in reaction efficiency seen for nanoporous solids was continued using 1,2-propanediol as a reactant, the results of which were discussed in Chapter 4. We observed higher current density for the electrocatalytic oxidation of 1,2-propanediol with nanoporous Pt than with the planar solid electrode.[81] Although the enhanced catalytic behavior was somewhat less than what was seen for the electro-catalytic oxidation of methanol, the difference in CV scans between the nanoporous and planar Pt electrodes indicated that the reaction pathways at these two electrode materials were not identical. We also cycled the reaction continuously, which revealed a monotonic decrease in current density with number of cycles for both Pt electrodes. The rate at which this decrease occurred was different for the planar and nanoporous Pt, which is consistent with the notion that different distributions of exposed crystal faces were present at the two electrodes. A potential shift was also observed for the oxidation wave with increasing number of scans, suggesting that there are changes in the electrode surface as the potential is cycled.[55] These data point collectively to the central role of metal morphology in mediating the electro-catalytic oxidation efficiency.

We continued our examination of the nanoporous Pt surfaces and with selected diols, because many diol species exist that could potentially be useful as energy sources and their chemical structures are useful for examining electrocatalytic reactions at nanoporous solid surfaces. We examined the electrocatalytic oxidation of 1,3-propanediol and the four isomers of butanediol to understand how the positions of the hydroxyl groups on the diols influence the electrocatalytic reaction pathways used as a function of electrode morphology. Chapter 5 probes this issue from a mechanistic view, while in Chapter 6 we examine the problem kinetically.

From the CV data discussed in Chapter 5, it was determined that the dominant factor in mediating the oxidation pathway is the proximity of the hydroxyl groups on the diol. It was also found that for the vicinal diols and 1,4-butanediol, the nanoporous Pt electrode produces a higher current density than the planar solid electrode. This however, was not the case for the 1,3-diols, as both the nanoporous and planar Pt produced essentially the same current densities. Collectively, these data point to the importance of the reactant structure relative to the morphology in mediating the reaction efficiency and in some cases, pathways. These data also suggest that the morphology of the nanoporous Pt is different than that of the planar solid Pt. These findings are supported by the work presented in Chapter 6, which focused on the kinetics. The scan-rate dependence of the diol oxidation reactions at the nanoporous and planar solid Pt electrodes indicates that, for fast scan rates, there can be a competition between the oxidation of reaction products and reduction of transient intermediate species. This behavior is sensitive to the particular diol.

The next step of this project would be to further examine the relative contributions of geometric and morphology issues to the observed electrocatalytic oxidation enhancement at nanoporous solid Pt electrodes. It was mentioned in Chapter 4 that changing the pore size of the nanoporous solids is a potential means to evaluate geometric issues. However, the intrinsic problem with this method is that as the size of the domain changes, there is a possibility that the exposed facets of the metal are also changing. This means that as the size of the silica spheres used in the template is increased, the electrodeposition of the metal may lead to different platinum or palladium morphologies as the nanoporous solid is formed. As presented in Chapter 5, resolving the differences between the nanoporous and planar Pt surface morphology is not simple, as traditional high vacuum surface techniques are incapable of accessing all surface sites in the nanoporous Pt. Methods that could potentially be used to probe this issue in a way where there is a less likelihood that the two variables are changing are underpotential deposition of selected metals and grazing incidence X-ray diffraction (GIXD).

As mentioned at the beginning of this Chapter, the overall goal of this project is to develop a flow-through catalytic membrane that can be used in fuel cells, thus building and improving upon the early experiments discussed in Chapter 2. This could be achieved by using supports for the nanoporous solids that are not solid substrates, (*e.g*. porous alumina) or using other ways of depositing the metal around the silica spheres.

Collectively, the information we gained from this work provides a basis for understanding the enhancement observed using nanoporous solids of Pt and Pd over planar solid electrodes. The results point to different crystalline facets that react preferentially with certain alcohols. This information will ultimately lead to more efficient catalysts for methanol and other direct fuel cell systems.

LITERATURE CITED

LITERATURE CITED

1. http://www.eia.doe.gov/totalenergy/

2. Cuesta, A.; Escudero, M.; Lanova, B.; Baltruschat, H. *Langmuir* **2009**, *25*, 6500.

3. Ohanian, M.; Zinola, C. F. *Journal of Power Sources* **2007**, *168*, 307.

4. Zheng, S. F.; Hu, J. S.; Zhong, L. S.; Wan, L. J.; Song, W. G. *Journal of Physical Chemistry C* **2007**, *111*, 11174.

5. Liu, H. S.; Song, C. J.; Zhang, L.; Zhang, J. J.; Wang, H. J.; Wilkinson, D. P. *Journal of Power Sources* **2006**, *155*, 95.

6. Rolison, D. R.; Hagans, P. L.; Swider, K. E.; Long, J. W. *Langmuir* **1999**, *15*, 774.

7. Liu, H. P.; Ye, J. Q.; Xu, C. W.; Jiang, S. P.; Tong, Y. X. *Journal of Power Sources* **2008**, *177*, 67.

8. Liu, Z. L.; Hong, L. *Journal of Applied Electrochemistry* **2007**, *37*, 505.

9. Zhang, J. T.; Ma, H. Y.; Zhang, D. J.; Liu, P. P.; Tian, F.; Ding, Y. *Physical Chemistry Chemical Physics* **2008**, *10*, 3250.

10. Casado-Rivera, E.; Volpe, D. J.; Alden, L.; Lind, C.; Downie, C.; Vazquez-Alvarez, T.; Angelo, A. C. D.; DiSalvo, F. J.; Abruna, H. D. *Journal of the American Chemical Society* **2004**, *126*, 4043.

11. Inc., E. G. T. S. *Fuel Cell Handbook (Seventh Edition)*; U. S. Department of Energy: Morgantown, WV, 2004.

12. Szekeres, M.; Kamalin, O.; Schoonheydt, R. A.; Wostyn, K.; Clays, K.; Persoons, A.; Dekany, I.; Vol. 12, p 3268.

13. Szamocki, R.; Reculusa, S.; Ravaine, S.; Bartlett, P. N.; Kuhn, A.; Hempelmann, R. *Angewandte Chemie-International Edition* **2006**, *45*, 1317.

14. Bartlett, P. N.; Birkin, P. R.; Ghanem, M. A. *Chemical Communications* **2000**, 1671.

15. Lin, S. Y.; Chow, E.; Hietala, V.; Villeneuve, P. R.; Joannopoulos, J. D. *Science* **1998**, *282*, 274.

16. Cichelli, J.; Zharov, I. *Journal of the American Chemical Society* **2006**, *128*, 8130.

17. Newton, M. R.; Bohaty, A. K.; White, H. S.; Zharov, I. *Journal of the American Chemical Society* **2005**, *127*, 7268.

18. Newton, M. R.; Bohaty, A. K.; Zhang, Y. H.; White, H. S.; Zharov, I. *Langmuir* **2006**, *22*, 4429.

19. Gao, G. Y.; Guo, D. J.; Li, H. L. *Journal of Power Sources* **2006**, *162*, 1094.

20. Yin, Z.; Zheng, H. J.; Ma, D.; Bao, X. H. *Journal of Physical Chemistry C* **2009**, *113*, 1001.

21. Jia, J. B.; Cao, L. Y.; Wang, Z. H. *Langmuir* **2008**, *24,* 5932.

22. Liu, Y.; Chen, J.; Misoska, V.; Swiegers, G. F.; Wallace, G. G. *Materials Letters* **2007**, *61*, 2887.

23. Herrero, E.; Franaszczuk, K.; Wieckowski, A. *Journal of Physical Chemistry* **1994**, *98,* 5074.

24. Bard, A. J., Faulkner, Larry R. *Electrochemical Methods: Fundamentals and Applications*; John Wiley and Sons, Inc.: Hoboken, NJ, 2001.

25. Shen, Q. M.; Min, Q. H.; Shi, J. J.; Jiang, L. P.; Zhang, J. R.; Hou, W. H.; Zhu, J. J. *Journal of Physical Chemistry C* **2009**, *113,* 1267.

26. Xu, C. W.; Cheng, L. Q.; Shen, P. K.; Liu, Y. L. *Electrochemistry Communications* **2007**, *9*, 997.

27. Reculusa, S.; Ravaine, S. *Chemistry of Materials* **2003**, *15,* 598.

28. Stober, W.; Fink, A.; Bohn, E. *Journal of Colloid and Interface Science* **1968**, *26,* 62.

29. Bogush, G. H.; Zukoski, C. F. *Journal of Colloid and Interface Science* **1991**, *142*, 19.

30. Matsoukas, T.; Gulari, E. *Journal of Colloid and Interface Science* **1988**, *124*, 252.

31. Matsoukas, T.; Gulari, E. *Journal of Colloid and Interface Science* **1989**, *132*, 13.

32. Okubo, T.; Ishiki, H.; Kimura, H.; Chiyoda, M.; Yoshinaga, K. *Colloid and Polymer Science* **2002**, *280*, 290.

33. Okubo, T.; Kobayashi, K.; Kuno, A.; Tsuchida, A. *Colloid and Polymer Science* **1999**, *277,* 483.

34. Philipse, A. P. *Colloid and Polymer Science* **1988**, *266*, 1174.

35. Vanblaaderen, A. V., J. Vrij, A *Journal of Colloid and Interface Science* **1992**, *154*, 481.

36. Vanblaaderen, A. V., A *Journal of Colloid and Interface Science* **1993**, *156*, 1.

37. Gornowich, D. B.; Blanchard, G. J. Personal Communication

38. Szablewski, P. M. a. M. *Langmuir-Blodgett Troughs: Operating Manual*; 6th ed., 2004.

39. Denkov, N. D.; Velev, O. D.; Kralchevsky, P. A.; Ivanov, I. B.; Yoshimura, H.; Nagayama, K. *Langmuir* **1992**, *8*, 3183.

40. Dimitrov, A. S.; Nagayama, K. *Langmuir* **1996**, *12*, 1303.

41. Mathur, A.; Brown, A. D.; Erlebacher, J. *Langmuir* **2006**, *22*, 582.

42. Perrin, J. *Annales De Chimie Et De Physique* **1909**, *18*, 5.

43. Wijnhoven, J.; Zevenhuizen, S. J. M.; Hendriks, M. A.; Vanmaekelbergh, D.; Kelly, J. J.; Vos, W. L. *Advanced Materials* **2000**, *12*, 888.

44. Hou, W. B.; Dehm, N. A.; Scott, R. W. J. *Journal of Catalysis* **2008**, *253*, 22.

45. Zhang, H.; Wang, Y.; Fachini, E. R.; Cabrera, C. R. *Electrochemical and Solid State Letters* **1999**, *2*, 437.

46. Jafarian, M.; Mahjani, M. G.; Heli, H.; Gobal, F.; Khajehsharifi, H.; Hamedi, M. H. *Electrochimica Acta* **2003**, *48*, 3423.

47. Chen, S.; Schell, M. *Electrochimica Acta* **2000**, *45*, 3069.

48. Tripkovic, A. V.; Popovic, K. D.; Lovic, J. D. *Electrochimica Acta* **2001**, *46*, 3163.

49. Pozio, A.; De Francesco, M.; Cemmi, A.; Cardellini, F.; Giorgi, L. *Journal of Power Sources* **2002**, *105*, 13.

50. Watt-Smith, M. J.; Friedrich, J. M.; Rigby, S. P.; Ralph, T. R.; Walsh, F. C. *Journal of Physics D-Applied Physics* **2008**, *41*.

51. Xu, C. W.; Wang, H.; Shen, P. K.; Jiang, S. P. *Advanced Materials* **2007**, *19*, 4256.

52. Tarnowski, D. J.; Korzeniewski, C. *Journal of Physical Chemistry B* **1997**, *101*, 253.

53. Morin, M. C.; Lamy, C.; Leger, J. M.; Vasquez, J. L.; Aldaz, A. *Journal of Electroanalytical Chemistry* **1990**, *283*, 287.

54. Perez, J. M.; Munoz, E.; Morallon, E.; Cases, F.; Vazquez, J. L.; Aldaz, A. *Journal of Electroanalytical Chemistry* **1994**, *368*, 285.

55. Lucas, C. A. *Electrochimica Acta* **2002**, *47*, 3065.

56. Xu, C. W.; Shen, P. K. *Journal of Power Sources* **2005**, *142*, 27.

57. Shekhar, R.; Barteau, M. A. *Catalysis Letters* **1995**, *31*, 221.

58. Gomes, J. F.; Busson, B.; Tadjeddine, A. *Journal of Physical Chemistry B* **2006**, *110*, 5508.

59. Susut, C.; Chapman, G. B.; Samjeske, G.; Osawa, M.; Tong, Y. *Physical Chemistry Chemical Physics* **2008**, *10*, 3712.

60. Clavilier, J.; Armand, D. *Journal of Electroanalytical Chemistry* **1986**, *199*, 187.

61. Zei, M. S.; Ertl, G. *Surface Science* **1999**, *442*, 19.

62. Xu, C. W.; Shen, P. K.; Liu, Y. L. *Journal of Power Sources* **2007**, *164*, 527.

63. Yu, E. H.; Scott, K.; Reeve, R. W. *Journal of Electroanalytical Chemistry* **2003**, *547*, 17.

64. Tripkovic, A. V.; Popovic, K. D.; Lovic, J. D.; Jovanovic, V. M.; Kowal, A. *Journal of Electroanalytical Chemistry* **2004**, *572*, 119.

65. Dimos, M. M.; Blanchard, G. J. *Journal of Physical Chemistry C* **2010**, *114*, 6019.

66. Mori, K.; Yamada, Y.; Sato, S. *Applied Catalysis a-General* **2009**, *366*, 304.

67. Huser, H.; Leger, J. M.; Lamy, C. *Electrochimica Acta* **1985**, *30*, 1409.

68. Huser, H.; Leger, J. M.; Lamy, C. *Electrochimica Acta* **1988**, *33*, 1359.

69. Ocon, P.; Beden, B.; Lamy, C. *Electrochimica Acta* **1987**, *32*, 1095.

70. Derlacki, Z. J.; Easteal, A. J.; Edge, A. V. J.; Woolf, L. A.; Roksandic, Z. *Journal of Physical Chemistry* **1985**, *89*, 5318.

71. Erbudak, M.; Kalt, P.; Nissen, H. U. *Physics and Chemistry of Minerals* **1982**, *8*, 197.

72. Tian, N.; Zhou, Z.-Y.; Sun, S.-G.; Ding, Y.; Wang, Z. L. *Science* **2007**, *316*, 732.

73. Kuzume, A.; Herrero, E.; Feliu, J. M. *Journal of Electroanalytical Chemistry* **2007**, *599*, 333.

74. Song, H.; Kim, F.; Connor, S.; Samorjai, G. A.; Yang, P. *Journal of Physical Chemistry B* **2005**, *109*, 188.

75. Horanyi, G.; Torkos, K. *Journal of Electroanalytical Chemistry* **1981**, *125*, 105.

76. Tsujino, T.; Ohigashi, S.; Sugiyama, S.; Kawashiro, K.; Hayashi, H. *Journal of Molecular Catalysis* **1992**, *71*, 25.

77. Pinxt, H.; Kuster, B. F. M.; Marin, G. B. *Applied Catalysis a-General* **2000**, *191*, 45.

78. Cao, J. Y.; Du, C.; Wang, S. C. C.; Mercier, P.; Zhang, X. G.; Yang, H.; Akins, D. L. *Electrochemistry Communications* **2007**, *9*, 735.

79. Geng, D. S.; Lu, G. X. *Journal of Physical Chemistry C* **2007**, *111*, 11897.

80. Caminati, W. *Journal of Molecular Spectroscopy* **1981**, *86*, 193.

81 Dimos, M. M.; Blanchard, G. J. *Journal of Electroanalytical Chemistry* **2011**, *654*, 13.

82. Betowska-Brzezinska, M.; Luczak, T.; Holze, R. *Journal of Applied Electrochemistry* **1997**, *27*, 999.

83. Hilmi, A.; Belgsir, E. M.; Leger, J. M.; Lamy, C. *Journal of Electroanalytical Chemistry* **1995**, *380*, 177.

84. Hilmi, A.; Belgsir, E. M.; Leger, J. M.; Lamy, C. *Journal of Electroanalytical Chemistry* **1997**, *435*, 69.

85. Tripkovic, A. V.; Popovic, K. D.; Lovic, J. D. *Electrochimica Acta* **2001**, *46*, 3163.

86. Liu, J.; Ye, J.; Xu, C.; Jiang, S. P.; Tong, Y. *Journal of Power Sources* **2008**, *177*, 67.

87. Sibille, S.; Moiroux, J.; Marot, J. C. *Journal of Electroanalytical Chemistry* **1978**, *88*, 105.

88. Lamy, C.; Belgsir, E. M.; Leger, J.-M. *Journal of Applied Electrochemistry* **2001**, *31*, 799.

89. Chbihi, M. E.; Takky, D.; Hahn, F.; Huser, H.; Leger, J. M.; Lamy, C. *Journal of Electroanalytical Chemistry* **1999**, *463*, 63.

90. Chbihi, M. E.; Takky, D.; Leger, J. M.; Lamy, C. *Annales De Chimie-Science Des Materiaux* **2008**, *33*, 397.